The Pursuit of Hypervelocities: A Review of Two-Stage Light Gas Gun Aeroballistic Ranges

Jacob A. Rogers[a], Nathaniel T. Bass[a], Mikayla L. Wiest[a], Zach Wantz[b], Justin W. Wilkerson[a], Thomas E. Lacy, Jr.[a,*]

[a] *J. Mike Walker '66 Department of Mechanical Engineering, Texas A&M University, College Station, Texas, 77843.*
[b] *Physics Applications, Inc., Dayton, OH, 45458.*

Abstract

The ongoing pursuit of space and hypersonic flight continues to expose critical gaps in the understanding of material behavior under hypervelocity impact (HVI) and hypersonic flow conditions. Such limitations pose serious risks for aerospace vehicles, spacecraft, hardened structures, defensive systems, *etc.* Consequently, the development of materials and systems that can endure HVIs and hypersonic flight is a major obstacle in the quest for sustainable space exploration, reusable air-breathing hypersonic vehicles, and enduring protective structures. HVIs ($\geq$3.0 km/s) can induce severe material deformation, erosion, fracturing, fragmentation, melting, vaporization, and sublimation. At the same time, hypersonic ($\geq$Mach 5) vehicles may be subjected to intense thermal and mechanical loads. Addressing these grand challenges requires a multifaceted and interdisciplinary approach, combining well-designed experiments with physics-based analytical and numerical modeling. Studying material behavior under HVIs and hypersonic conditions has been facilitated by two-stage light gas gun (2SLGG) aeroballistic ranges for almost seven decades. This current study surveys over 90 2SLGG aeroballistic ranges operational since 1990 to assess global launch and experimental capabilities. The 2SLGG's origins and research applications are explored, highlighting its significance in various fields, including shock physics, planetary science/defense, military defense, nuclear physics, hypersonic vehicle survivability and performance, and spacecraft micro-meteoroid/orbital debris protection. A summary of relevant HVI phenomena is presented to underscore the importance of 2SLGGs and to elucidate similarities and differences among various 2SLGG aeroballistic ranges and their supporting methods/tools. The 2SLGG's working principles are explained, and configurations and operations are compared. Modifications resulting in "three-stage light gas guns" are briefly mentioned for completeness. The full range of current 2SLGG performance capabilities is assessed with impact kinetic energies ranging from $\sim$10 joules to nearly 100 megajoules, and the facility survey results are used to explain the variations in aeroballistic

*Corresponding author. J. Mike Walker '66 Department of Mechanical Engineering, Texas A&M University, College Station, Texas, 77843, United States.
Email address: telacyjr@tamu.edu (Thomas E. Lacy, Jr.)

range tankage, experiment types, research applications, and diagnostic systems. Finally, an overview of 2SLGG performance prediction methods is provided, featuring notable empirical, analytical, and numerical approaches.

Keywords: two-stage light gas gun (2SLGG), aeroballistic range, hypervelocity impact, hypersonics, ballistics, terminal ballistics, high-speed imaging, flash X-ray imaging, photon doppler velocimetry (PDV), planar impacts, aerothermophysics, hypervelocity launchers, nuclear/pellet injection

---

Contents

1. Introduction and Motivation

For many centuries, free flight ballistic ranges were used to study high-velocity projectile dynamics and impact physics. Such ranges nearly all employed some form of launch tube in which an energetic powder

was burned to generate the pressures necessary to accelerate projectiles to high velocities (*e.g.*, a cannon or gun). The first gun originated around the 12th century in Europe or Asia [1]. Formal scientific study of the physics of classical internal ballistics, projectile flight characteristics, and terminal impact effects did not begin in earnest until around the beginning of the 19th century. Throughout history, a number of eminent scholars worked on these ballistic problems, including Galileo, Newton, Robins, Lagrange, Poisson, Résal, Hélie, Serrau, Moisson, Hugoniot, Gossot and Liouville, Charbonnier, Rōggla, Love and Pidduck, Cranz, Fowler *et al.*, Corner, Thornhill, Hunt, and Nelson, among many others [2]. The earliest recorded existence of a single-stage *laboratory* gun (cannon) was in 1742 when Benjamin Robins used a ballistic pendulum to measure the muzzle velocity of a projectile [3]. His experiments proved that aerodynamic effects on the projectile were nonnegligible and that the existing prevailing theories for predicting projectile ballistics needed significant modifications.

Over the next two centuries, many studies focused on optimizing projectile shapes to minimize aerodynamic drag (*cf.* [2, 3]). These were conducted with single-stage compressed gas or nitrocellulose powder guns. In general, a single-stage gun consists of three main components: a pressure breech containing the driver gas, a projectile, and a launch tube (barrel) as shown in Fig. 1a. These launchers can have overall dimensions on the order of centimeters (*e.g.*, small firearms) to 10–50 m (*e.g.*, Schwerer Gustav [4]) and can accommodate projectile diameters and masses ranging several orders of magnitude. Hypervelocity phenomena were not widely considered until the 1930s when astronomers began to study planetary impacts. This work gained little traction until the late 1940s [5] when the advent of supersonic jets, hypersonic rockets, and missiles at the end of the Second World War necessitated the study of hypervelocity impacts (HVIs) (*circa.* 1945) [6]. The introduction of ballistic missile technology and spacecraft shielding required laboratory launch velocities of up to 6.0 km/s and >7.0 km/s, respectively. Conventional, single-stage compressed gas and nitrocellulose powder guns, though, could only accommodate launch velocities up to 2.75 km/s (roughly Mach 8) [6]. Significant improvements in launcher design were required in order to develop these emerging technologies.

Rocket motors, jet engines, shock tubes, and wind tunnels all appeared to be viable tools to extend the launch velocity ceiling but possessed significant limitations in fully replicating projectile/vehicle flight dynamics [6]. Several launching methods were designed, developed, and implemented to accelerate objects up to ∼10 km/s (*e.g.*, Van de Graaff accelerators, plasma guns, and electromagnetic rail guns). Other launching techniques, such as magnetically launched flyers, reached velocities well beyond the scope of this work (15–44 km/s) [7]. In contrast, the basic structure and working principles of the single-stage powder gun provided many advantages in generating the required projectile launch conditions: (*i*) the solid propellant was relatively stable and non-toxic, (*ii*) the propellant ignition was more reliable compared to certain rocket

fuels, (*iii*) the high-pressure combustion gases were safely contained within the gun barrel, (*iv*) the muzzle velocity was easily controllable and repeatable, (*v*) the projectile base pressure could be maintained for a relatively long duration, and (*vi*) the high achievable projectile accelerations enabled launchers to be relatively small and easily manufacturable [8].

During the 1940s and 1950s, Crozier and Hume [2, 6], Charters *et al.* [8], and Slawsky *et al.* [9] conducted groundbreaking research that involved adding an extra stage to a single-stage gun. This innovation dramatically raised the launcher's velocity ceiling while retaining its original benefits. The resulting novel apparatus soon became known as the two-stage light gas gun (2SLGG). In the nearly eight decades since its inception, the 2SLGG has been reliably used to launch objects to velocities ranging roughly 2.0–10.0 km/s. Even higher velocities have been reached with modifications to the 2SLGG, creating so-called "three-stage light gas guns" (3SLGGs). The single-, two-, and three-stage guns are all pressure-driven launchers. Single-stage launchers rapidly propel projectiles down a launch tube (barrel) using high-pressure gas, generated either through controlled combustion or mechanical compression and initially contained within a pressure breech [2, 10]. 2SLGGs employ the single-stage launching technique to accelerate a (usually) consumable piston down a "pump tube," rapidly compressing a light gas to extremely high pressures and temperatures. This high pressure "working" gas is then released *via* a single-use, rapidly opening valve and accelerates a projectile to hypervelocities (Fig. 1b). A comprehensive discussion of 2SLGG operating principles is included later in this paper. The 3SLGG (or "modified 2SLGG") uses yet another stage (see Section 3.3) to achieve even higher velocities (Fig. 1c) [11]. The conceptual schematics presented in Fig. 1 highlight key similarities and differences between each gun by clearly indicating all components, including the pressure breech, driver gas, projectile, launch tube (barrel), pump tube, piston, working gas, diaphragm, and flyer plate launcher [6, 12, 13]. The achievable impactor velocity-scale ranges for single- and multi-stage guns are compared to some other relevant launching methods in Fig. 2 [7, 14]. To date, multi-stage gas guns remain the predominant technique for launching macroscale projectiles to velocities exceeding roughly 5 km/s. More details on these multi-stage launchers can be found in Refs. [6, 12, 13, 15].

Early ballistics, hypersonics, and HVI research led to over 70 years of scientific advances, starting with the inception of the 2SLGG [5]. Swift [6] loosely categorized this period into five eras based on the significant scientific contributions and corresponding political environment: the Early Days (1945–1957), the Space Race (1958–1969), the "Dark Ages" (1970–1977) the Cold War (1978–1991), and the Commercial Space Age (1996–present) [6]. Figure 3 displays a graph summarizing the findings of a previous study that examined the temporal distribution of high-velocity and hypervelocity related publications over a period of 70+ years [5]. The figure has been adapted to emphasize significant 2SLGG-related historical milestones, as they correlate well with scientific advancements made during this period [6, 11, 13, 16–32]. In the Early Days, research

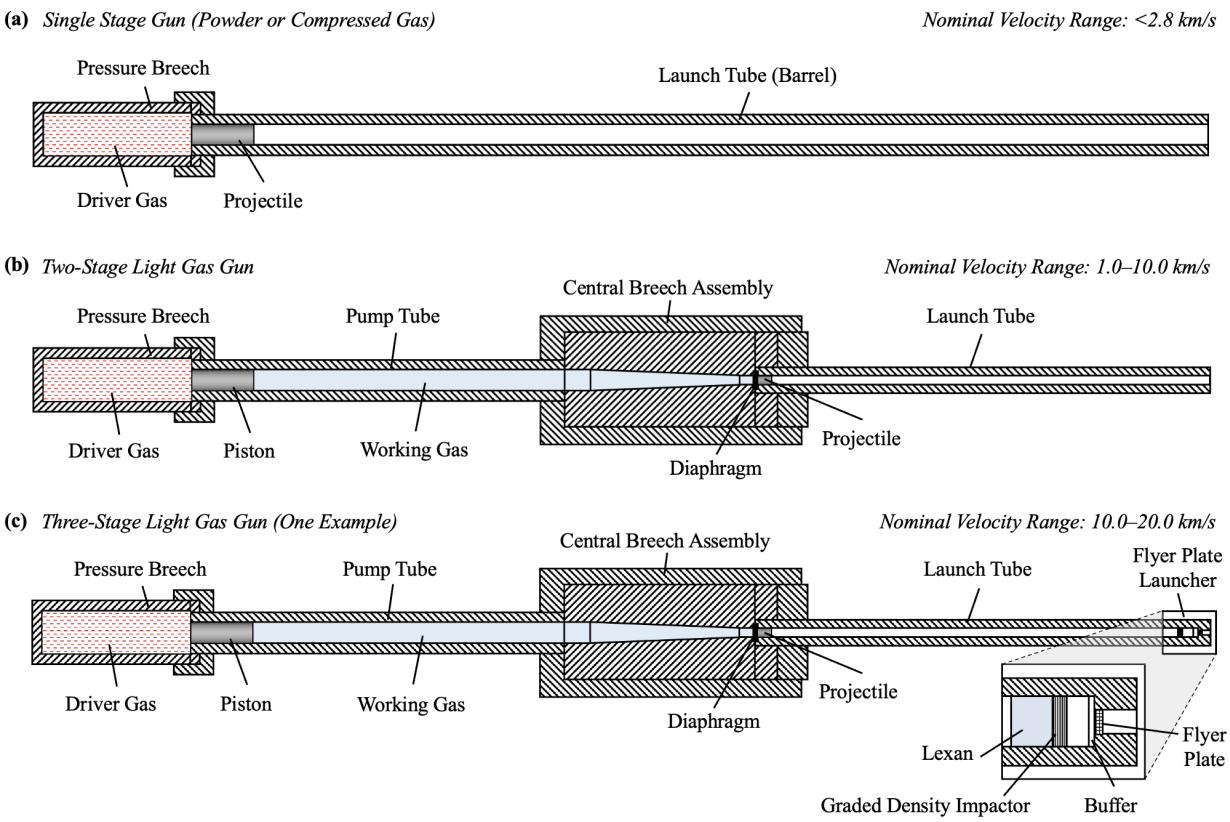

Figure 1: Conceptual schematics of a (a) single-, (b) two- [6], and (c) three-stage gun ("modified two-stage gun") with key elements/components highlighted to indicate differences [12, 13].

was primarily focused on developing and optimizing the 2SLGG, with an emphasis on maximizing muzzle velocity. The first peak in scientific productivity was largely motivated by the Space Race, during which the first NASA 2SLGG was developed [17], the Aeroballistic Range Association (ARA) was founded [18], and the largest 2SLGG to date was constructed [19]. This surge in scientific output was succeeded by a significant dip that began and lasted throughout much of the Cold War. Only near the end of the Cold War was there another strong peak in scientific productivity due to the declassification of relevant data [5]. This nearly 25 year period of maximum scientific discovery aligned with the founding of the Hypervelocity Impact Society (HVIS) [22] and the establishment of two commercial 2SLGG manufacturers, Thiot Engineerie and Physics Applications, Inc. (PAI) [23, 24]. The noticeable decline in the number of publications after approximately the year 2000 likely resulted from a shift in defense funding towards the War on Terror, a change that was largely driven by the September 11, 2001, attacks on the World Trade Center. Following the Cold War and post-Cold War periods, 2SLGG research has been primarily motivated by commercial space efforts, hypersonic technological developments, and the pursuit of ever-higher velocities. The need to develop next generation protective structural concepts and materials essential to ensure safe space travel and enable

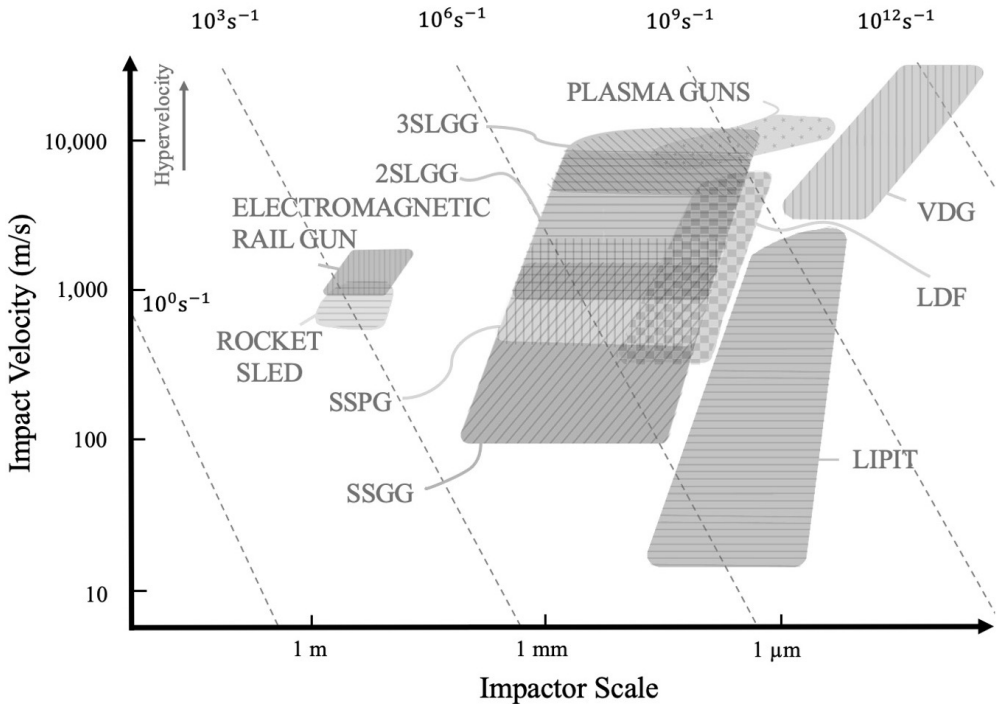

Figure 2: Impact velocity as a function of impact size for common impact testing techniques, with lines indicating constant characteristic strain rates. Techniques include single-stage gas gun (SSGG), single-stage powder gun (SSPG), two-stage light gas gun (2SLGG), three-stage light gas gun (3SLGG), Van de Graaff accelerators (VDF), laser-driven flyers (LDF), laser-induced particle impact tests (LIPIT), rocket sleds, rail guns, and plasma guns. The hatched shaded regions of the same color as the all-caps labels represent the specific velocity-scale domains in which the corresponding techniques are used. Adapted from Ref. [14].

hypersonic vehicle operations is anticipated to lead to an increase in scientific productivity over the next decade and beyond [33–42].

Ultimately, the launcher is but one part of an "aeroballistic range." Range tankage, instrumentation, data acquisition systems, and various supporting equipment make an aeroballistic range a powerful tool to study a variety of scientific phenomena. Depending on the research application, typical launch packages can range from simple geometries, such as spheres, cylinders, and cubes, to complex scale models of spacecraft with sizes ranging from 100 microns in diameter and weighing a few micrograms [43] to 175 mm in diameter weighing several kilograms [44]. Velocities of 7 km/s are routinely achieved, and specially designed launch packages have been reportedly accelerated to roughly 11 km/s [31]. Unique projectiles have carried on-board diagnostic instrumentation, multiple bodies have been packaged to launch simultaneously, and even liquids and powders have been successfully launched [6]. These special use cases would not be possible without a unique feature of the 2SLGG: the ability to optimize the loading parameters to vary the projectile acceleration profile while still producing the same muzzle velocity. Instrumentation, diagnostic equipment, and data acquisition systems are constantly evolving due to technological advancements and are typically specific to the types

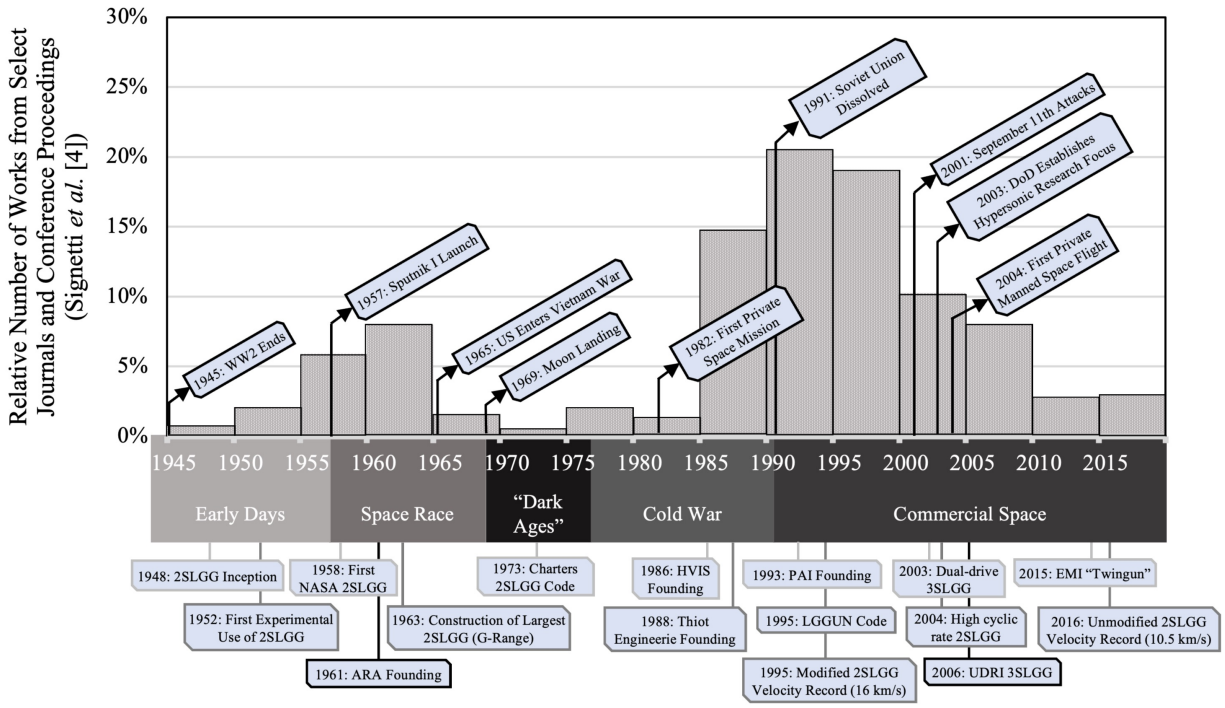

Figure 3: A temporal distribution of scientific publications on the experimental characterization, theoretical modeling, and numerical simulation of high-velocity and hypervelocity impacts, with an emphasis on key historical milestones. The figure was adapted from previous work by Signetti *et al.* [5] and Swift [6]. Key events were sourced from Refs. [6, 11, 13, 16–32].

of experiments that a given facility was designed to conduct. Some currently employed diagnostic methods include ultra-high-speed videography, schlieren and shadowgraphic imaging, photon Doppler velocimetry (PDV), flash X-ray radiography (FXR), velocity inteferometer system for any reflector (VISAR), and laser velocimetry (see Section 6) [45–49]. The sensitivity and function of the instruments along with the data they provide determine the quality and usefulness of the actual scientific findings produced by a given facility.

Establishing a 2SLGG aeroballistic range is particularly challenging from time and cost perspectives due to the intrinsic complications associated with the operational aspects of the 2SLGG itself, safety concerns (use of explosives, high-pressure gas, impact ejecta, *etc.*), and experimental turnaround time. These difficulties are exacerbated by the need for megahertz-rate triggering, timing, and diagnostic systems to capture impact events *in-situ*. 2SLGG performance largely depends on interactions between pump tube piston mass, driver gas pressure and composition, initial light working gas pressure, projectile release pressure, and projectile mass. Additionally, structural features of the launcher such as chamber volume, pump tube and launch tube length and diameter, and convergence angle of central breech play a role. Peak light gas pressures can be intense enough to shatter projectiles or even deform/rupture gun components [6]. These considerations do not include the time and cost invested in designing experiments (targets, projectiles, test matrices, *etc.*) and additional experimental capabilities or performing pre- and post-impact characterization. Of course,

these difficulties grow nonlinearly with the scale of the range and complexity of the experiment. Hence, a significant portion of 2SLGG-related research efforts have been dedicated to designing, developing, installing, calibrating, using, and improving equipment and capabilities (see, *e.g.*, [50–56]).

Due to the vast array of potential research applications of 2SLGGs, there is a considerable diversity of aeroballistic range capabilities and configurations. Furthermore, the research demands and experimental capabilities are in a state of rapid evolution, with new developments and advancements emerging continuously. Several previous studies have attempted to catalog aeroballistic ranges, diagnostics, and research associated with 2SLGGs worldwide (see, *e.g.*, [6, 57, 58]). These studies, however, were either limited to a few select aeroballistic ranges or were conducted over 50 years ago. Consequently, the present work aims to serve as an extensive review of 2SLGG aeroballistic ranges operational as of 1990 to expand the scope of known facilities and capabilities. A more complete understanding of the available launching and diagnostic capabilities facilitates and motivates scientific discovery. In addition, relevant research activities are briefly summarized to better understand the diversity in aeroballistic ranges. Sources for this survey include journal publications, conference proceedings, technical reports, textbooks, websites, and dissertations/theses, with a percentage breakdown of the sources provided in Figure 4. Relevant information from over 90 2SLGG aeroballstic ranges was compiled to provide a comprehensive overview and reference of modern aeroballistic ranges as of 2023. HVI phenomena are first briefly discussed. Physical limitations with single-stage guns are used to motivate the working principles of 2SLGGs. The method by which 2SLGGs accelerate projectiles to hypervelocities is then presented in detail with references to the current technology. The types of experiments performed at aeroballistic ranges are summarized. An overview of conventional and modern diagnostic methods is presented. Finally, key empirical, analytical, and numerical 2SLGG performance prediction methods are surveyed.

2. A Brief Overview of Hypervelocity Impact Phenomena and Research

The types of experiments that a given 2SLGG aeroballistic range is designed to conduct heavily influence its configuration and supporting diagnostic equipment. Typically, experiments can be classified into one of four categories: penetration/perforation mechanics, hypersonics/aerothermophysics, planar impacts, or nuclear/pellet injection. The differences within and among each type of experiment, and therefore the setup of the facilities used to conduct them, are mostly determined by the complex scenarios that occur during and after HVI events. Hence, fully understanding current aeroballistic range capabilities and experiment types requires some knowledge of HVI phenomena. Any previous or current impact study can be organized into one or more of the four key velocity regimes: low/high-velocity, terminal ballistic, transi-

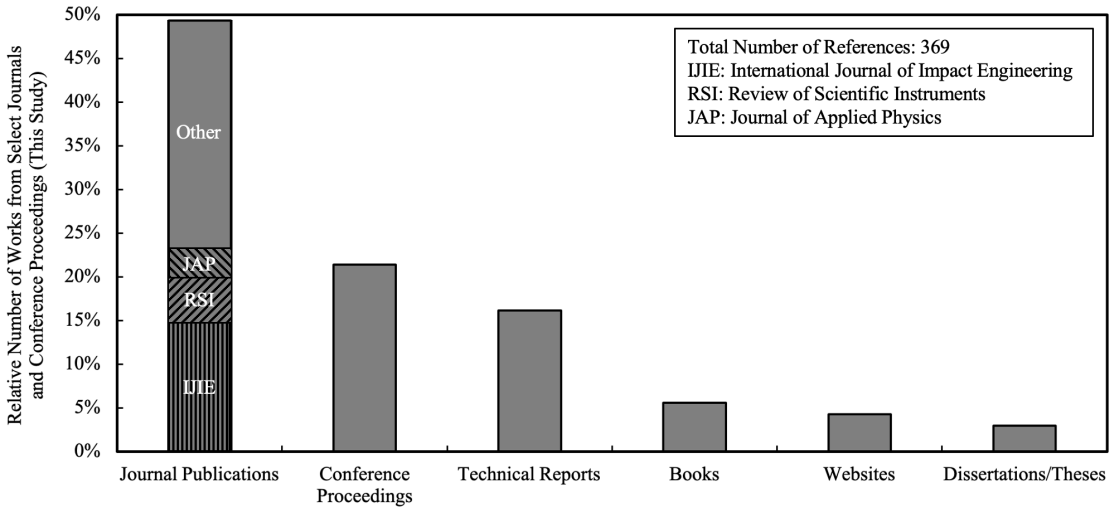

Figure 4: A percentage breakdown of the sources used in the review, encompassing a range of scholarly materials such as textbooks, technical reports, academic journals, conference proceedings, and lectures. The most common academic journals, including *International Journal of Impact Engineering* (IJIE), *Journal of Applied Physics* (JAP), and *Review of Scientific Instruments* (RSI), are shown for reference.

tion, and hypervelocity [5, 59]. The physics, mechanics, thermodynamics, and chemistry occurring in each regime can differ widely in some cases while in others phenomena overlap significantly, making analytical and numerical modeling challenging. In addition, most historic and current HVI studies have applications in one or more of six key application areas, including ultra-high strain rate material behavior, planetary science/defense, nuclear physics, spacecraft micro-meteoroid/orbital debris (MMOD) protection, hypersonic vehicle survivability and counter hypersonics, and protective structures for military defense (Fig. 5a). Efforts to understand impact/penetration events typically employ one or more of three approaches: experiments, analytical models, and numerical simulations (Fig. 5b) [7]. Previous studies have frequently defined hypervelocity as impact velocities exceeding 2.5–3.0 km/s. However, this rigid definition is an oversimplification that can lead to confusion and misunderstanding. To comprehend the importance and challenges of launching projectiles to hypervelocities with reliability, it is essential to gain a precise understanding of the transition from high-velocity to hypervelocity, as well as the associated phenomenology.

Most everyday moving objects (baseballs, automobiles, rifle bullets, *etc.*) travel at velocities in the low/high or terminal ballistic regimes. Hypervelocity objects are only encountered in more extreme environments like those where intercontinental ballistic missiles (ICBMs), rockets, explosives, hypersonic vehicles, reentry vehicles, or meteors are considered. The mechanical and thermal loading and physical response of materials in a ballistic event can be largely determined by the impact velocity. At increasingly higher velocities, the material response can include elastic-plastic deformation, rate-dependency, a variety of failure mechanisms, phase transitions, incompressible and compressible flows, shock wave propagation, thermo-

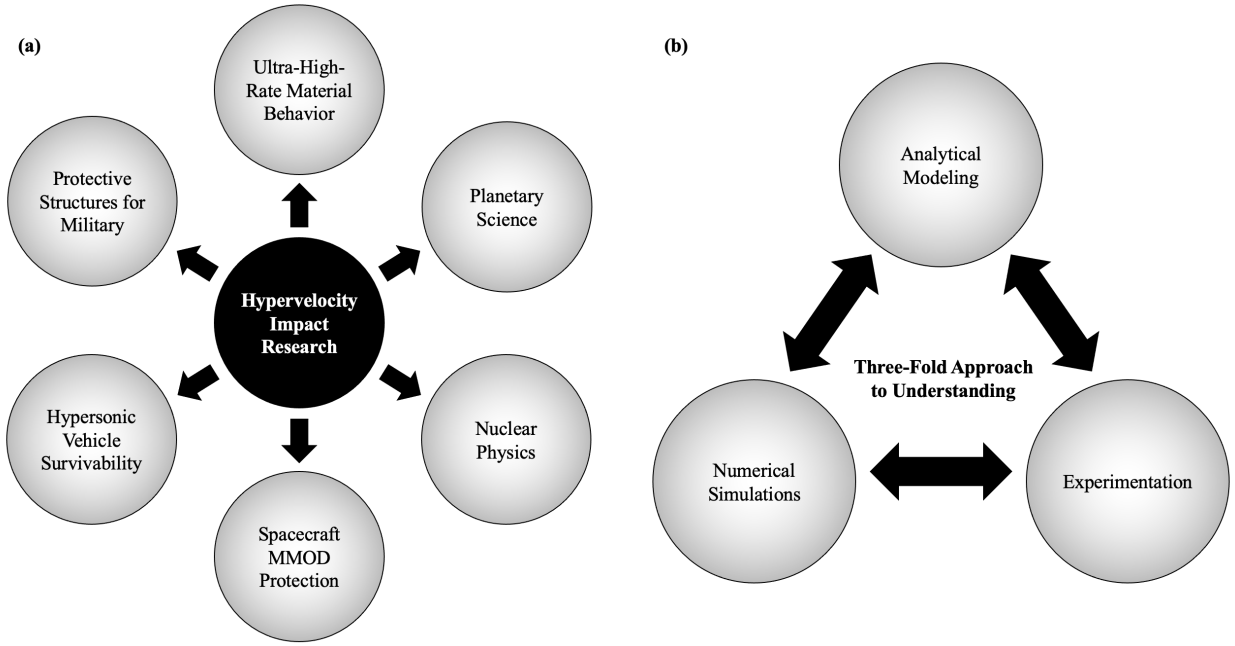

Figure 5: An overview of HVI research, including (a) the six key HVI research application areas and (b) the three-fold approach to understanding impact/penetration events presented by [7].

dynamic processes, *etc.* Impact velocity alone, therefore, is insufficient in describing velocity transitions without consideration of projectile/target material properties [5]. Generalizations of velocity regimes should be made with caution, especially when guiding theoretical, numerical, and/or experimental development and/or interpretation. Although the impact velocity regime is projectile/target material dependent, designating general broad impact regimes can be convenient from a conceptual perspective. In a similar way, the subsonic (<Mach 0.7), transonic (Mach 0.7–Mach 1.2), supersonic (Mach 1.2–Mach 5), and hypersonic (>Mach 5) regimes have been defined relative to a medium's speed of sound with physical phenomena marking transitions between regimes.

Low/high and terminal ballistic velocity impacts are characterized by, phenomenologically speaking, rigid body penetration at the low end of the velocity regime to eroding projectiles at the high end. Strain rates experienced by the projectile and target materials can range from 10^2–10^5 s^{-1} [5, 60, 61]. A key characteristic of impacts in the low/high and terminal ballistic velocity regimes is the strength-dominated material response (even with thermal softening and melting present). Hence, material flow and strain-rate dependent strength effects are prevalent even at the upper bound of the terminal ballistic regime, and dynamic material behavior is generally captured using constitutive models (*e.g.*, Johnson-Cook [62], Cowper and Symonds [63], Zerilla-Armstrong [64], Arrhenius-type [65], Preston-Tonks-Wallace [66], and Steinberg [67]) and fracture/failure models (*e.g.*, Johnson-Cook [68], Xie-Wierzbicki [69], and Grady and Olsen [70]). Depending on the loading rate, constitutive parameters are typically determined using one or more dynamic

experimental techniques, including quasi-static or dynamic tension tests (10^{-4}–10^{1} s^{-1}), Split Hopkinson Pressure Bar experiments (10^{2}–10^{4} s^{-1}) [71], Modified Taylor Tests (10^{4}–10^{6} s^{-1}) [61, 72], and/or Inverse Planar-Plate-Impact Tests (10^{6}–10^{9} s^{-1}) [61]. To accurately capture the material constitutive response, plastic heating must also be modeled, for example, by incorporating the Taylor-Quinney (TQ) coefficient [73]. The actual material loading conditions during impact, though, can differ significantly from established dynamic material characterization approaches that load materials in pure tension, compression, or shear.

The hypervelocity regime (strain rates $\geq 10^{6}$–10^{8} s^{-1}) is characterized by hydrodynamic material behavior (*i.e.*, deviatoric stresses are negligible), implying that material strength does not play a significant role in the impact behavior. For this reason, material behavior is often characterized by density and pressure-volume relationships, *i.e.*, equation-of-state (EOS) models (*e.g.*, Mie-Grüneisen [74], Tillotson [75], and SESAME [76]). The dominating phenomena are shock wave generation and propagation, which dramatically increase internal energy and lead to material melting, vaporization, sublimation, superheated vapor generation, or even plasma production [5]. Such near-instantaneous changes in density, temperature, and pressure (up to 1.0 TPa [6]) must be addressed from the perspective of thermodynamic principles (*e.g.*, Rankine-Hugoniot conditions). Impact scenarios with low target-thickness-to-projectile-diameter ratios ($t/D \leq 1$) are characterized by propagating shocks that accelerate the target material surrounding the impact region. Rarefaction waves frequently shatter both the projectile and target, generating ejecta/debris clouds [5, 77]. Global deformation is negligible in semi-infinite targets due to their inertia, and failure is governed by compression-driven cratering, melting or vaporization (due to local increases in internal energy), and possible spallation [5, 78–80]. Because the transition between the terminal ballistic and hypervelocity regime is not a discontinuity, a transition regime exists where the material response exhibits a combination of phenomena belonging to both regimes, making impacts in this regime difficult to model. The transition to hypervelocity, however, can be roughly described using a simple sonic ($v_o/\sqrt{K/\rho_0}$) [5, 81] or strength-based ($\rho_p v_0^2/\sigma_{y,p}$ and $\rho_p v_0^2/\sigma_{y,t}$) [82] criterion, where ρ_0 is the target mass density, ρ_p is the projectile mass density, v_0 is the impact velocity, and $\sigma_{y,p}$ and $\sigma_{y,t}$ are the projectile and target yield stresses, respectively. Even still, these criteria are an oversimplification as they do not include thermal effects or thermodynamic considerations. A more recent criterion defines the transition regime based on incipient and full melting of projectile/target materials [83]. Understanding the regime to which a given impact belongs is critical, as it determines which physical phenomena are present, what simulation/modeling tools can be applied, and which experiments should be performed. Despite a given impact regime's medium dependency, the HVI community generally defines the transition to occur at impact velocities between 2.5–3.0 km/s [84–90], corresponding to the muzzle velocity ceiling of single-stage, powder guns (∼2.8 km/s) [16]. For consistency, "hypervelocity" will herein correspond to projectile velocities ≥3.0 km/s, and "ultra-high strain rates" will refer to those $\geq 10^{6}$ s^{-1}.

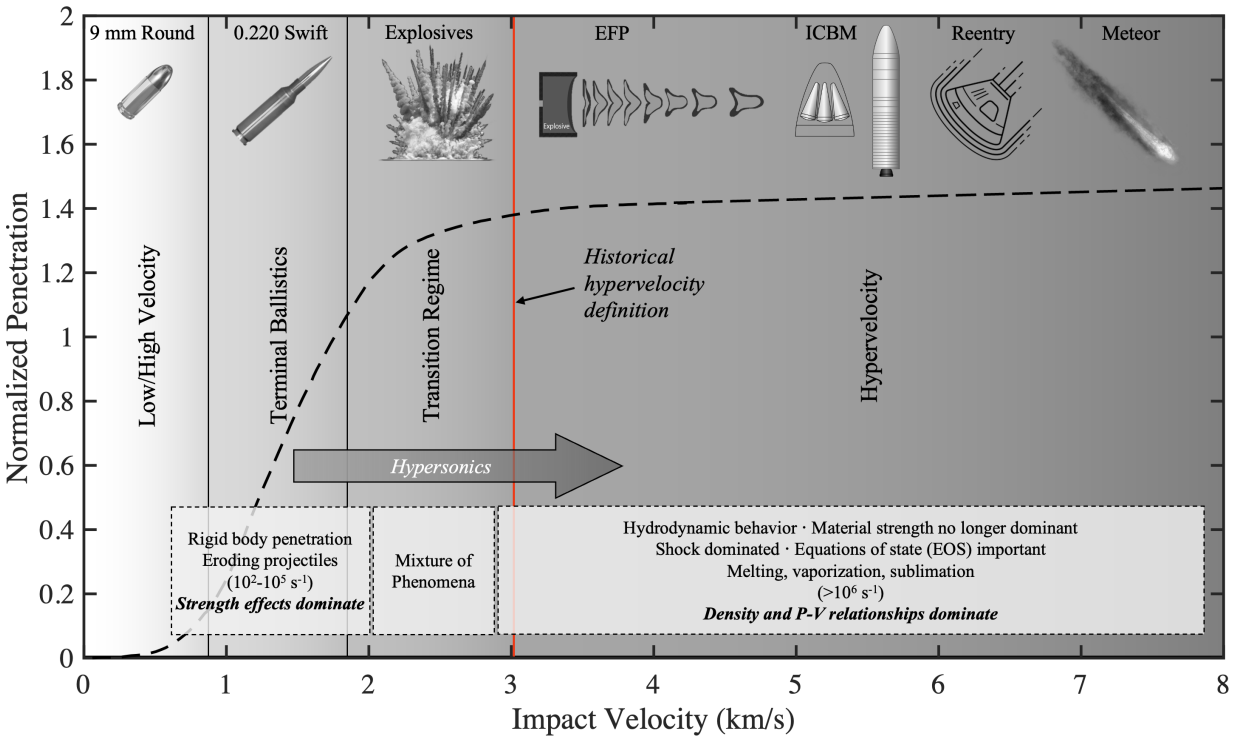

Figure 6: An illustrative plot of normalized projectile penetration as a function of impact velocity to emphasize the different physical phenomena occurring and provide examples of moving objects in each impact velocity regime [5, 83]. Here, EFP and ICBM denote explosively formed penetrator and intercontinental ballistic missile, respectively.

The transition regimes for both impact velocities and aerodynamic sonic speeds can be visualized for comparison *via* a variety of plots. For example, Fig. 6 shows a penetration efficiency curve (projectile-length-normalized depth of penetration as a function of impact velocity): the different impact regimes are clearly demarcated by changes in material impact response [83]. Specifically, the terminal ballistics regime is characterized by the linear portion of the curve while the hypervelocity regime exhibits a somewhat plateaued response. This trend is qualitative and only meant to emphasize the need to identify regimes. Also included in Fig. 6 are key phenomena exhibited by impacted materials in each regime, where hypersonic impacts land on the spectrum, and some relevant examples within each regime. This figure reinforces the challenges associated with studies in impact and penetration mechanics. Appropriately addressing HVI problems may require cross-disciplinary expertise in mechanics, computational and physical chemistry, thermodynamics, materials science, applied and computational physics, and planetary science. The complexity and diversity of modern HVI and hypersonics research play a central role in understanding the importance of and variations in 2SLGG aeroballistic ranges.

3. The Two-Stage Light Gas Gun (2SLGG)

While there are variations in the configurations of *aeroballistic ranges*, the operational concepts and fundamental physical components of all currently utilized 2SLGGs are similar. The present section aims to explain the working principles of 2SLGGs by initially providing a concise overview of the physical limitations of conventional single-stage guns. Subsequently, a detailed outline of the components that characterize a conventional 2SLGG is provided. The arguments regarding the predominant configurations of 2SLGGs are substantiated by data gathered from existing literature.

3.1. The 2SLGG Working Principles

In general, single-stage guns convert the potential energy stored in compressed gas into projectile kinetic energy. This potential energy is typically produced by utilizing high-pressure gas generated through a controlled combustion process or, alternatively, mechanical compression. Once the gas is released, it rapidly expands within the gun barrel, accelerating the projectile. The efficiency of this energy conversion process depends on various factors, including the gas composition and the design of the gun barrel. In essence, the local expansion and acceleration of driver gas particles increase the gas velocity at the expense of a decrease in pressure [91]. Depending on the gas composition and the projectile velocity, the expansion and acceleration of the gas can occur much more quickly than the projectile moves down the barrel, such that any difference in net force on the projectile does not strongly influence projectile acceleration and is, therefore, negligible. As the projectile velocity increases, however, these gas particles cannot "react" quickly enough to the changes in volume, and the projectile begins to outpace the expanding gas regions. The inefficiencies associated with this phenomenon will necessarily limit the maximum projectile velocity. Launchers that are unable to efficiently transmit pressure increases from the high-pressure reservoir to the projectile's base are referred to as "communication-limited" [6]. The progression of successive, incremental movements describes an acoustic rarefaction pressure wave, and the maximum velocity they can "react" is the definition of the speed of sound in the gas [91].

The rise of supersonics as a field of study and the corresponding derivation of compressible flow mathematical models motivated efforts to theorize and, later, prove that the constraining factor for conventional single-stage powder guns was the molecular weight of the gaseous products of combustion [91]. This groundbreaking finding was motivated by the fact that the gas used to accelerate the projectile must also accelerate. Thus, as the molecular weight of the gas increases, the energy available to accelerate the projectile decreases. This phenomenon is subtle but incredibly important to understanding the 2SLGG working principles and can be simply demonstrated by analyzing the maximum theoretical velocity of a generalized gun. The maximum attainable muzzle velocity for both single- and multi-stage guns has been theorized at great length

[25, 51, 92–95]. Corner [10] presented various analyses developed by several researchers. A simple but powerful derivation attributed to Langweiler [96] gives the maximum achievable velocity (U_P) as

$$U_P \approx \sqrt{\frac{2\frac{RT}{M}}{\gamma - 1}}, \tag{1}$$

where R is the universal gas constant, M is the gas molecular weight, T is the gas temperature, and $\gamma = c_p/c_v$ is the ratio of specific heats. Despite the associated simplifying assumptions, Eq. (1) closely correlates with observed peak velocities for single-stage gas guns, single-stage powder guns, and 2SLGGs much better than some of the more rigorous treatments [10]. It is apparent from Eq. (1) that careful selection of the gas is critical to achieving the highest possible muzzle velocity. Considering $\gamma \approx 1.00$–1.80 for most gases and that nearly all ideal gases have $\gamma = 1.40$ or $\gamma = 1.67$, the importance of low molecular weight is clearly paramount. However, simply using low molecular weight gas is not enough—high temperatures and pressures are required to achieve hypervelocities. These ideas are emphasized in Fig. 7a, where the maximum achievable projectile velocity, U_P, is plotted as a function of gas molecular weight at various temperatures ($\gamma = 1.4$ assumed for all gases for comparison purposes). The red vertical lines in the plot indicate key gases used in conventional launchers: hydrogen, helium, powder gases (H_2O, CO_2, and N_2), and air. This figure clearly shows that low molecular weight and high temperatures are required to achieve hypervelocities (*i.e.*, maximum velocity is proportional to the speed of sound and temperature and inversely proportional to gas molecular weight).

Merely achieving high gas pressures and temperatures in the reservoir of a gun is not sufficient to reach the theoretical maximum muzzle velocity. To approach this limit, it is necessary to maintain these gas pressures at the base of the projectile for a certain time period or distance. Hence, the muzzle velocity is proportional to the barrel length, provided positive pressure is maintained at the projectile's base and frictional effects are negligible [97]. One way to maintain muzzle velocity while decreasing peak reservoir pressure (and peak projectile acceleration) is to extend the launch tube length. In essence, the projectile base pressure is converted into kinetic energy. Specifically, the velocity and translational kinetic energy of a projectile within a barrel are proportional to the integrals of the pressure-time and pressure-distance histories, respectively:

$$v = \frac{A}{m}\int p\,dt, \qquad KE = \frac{1}{2}mv^2 = \frac{A}{m}\int p\,dx, \tag{2}$$

where A is the projectile base area, m is the projectile mass, p is the base pressure, t is time since launch, and x is downrange position since launch (Fig. 7b) [97]. Clearly, projectile velocity and kinetic energy are dependent on the magnitude and duration of the base pressure. In 2SLGGs, high working/driver gas temperatures and pressures need to be reached and maintained while the projectile is in the launch tube.

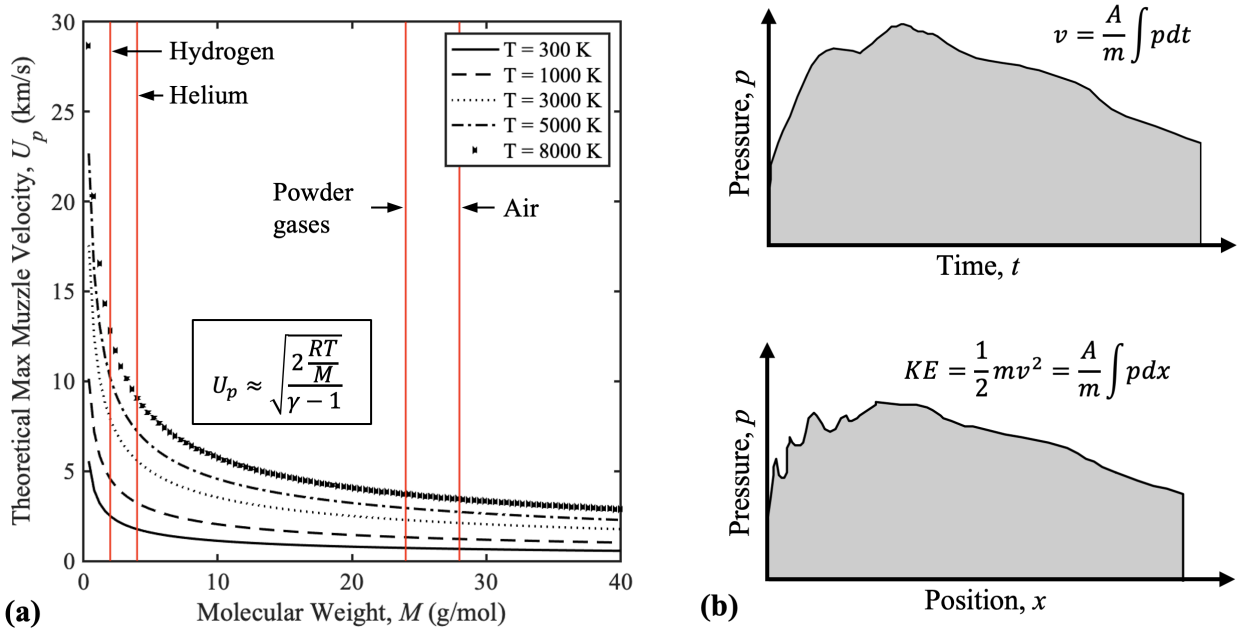

Figure 7: The working principles of pressure-driven launchers (guns), with (a) a graph of theoretical maximum muzzle velocity (U_P) as a function of gas molecular weight for relevant gases at a series of temperatures ($\gamma = 1.4$ for qualitative comparison) and (b) plots of pressure (p) versus time (t) and pressure versus downrange position (x) adapted from Ref. [95]. The maximum muzzle velocity is proportional to temperature and pressure and inversely proportional to molecular weight. Here, v is projectile velocity, A is projectile base area, m is projectile mass, and KE is projectile kinetic energy.

These requirements could not be satisfied by a single-stage gun due to limitations on gas conditions in the reservoir (compressed-gas guns) or gas speed of sound (powder guns).

In essence, a 2SLGG utilizes the energy generated by a single-stage launch system to compress a light working gas (WG), which, then, propels a projectile. Initially, helium was used as the 2SLGG WG to increase the velocity ceiling from 2.8 km/s to roughly 4.5 km/s [6]. Serious problems were soon encountered as performance increased: interior gun surfaces exposed to peak gas pressures would melt and/or boil. Evidence existed of metal droplets impacting range components, and experts speculated that vaporized steel (iron gas) mixed with the helium, significantly increasing the WG molecular weight. These problems were linked to helium's relatively high ratio of specific heats (γ) and heat convection properties [6]. The relatively small He atoms and their chemical inertness make them highly effective for convective heat transfer, which exacerbates 2SLGG barrel heating during launch. As a result, a shift towards hydrogen as the WG started in the early 1960s.

Despite decades of research and optimization, the essential components of 2SLGGs have remained largely unchanged since 1948 and consist of seven structural and consumable elements, including a pressure breech, pump tube, central breech, launch tube, piston, petal valve, and projectile package (*cf.* Fig. 1). These components perform the same basic functions during all operational cycles, with the pressure breech, pump

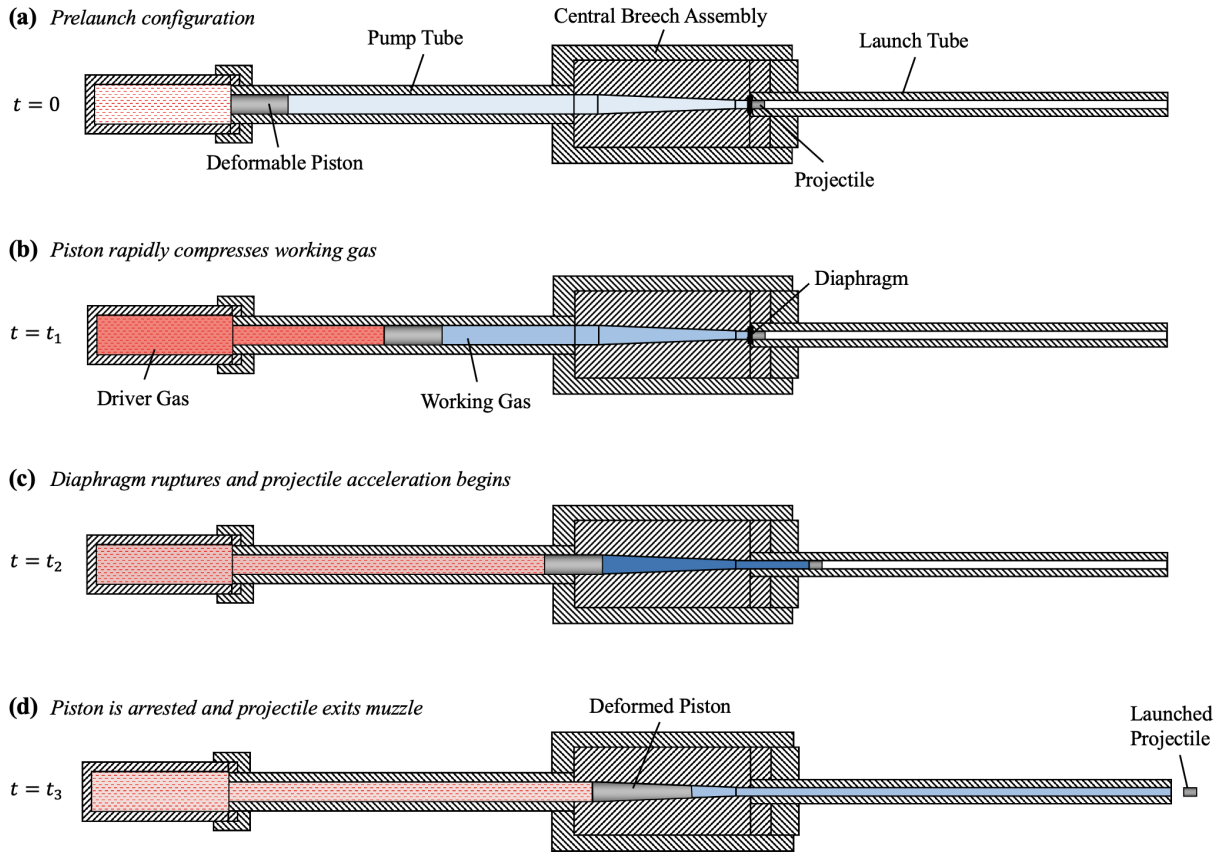

Figure 8: A schematic overview of 2SLGG working principle: (a) just before launch, (b) during WG compression, (c) when diaphragm ruptures and projectile acceleration begins, and (d) just after the projectile leaves the muzzle.

tube, central breech, and launch tube being coaxially arranged and rigidly coupled with gas-tight seals between each component. For illustration, Fig. 8 displays a representative 2SLGG during four key instances during a launch sequence. At the start of the internal-ballistic cycle, the piston is located at the uprange end of the pump tube, while the projectile is located at the uprange end of the launch tube, just downrange of the petal valve diaphragm (Fig. 8a). A specific amount of low-molecular-weight WG, typically hydrogen or helium, is loaded into the pump tube. When the high-pressure gas generated within the pressure breech is released, it accelerates the piston downrange within the pump tube, rapidly increasing the WG pressure and temperature (Fig. 8b). Upon reaching a critical pressure, the petal valve diaphragm ruptures, exposing the projectile's base to the WG, which then accelerates the projectile down the launch tube (Fig. 8c). Ultimately, the projectile exits the muzzle of the 2SLGG at some high-velocity or hypervelocity (Fig. 8d) and enters the range tankage (more later). These critical cycle steps are universal among most unmodified 2SLGGs documented in the literature and provide a reliable and consistent means of achieving hypervelocity projectiles [15, 26, 32, 43, 98–143].

One powerful feature of the 2SLGG is that the piston velocity can be tailored to control the WG pressure

curve and, consequently, projectile acceleration. In fact, there are several potential loading parameters, such as pressure breech conditions, piston mass, and initial WG pressure, that can be varied to achieve the same muzzle velocity. Figure 9, which displays a representative WG pressure envelope for a 2SLGG [95, 97], helps illustrate the regions where these loading conditions can be changed. The petal valve diaphragm ruptures at a known pressure as the piston traverses the pump tube, with higher piston velocities corresponding to higher peak WG pressure in the central breech. However, increasing the peak WG pressure has diminishing returns, as acceleration-induced stresses can surpass the dynamic yield stress or toughness of the projectile material, leading to projectile failure during launch. The loading parameters are, thus, typically chosen to prevent over-accelerating the projectile. Additionally, the WG *temperature* must also be controlled to achieve desired velocities. The currently available methods for dynamically generating both the high temperatures and pressures in a 2SLGG WG are (*i*) shock compression and (*ii*) isentropic compression [6]. Shock compression of the gas appears the more advantageous of the two because it can yield very high pressures and temperatures on the downrange side of the shock wave. These extreme pressures, while desirable, present significant challenges to designing practical containment structures (*i.e.*, the barrel). Furthermore, these shocks will travel back and forth throughout the gas column, reflecting off the projectile base. These sharp pressure and temperature rises are only applied in very short bursts and cause substantial positive and negative accelerations to the projectile. Isentropic compression is therefore the more favorable choice and is often used in modern 2SLGGs [2].

Although 2SLGGs share common operational conditions and key components, there are significant variations in how these conditions are achieved, the geometry of key components, and the resulting performance capabilities. Despite these known differences, there has been little recent systematic documentation of 2SLGGs worldwide, making it challenging to compare the performance of different 2SLGG designs and identify areas for improvement. To address this gap, an extensive dataset summarizing the features of more than 90 2SLGGs worldwide, all of which are operational at least as of 1990, was compiled. The dataset, which is presented in Table 1, includes information on each 2SLGG's parent facility, country of origin, maximum reported projectile velocity, launch tube bore diameter, and "drive type" (more in Section 3.2.1). The 2SLGGs in Table 1 have been numbered by facility for consistency and ease of comparison, even though some may have specific names designated by the parent organization. Additionally, Table 6 in Appendix A provides more detailed information on the associated aeroballistic ranges, including some diagnostics, experimental capabilities, and configurations. These tables provide a valuable resource for researchers, engineers, operators, students, project managers, and other stakeholders interested in assessing the diversity of 2SLGGs and identifying trends, challenges, and opportunities for innovation. The following section highlights the configurational and operational differences observed among the surveyed 2SLGGs.

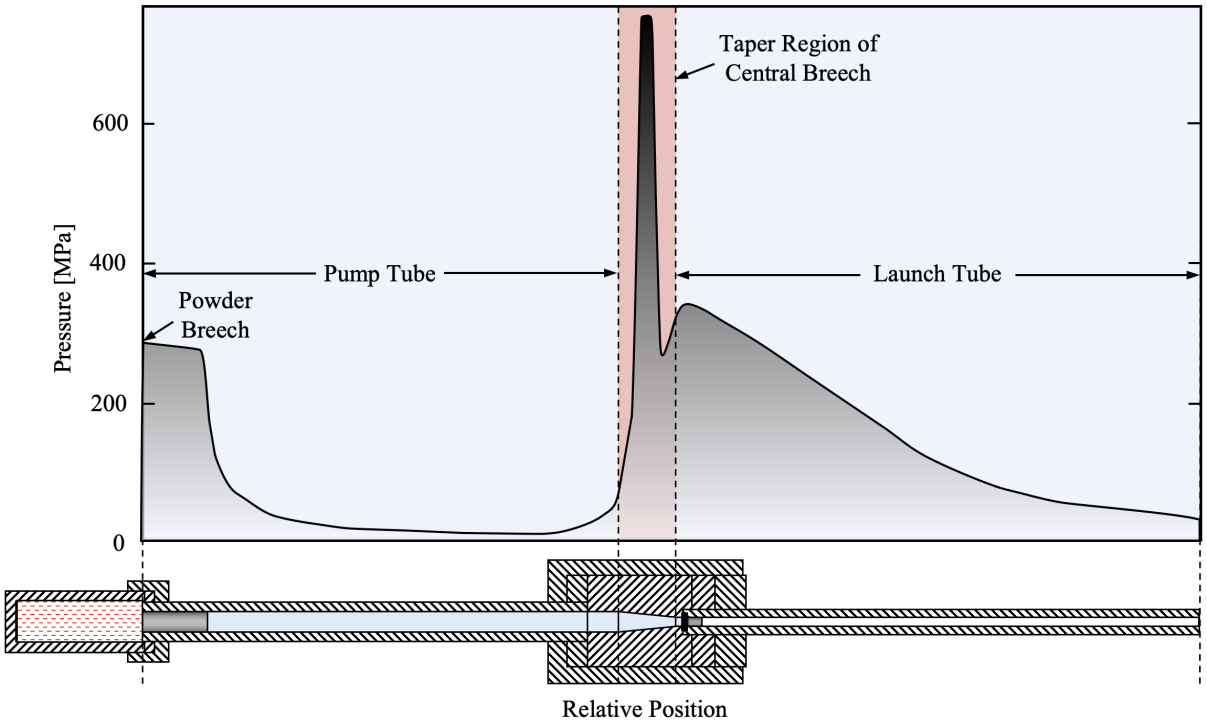

Figure 9: A representative internal pressure envelope for a 2SLGG, with pressure data sourced from Ref. [95, 97]. The plot provides insights into the 2SLGG working principles.

Table 1: An overview of the operational 2SLGG aeroballistic ranges as of 1990, detailing key information such as country of origin, maximum reported launch velocity, launch tube diameter(s), and first stage drive type. 2SLGGs can be driven by powder (P), compressed gas (C), or gaseous detonation (GD). Additional information regarding these 2SLGGs is provided in Appendix A. "*" denotes estimated values from indirect evidence in published works.

No.	Facility	Country	Max. Velocity (km/s)	Launch Tube Dia (mm)	Drive Type
1	Mississippi State University - I [32]	US	6.00	1.00	P
2	Drexel University [43, 136]	US	4.00	1.58	C
3	Caltech [100]	US	10.00	1.80	P
4	Commissariat a l'Energie Atomique - I [144, 145]	France	5.00	2.00*	P
5	National Defense Academy [101]	Japan	5.90	2.10	P
6	Commissariat a l'Energie Atomique - II [146]	France	3.40	3.00, 4.00	C
7	NASA MSFC - I [126]	US	7.50	4.00	P
8	University of Kent [137]	UK	7.70	4.30	P
9	Rice University [138, 139]	US	7.10	4.30	P
10	NASA WSTF - I [105]	US	8.50	4.32	P
11	Oak Ridge National Lab [147, 148]	US	5.00	1.90, 2.60, 3.20, 4.40	C
12	The Open University [149]	UK	7.00	4.70	P
13	NASA JSC [107]	US	8.00	5.00	P

Table 1: An overview of the operational 2SLGG aeroballistic ranges as of 1990, detailing key information such as country of origin, maximum reported launch velocity, launch tube diameter(s), and first stage drive type. 2SLGGs can be driven by powder (P), compressed gas (C), or gaseous detonation (GD). Additional information regarding these 2SLGGs is provided in Appendix A. "*" denotes estimated values from indirect evidence in published works.

No.	Facility	Country	Max. Velocity (km/s)	Launch Tube Dia (mm)	Drive Type
14	PERC, Chita [150, 151]	Japan	7.00	5.00*	P*
15	NASA MSFC - II [126]	US	7.50	5.59	P
16	Mississippi State University - II [99]	US	7.00	5.60	P
17	University of Nevada, Las Vegas [108]	US	6.80	5.60	P
18	Fraunhofer EMI - I [102]	Germany	7.00	4.00, 6.00	P
19	University of Padua [26]	Italy	5.50	4.72, 6.00	C
20	Japan Aerospace Exploration Agency [109]	Japan	7.00	7.00	P
21	Johns Hopkins University [134]	US	7.00	7.60	C
22	Cranfield University [152]	UK	...	7.60	...
23	Hypervelocity Aerodynamics Institute - I [133]	China	7.00	7.60	P
24	Denver Research Institute [153, 154]	US	7.00	7.62	...
25	Brookhaven National Lab [155]	US	1.5	7.62	C
26	KAIST [156, 157]	South Korea	3.2	7.62*	C
27	National Research Tomsk University - I [132]	Russia	5.00	8.00	C
28	Corvid [158]	US	7.00	8.00	...
29	Fraunhofer EMI - II [103]	Germany	9.00	8.50	P
30	University of New Brunswick - I [159, 160]	Canada	8.00	10.0	C
31	Imperial College London [152]	UK	4.00	10.0	C
32	Kyushu Institute of Technology [161, 162]	Japan	8.00	10.0*	P
33	TiTech [111]	Japan	8.90	11.8	P
34	Thiot Ingenierie [140, 141]	France	9.85	12.0	C
35	Texas A&M University [112, 113, 163]	US	7.00	12.7	P
36	NASA WSTF - II [105]	US	7.00	12.7	P
37	First Light Fusion - I [114]	UK	7.50	12.7	P
38	Argonne National Lab [164]	US	6.00	12.7	...
39	NASA AVGR [110, 165]	US	7.00	7.62, 12.7	P
40	Naval Surface Warfare Center - I [166]	US	6.00	7.0, 7.6, 12.7	P
41	Royal Military College of Science [115]	UK	7.00	15.0	P
42	Tohoku University - I [142]	Japan	1.00	15.0	C
43	Hypervelocity Aerodynamics Institute - II [15]	China	8.60	16.0	P
44	China Academy of Space Technology - I [167]	China	7.00	18.0	...
45	Arnold Engineering Development Complex - I [116]	US	8.00	19.0	P
46	Tohoku University - II [118]	Japan	7.50	20.0	P
47	UDRI - I [119]	US	7.50	20.0	P

Table 1: An overview of the operational 2SLGG aeroballistic ranges as of 1990, detailing key information such as country of origin, maximum reported launch velocity, launch tube diameter(s), and first stage drive type. 2SLGGs can be driven by powder (P), compressed gas (C), or gaseous detonation (GD). Additional information regarding these 2SLGGs is provided in Appendix A. "*" denotes estimated values from indirect evidence in published works.

No.	Facility	Country	Max. Velocity (km/s)	Launch Tube Dia (mm)	Drive Type
48	University of British Columbia [168]	Canada	4.00	20.0	P
49	University of New South Wales [169, 170]	Australia	4.50	22.0	C
50	Commissariat a l'Energie Atomique - III [171, 172]	France	7.90	22.0	P
51	National Research Tomsk University - II [143]	Russia	8.00	23.0	P
52	University of California, Davis [120]	US	8.00	25.0	P
53	China Academy of Space Technology - II [173, 174]	China	7.50	25.0	C
54	Hypervelocity Aerodynamics Institute - III [15]	China	···	25.0	P
55	Seoul National University [175]	South Korea	7.50	25.0	···
56	University of New Brunswick - II [159, 160]	Canada	···	25.0	P
57	National Institute for Material Science [176, 177]	Japan	7.00	18.0, 25.0	P
58	NASA WSTF - III [106]	US	7.00	25.4	P
59	Engineering Research Development Center [121]	US	7.50	25.4	P
60	Wuhan University [178]	China	5	25.4	C
61	Lawrence Livermore National Laboratory - I [179]	US	8.00	28.0	P
62	Sandia National Labs [123, 124]	US	8.00	28.0	P
63	Chinese Academy of Sciences [55]	China	···	30.0	GD
64	Los Alamos National Lab - II [180, 181]	US	8.00	28.00	···
65	UDRI - II [119, 182]	US	6.50	30.0	P
66	Northwest Institute of Nuclear Technology - I [183]	China	3.00	30.0	C
67	Swedish Defence Research Agency [184]	Sweden	···	30.0	P
68	Eglin Air Force Base [185, 186]	US	···	30.0	P
69	Southwest Jiaotong University [187]	China	8.00	30.0	···
70	University of Alabama in Huntsville - I [126]	US	8.00	19.0, 30.0	P
71	Institute of Saint-Louis [188]	France	7.00	10.0, 20.0, 30.0	···
72	Lawrence Livermore National Laboratory - II [128]	US	7.00	12.0, 20.0, 35.0	P
73	University of Alabama in Huntsville - II [126]	US	6.50	30.0, 36.0	P
74	Southwest Research Institute [127]	US	7.00	38.0	P
75	First Light Fusion - II [189]	UK	6.50	38.0	P
76	New Mexico Tech - EMRTC [130]	US	6.70	38.0	P
77	NASA Ames HFFAF [190]	US	9.00	12.7, 25.4, 38.1	P
78	Naval Surface Warfare Center - II [166]	US	7.00	19.0, 43.0	P
79	Los Alamos National Lab - I [129]	US	3.60	50.0	P,C
80	Hypervelocity Aerodynamics Institute - IV [15, 131]	China	6.75	37.0, 50.0	P
81	Arnold Engineering Development Complex - II [116, 117]	US	6.75	64.0	P

Table 1: An overview of the operational 2SLGG aeroballistic ranges as of 1990, detailing key information such as country of origin, maximum reported launch velocity, launch tube diameter(s), and first stage drive type. 2SLGGs can be driven by powder (P), compressed gas (C), or gaseous detonation (GD). Additional information regarding these 2SLGGs is provided in Appendix A. "*" denotes estimated values from indirect evidence in published works.

No.	Facility	Country	Max. Velocity (km/s)	Launch Tube Dia (mm)	Drive Type
82	Lawrence Livermore National Laboratory - III [128]	US	8.00	20.0, 28.0, 64.0	P
83	Fraunhofer EMI - III [104]	Germany	7.80	25.0, 50.0, 70.0	P
84	TAMU Ballistics Aero-optics and Materials [191, 192]	US	···	102	P
85	University of Alabama in Huntsville - III [126]	US	6.00	56.0, 152	P
86	Arnold Engineering Development Complex - III [116, 117]	US	6.90	83.8, 102, 203	P
87	Agency for Defence Development [193]	South Korea	···	···	C
88	Harbin Institute of Technology [194]	China	3.00	···	···
89	Northwest Institute of Nuclear Technology - II [195]	China	7.20	···	···
90	Beihang University [196]	China	6.50	···	···
91	Shenyang Ligong University [197]	China	7.00	···	···

3.2. A Configurational and Operational Comparison of 2SLGGs

All 2SLGGs operate by compressing a light WG (He, H_2, *etc.*) using a drive mechanism similar to that used in a single-stage launcher to directly accelerate a projectile. However, the compressed WG achieves higher pressures and temperatures than those attainable by single-stage launchers, thereby facilitating more efficient energy transfer to the projectile. Five key components are generally shared across all 2SLGGs: (1) a pressure breech, (2) a pump tube, (3) a central breech, (4) a petal valve (burst) diaphragm, and (5) a launch tube (barrel). 2SLGG pressure breech drive type, pump tube diameter and length, central breech transition geometry, launch tube diameter and length, and pump-tube-to-launch-tube diameter ratio can all be readily varied to meet specific performance and launch demands. The customizability of these design features has resulted in vast differences among 2SLGGs in operation today as partially outlined in Table 1.

3.2.1. Pressure Breeches and Drive Types

The uprange-most component of a given 2SLGG is the pressure breech (*cf.* Figs. 1 and 8). The configuration and working principle of the pressure breech determines a given 2SLGG's "drive type." 2SLGGs can be powder-driven [98, 102, 110, 116, 121, 127, 198], gas-driven [26, 118, 129, 134, 136], or gaseous-detonation-driven [55]. Powder-driven 2SLGGs are simple and widely used, while gas-driven systems offer more precise control and potentially cleaner operation. Much less prevalent is the gaseous detonation method, which uses a controlled detonation of a gaseous mixture. Despite these variations in drive type, the purpose of the pressure breech is consistent: to accelerate the compression piston downrange.

Powder-driven guns use the expanding gases from a chemical propellant (*e.g.*, nitrocellulose or gunpowder) housed in a sealed powder chamber to begin the operational cycle (*i.e.*, "powder-driven"). The pressure breech is sealed on the uprange end by a breech block and on the downrange end by a (most often) deformable compression piston, typically machined from a polymeric material. Commonly, the main powder charge is ignited by a smaller, faster burning charge in conjunction with a booster (Fig. 10). The entire 2SLGG cycle is initiated by a remote control firing system. The rapidly expanding gases can reach breech pressures on the order of hundreds of megapascals, accelerating the piston downrange and rapidly compressing the WG. This method is employed in guns of all sizes, ranging from some of the smallest [32] to mid-range [105] to the largest [44] operational 2SLGGs.

Alternatively, "cold" compressed gas-driven 2SLGGs employ large reservoirs of high-pressure gas (*e.g.*, air, nitrogen, helium) and fast-acting valves to induce compression piston motion (Fig. 10b). Typically, the advantages associated with this method are greater repeatability in 2SLGG muzzle velocity and less involvement of hazardous materials. On the other hand, gas-driven guns generally possess a lower velocity ceiling for a given projectile size/mass. Moreover, they are typically not viable for relatively larger projectiles because the volume of the compressed gas reservoirs required for launch within the hypervelocity regime becomes cost and/or space prohibitive. Nonetheless, many facilities with small [26, 136] and medium sized [118, 134] 2SLGGs still prefer this method to accelerate the piston.

Lastly, gaseous detonation may be used to accelerate the piston, where an ignition device is used to initiate the process. Once the gas pressure reaches some critical pressure, a diaphragm ruptures and piston acceleration begins (Fig. 10c). This approach, however, is much less prevalent than the powder and cold-gas methods. Roughly 76% of surveyed 2SLGGs operational worldwide are powder-driven, while only 23% and 1% are cold gas-driven and gaseous-detonation-driven, respectively (Fig. 10d). The majority of currently operational guns designed and built prior to 1990 are powder-driven, largely due to the intrinsic performance advantages. Regardless of the drive type, the pressure breech is ultimately used to generate high-pressure gas to accelerate the (usually) consumable piston down the pump tube and rapidly compress the WG.

3.2.2. Pump Tubes

The sole purpose of the pressure breech is to launch the deformable compression piston down the pump tube at velocities near 1 km/s. Common to all 2SLGGs, pump tubes are thick-walled, hollow, metal cylinders ($L/D \approx 50$–100) through which the piston travels and compresses the WG. The pump tube is thus both simultaneously a barrel *and* a dynamically evolving reservoir (piston cylinder). In fact, the pressure breech combined with the pump tube is analogous to a single-stage powder or gas gun (*cf.* Fig. 1) with the key difference, of course, being that the "projectile" in this case is the piston. Pump tubes are usually several

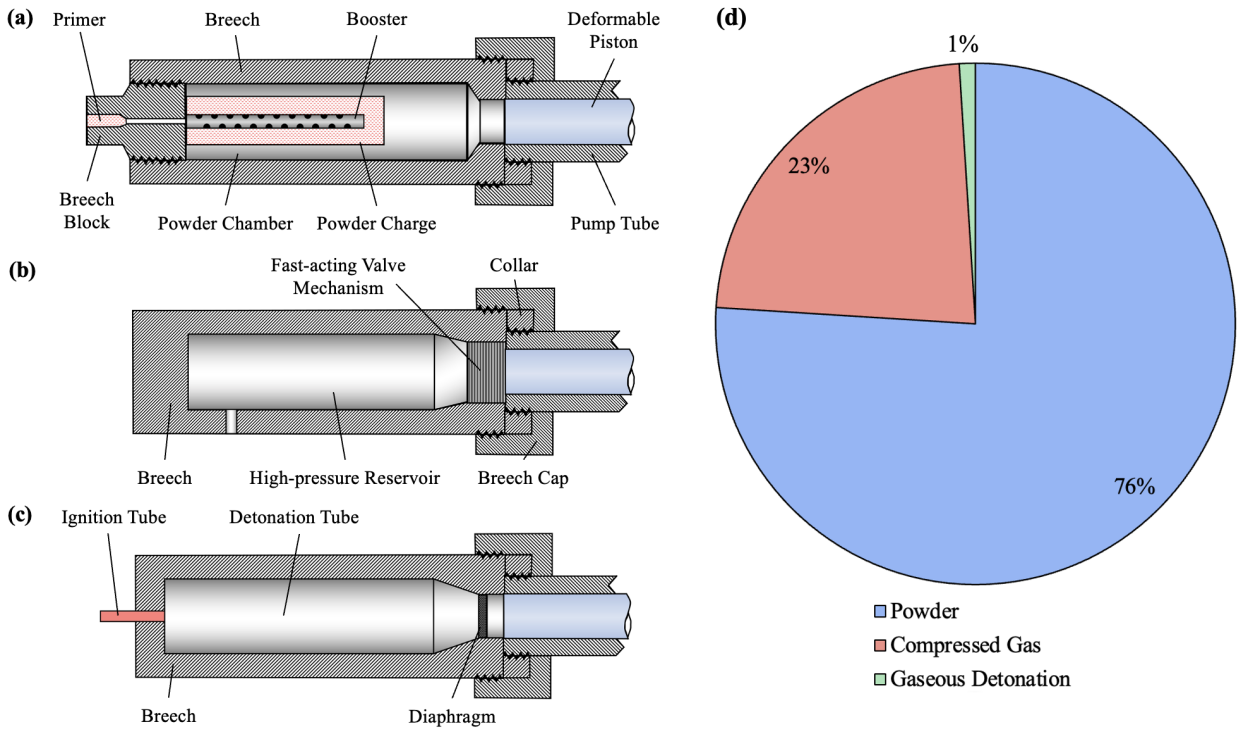

Figure 10: The three common driver systems for 2SLGGs, with simple schematics of the (a) powder-driven, (b) compressed-gas-driven, and (c) gaseous-detonation-driven components and (d) a breakdown of the percentage of 2SLGGs that employ each system.

times larger in diameter than the 2SLGG launch tube to ensure projectile base pressures are maintained during acceleration.

3.2.3. Central Breech Assemblies

The pump tube facilitates WG compression into the central beech assembly (also termed "high-pressure section," "high pressure coupling," or "accelerated reservoir" [6, 97, 124, 199]), which couples the downrange end of the pump tube to the uprange end of the launch tube. The breech core serves as a transition between the pump tube and launch tube inner diameters and is typically a hollow cylinder of conical cross-section with included neck-down transition angle, β. A rupture diaphragm (*i.e.*, burst disc, petal valve) with accompanying cassette assembly is fixed between the downrange end of the central breech and uprange end of the launch tube. During a given cycle, the WG pressure and temperature reach maximum values within the central breech (*e.g.*, up to 1 GPa and >1000 K, respectively). For this reason, most central breech assemblies include coupling devices and high-pressure seals that are specially designed to prevent central breech decoupling and gas leakage during WG compression [6].

The dual collar-breech-cap mechanism serves as one simple way to compress the central breech core between the pump and launch tubes (Fig. 11a). Breech caps and annular metallic collars are fixed to

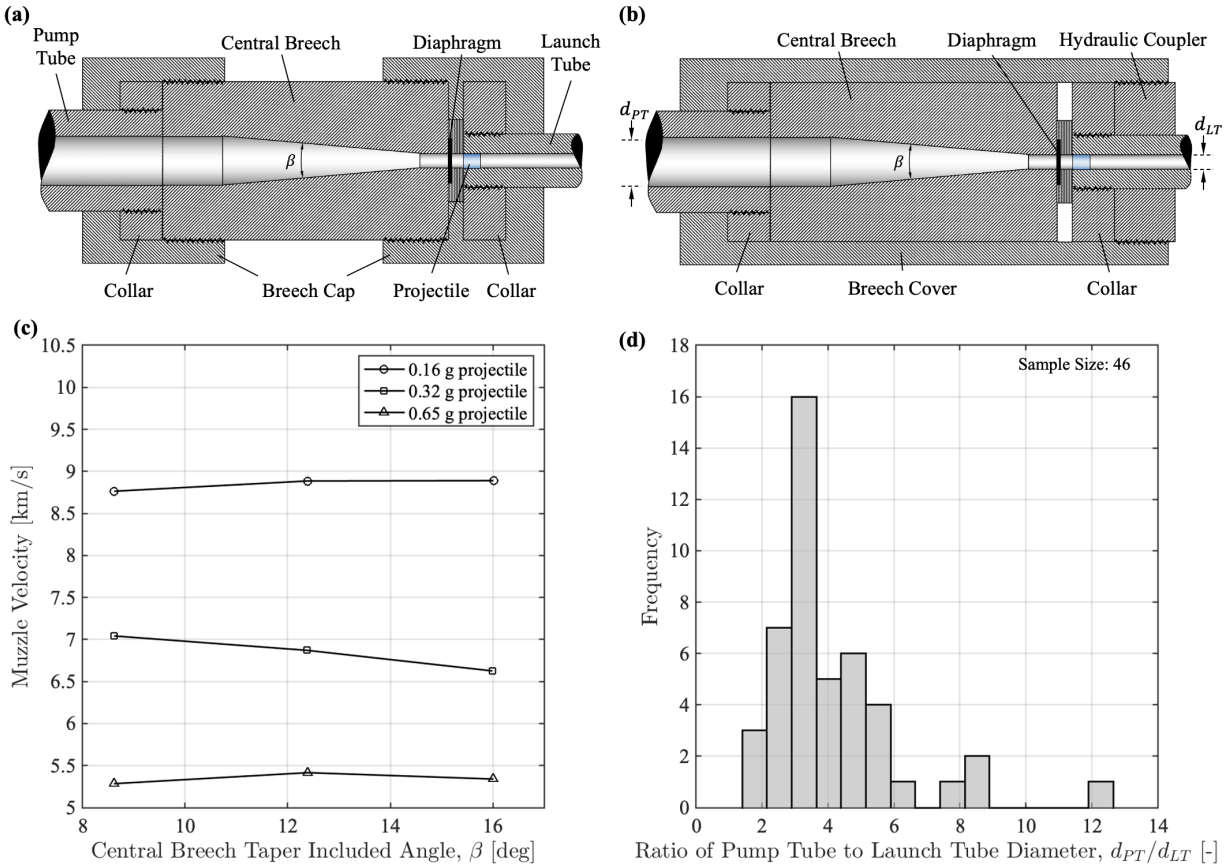

Figure 11: An overview of the central breech assembly used in 2SLGGs, featuring (a,b) schematics of two common central breech assembly configurations, (c) a demonstrative plot of experimental muzzle velocity *versus* central breech taper angle (β), and (d) a histogram of the pump-tube-to-launch-tube-diameter ratios (d_{PT}/d_{LT}). The histogram reveals that the most prevalent ratio is approximately three. Data in (c) is obtained from NASA Ames 7.1 mm/39 mm 2SLGG, and the figure was adapted from Ref. [2].

the downrange end of the pump tube and uprange end of the launch tube. The breech caps are then tightened onto the threaded central breech core, compressing the seals located at the pump tube and launch tube interfaces. Since the inception of 2SLGGs, the designs of seals have undergone significant evolution. References [2, 6] present overviews of these designs.

Another way to couple the central breech between the pump and launch tubes is *via* a "breech cover" design. Instead of compressing each central breech interface individually, the entire central breech assembly is compressed by equal and opposite axial forces applied to the collars by the breech cover and a hydraulic coupler (Fig. 11b). The hydraulic coupler can readily apply coupling forces that exceed 500 kN. Since coupling forces must grow with geometric scale, the breech cover design is typically employed in medium- to large-scale 2SLGGs. While these two central breech assembly configurations outline common coupling mechanisms, other designs do exist.

The prevailing central breech geometry used in current isentropic 2SLGGs owes its origins to Curtis

[2, 200]. Key features of this geometry include a slender central breech taper section with a transition angle ranging $\beta = 6°$–$16°$ and a relatively heavy piston typically constructed from a deformable yet incompressible plastic such as polyethylene. During the pump tube WG compression phase, the piston enters the tapered region of the central breech and experiences deceleration due to retarding forces from the conical wall and increasing WG pressure. This process generally halts the piston's motion, minimizing the need for additional gas buffers and enabling an optimized WG compression ratio in a non-destructive manner. The slender taper ensures a smooth flow transition with minimal central breech erosion/wear; however, it can generate and intensify shock waves as the piston enters the taper [201, 202]. As the piston extrudes into the taper, its downrange face velocity increases inversely proportional to the corresponding area change, potentially causing compression waves to rapidly merge into shock waves if the acceleration is significant. These shock waves may increase projectile velocity but can also cause undesirable base pressure fluctuations. Nevertheless, using a slender taper may lead to enhanced projectile velocities relative to those attainable using a constant diameter section. The accelerated gas particles may also gain additional kinetic energy, reducing the pressure drop between the reservoir and the projectile. This effect is more prominent in high-speed piston guns but may be less significant in guns with large chambrage and slow pistons [2].

The effect of transition/taper angle (β) on muzzle velocity has been previously investigated. For example, 0.16 g, 0.32 g, and 0.65 g projectiles were launched by the NASA Ames 7.1 mm/39 mm 2SLGG using equivalent loading conditions and only varying β [2]. The experimental data from this study are plotted in Fig. 11c, which clearly shows that muzzle velocity is not significantly influenced over the range $\beta = 8°$–$16°$. Other studies have shown a decrease in performance for higher transition angles [51, 203]. The optimal taper angle is still an active area of research and development, with currently available central breech and piston materials being key limiting factors. Recent studies, however, indicate that the optimal transition angle is generally between $\beta = 7°$–$14°$ [91, 203].

Another factor that affects the central breech's geometry is the ratio of the pump tube inner diameter to the launch tube bore diameter (d_{PT}/d_{LT}). This ratio not only enables the comparison of 2SLGGs across various length scales but also significantly impacts their performance and efficiency. Consequently, this ratio has been the focus of numerous 2SLGG optimization studies (*cf.* [50, 51, 53, 54, 183, 204–207]). This has led to a relative decrease in both pump tube diameters and lengths and an increase in WG starting pressure since 2SLGG operations began in the 1950s. Operational 2SLGGs have a wide range of d_{PT}/d_{LT} ratios due to laboratory space restrictions, modest performance requirements, *etc.* Figure 11d shows a histogram of all d_{PT}/d_{LT} values available for the 2SLGGs from Table 1. Clearly, $d_{PT}/d_{LT} \approx 3$ is most common, which aligns with designated optimal values from the literature [2, 50, 51]. As an aside, most larger values of d_{PT}/d_{LT} correspond to 2SLGGs with *multiple* launch tubes of various diameters for a single pump tube. In general,

both β and d_{PT}/d_{LT} are chosen for a given gun based on design/performance requirements.

3.2.4. Rupture Diaphragms (Petal Valves)

For all 2SLGGs, the WG is compressed in the pump tube and the central breech until its pressure reaches some critical value necessary to burst the rupture diaphragm (*cf.* Figs. 11a and 11b). In most cases, the rupture diaphragm (aka petal valve) is a metallic circular disc of thickness e with two perpendicular radial grooves of depth ε (Fig. 12a). The pressure at which the diaphragm ruptures can be partially controlled by varying the depth of the grooves for a given disc thickness. This rupture pressure (or release pressure) has a second-order effect on 2SLGG performance, with higher rupture pressures resulting in modest muzzle velocity gains [2]. Most often, the rupture pressure (p) is determined experimentally as a function of petal valve geometry, leading to simple empirical expressions, such as

$$p = \frac{A}{B} e^{3/2} (\varepsilon/e)^{-1/2}, \tag{3}$$

where empirical parameter A depends on diaphragm dimensions, groove depth, and material properties (elastic limit, fracture toughness, *etc.*), $B = 1 + 3.75(\varepsilon/e)^3$, and $0.05 < \varepsilon/e < 0.4$ [95, 208]. For illustration, Eq. (3) is plotted as a function of ε/e for various values of A in Fig. 12b, with common burst pressures highlighted. Simple expressions like Eq. (3) facilitate critical burst pressure optimization and, ultimately, muzzle velocity enhancement. For a given 2SLGG, the burst diaphragm material and geometry, however, are often held constant across experiments to nominally remove projectile release pressure as a variable.

3.2.5. Launch Tubes

Once the WG reaches the critical release pressure, the rupture diaphragm opens (Fig. 12b inset), and the hot, high-pressure WG rapidly travels into the uprange end of the launch tube, initiating projectile acceleration. Similar to pump tubes, launch tubes are thick-walled, hollow cylinders with length-to-diameter ratios ranging $L_{LT}/D_{LT} \sim$ 100–400. The launch tube functions similar to a traditional gun barrel, as it contains high-pressure gas that accelerates the projectile. The term "launch tube" is used primarily to differentiate it from the pump tube, rather than to indicate any significant functional differences. Launch tubes can be categorized as either rifled or smooth-bore. Rifled launch tubes provide projectile spin stabilization and enable sabot separation (see Section 3.2.6) in a vacuum through gyroscopic forces; however, they also introduce uncertainty in projectile rotational kinetic energies. In contrast, smooth bore launch tubes contribute negligible rotational kinetic energy but require aerodynamic drag for sabot separation. Rifling for larger bore diameters can be challenging, particularly if the launch tube is segmented. Therefore, smooth bore launch tubes become more prevalent as the diameter increases (*e.g.*, $D_{LT} \geq 12.7$ mm).

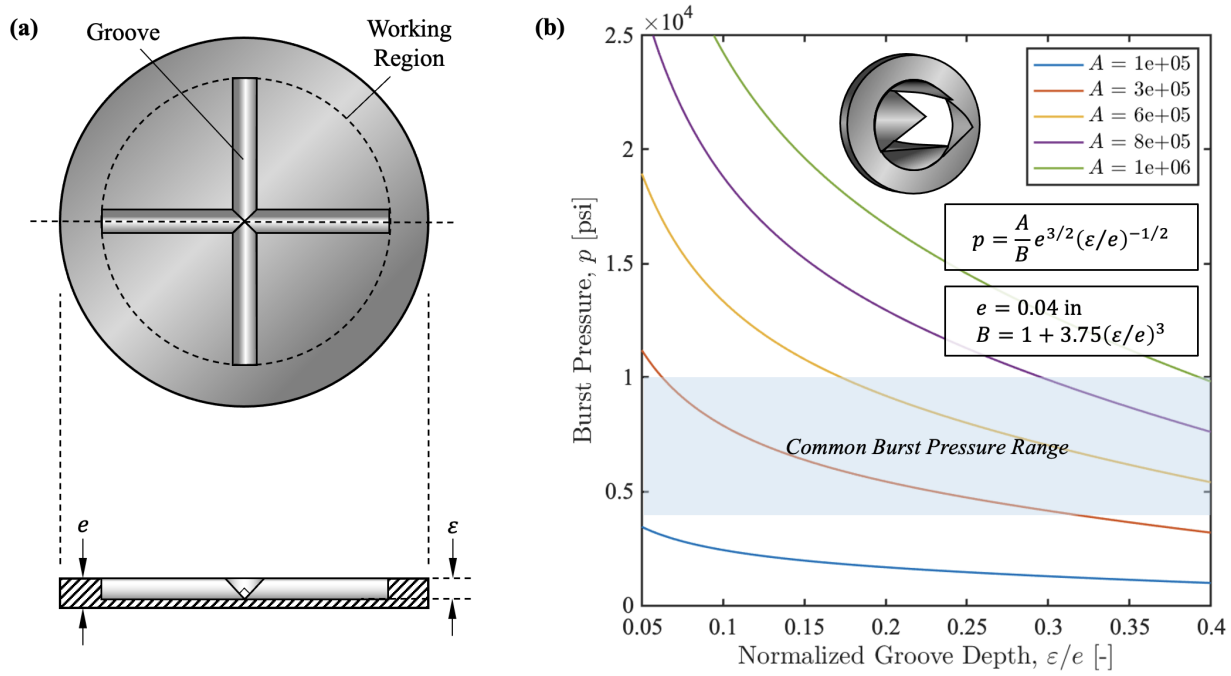

Figure 12: An overview of the rupture diaphragm (petal valve) configuration commonly used in 2SLGGs, featuring (a) a schematic of the petal valve with total thickness e and groove thickness ε, and (b) an empirical plot of the petal valve burst pressure as a function of groove depth for various values of constant A. This relationship is valid for groove thicknesses in the range of $0.05 < \varepsilon/e < 0.4$. The constant A depends on diaphragm dimensions, groove depth, and material properties such as the elastic limit and stress intensity factor for crack propagation, as described in Refs. [95, 208].

Since the diameter of the launch tube determines the diameter of the projectile or model that can be launched, a given 2SLGG is typically described by its "bore size" alongside its range of attainable muzzle velocities. Furthermore, the launch tube diameter serves as the most reliable indicator of overall 2SLGG size, as all components typically scale in proportion to the bore size. Figure 13a presents a histogram of launch tube bore sizes for the 2SLGGs examined in this study (Table 1). Although bore sizes can exceed 200 mm (*e.g.*, Arnold Engineering Development Complex (AEDC) Range-G), the majority of 2SLGGs feature launch tubes with diameters under 40 mm (*cf.* Table 1). This observation aligns with expectations, as the cost and complexity of aeroballistic ranges escalate nonlinearly with gun size. Consequently, national research priorities and long-term available funding play substantial roles in the distribution of launch tube diameters (L_{LT}/D_{LT}).

Another key parameter for 2SLGGs is the length-to-diameter ratio of the launch tube. For a given 2SLGG and set of operational parameters, increasing L_{LT}/D_{LT} has been demonstrated to increase muzzle velocity up to a certain threshold [2]. Beyond this critical point, frictional (and other) losses hinder further velocity gains and can, in fact, considerably reduce the projectile velocity. For example, Fig. 13b shows muzzle velocity *versus* launch tube length-to-diameter ratio ("bore-normalized launch tube length") data for two different mass projectiles taken from the NASA Ames 7.1 mm/39 mm 2SLGG [2]. A peak in muzzle velocity

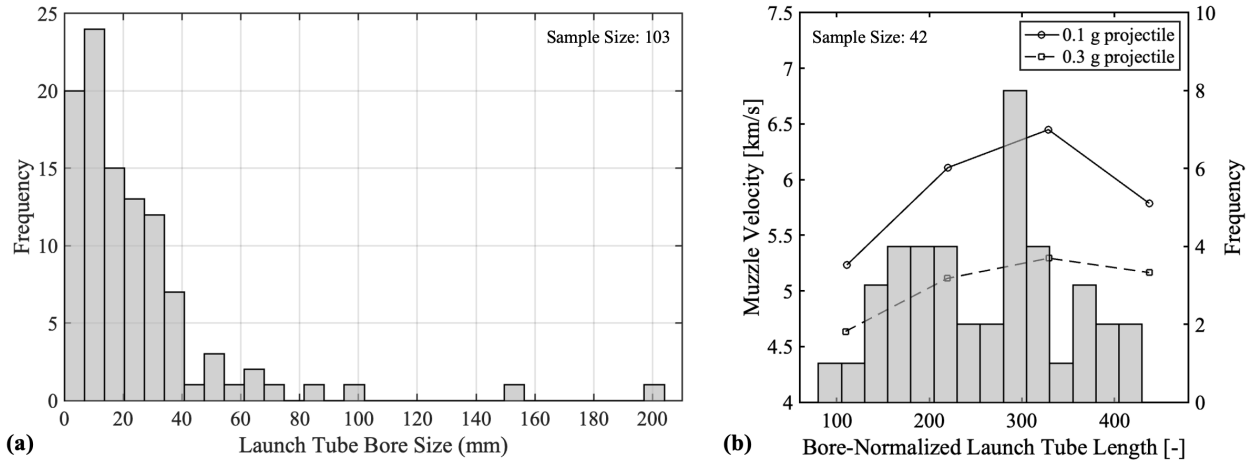

Figure 13: 2SLGG launch tube geometry: (a) an illustrative plot of experimental muzzle velocity *versus* bore-normalized launch tube length superimposed on a histogram of bore-normalized launch tube length and (b) a histogram of the bore sizes of launch tubes used in 2SLGGs worldwide. The histogram demonstrates that the majority of 2SLGG launch capability is reserved for projectiles with a diameter of approximately 40 mm or smaller. The sample size in the histogram is larger than the total number of 2SLGGs, as some facilities possess multiple launch tubes for the same 2SLGG.

for both projectile masses corresponds with an optimal ratio of $L_{LT}/D_{LT} \approx 325$. Superimposed on these trends is a histogram of all available launch tube length-to-diameter ratios for the 2SLGGs from Table 1. This distribution shows that research, performance, and laboratory space requirements have led to notable differences not only in launch tube diameters but also launch tube length-to-diameter ratios. The initial projectile velocity increase with increasing launch tube length in Fig. 13b is consistent with elementary predictions obtained using Eq. (2), which suggests that sustaining a positive projectile base pressure for extended durations or distances enhances muzzle velocity (*cf.* Figs. 7a and 7b). The trend holds until the negative frictional forces between the projectile and the bore surpass the positive force exerted on the projectile's base by the WG or there is a loss of positive base pressure (*i.e.*, finite reservoir effects). Expanding the velocity ceiling is not the sole purpose for adjusting the launch tube length-to-diameter ratio; lengthening the launch tube at a fixed diameter also moderates the acceleration profile needed to propel a specific projectile to a desired velocity. This feature may be advantageous when launching fragile or intricate projectiles or models to hypervelocities.

3.2.6. Projectiles and Sabots

Throughout this discussion, the term "projectile" has been used broadly to denote the object being launched. Specifically, projectiles can encompass single, full-caliber geometries with diverse length-to-diameter ratios or, more frequently, projectile "packages" comprised of a sub-caliber projectile and its corresponding sabot [2, 209]. Sabot geometries can vary substantially, but their primary functions include obturating the launch tube (inhibiting WG blowby) and sustaining the projectile during acceleration. Of

course, it is undesirable for the sabot to interfere with the experiment. To avert this issue, segmented sabots are strategically designed to facilitate radial separation of each sabot component during the projectile's free flight *via* gyroscopic or aerodynamic forces. Eventually, the projectile traverses a thick, metallic annular disc that captures the sabot fragments (see Section 5.1). Ideally, only the projectile enters the diagnostic field of view and/or comes into contact with the target. Complex sabot designs and separation mechanics can differ significantly than described here and are driven by the specifics of a given experiment (see Section 5.2) [2, 209–213]. As such, an in-depth discussion on sabots is beyond the scope of this present work.

3.3. Notable Modifications to the 2SLGG

The pursuit of increasingly higher muzzle velocities has resulted in significant modifications to the 2SLGG, giving rise to what is known as "three-stage light gas guns" (3SLGGs). As these devices fall somewhat outside the focus of this review, they are only *briefly* discussed here to provide some illustrative examples, broader insights, and perspectives. 3SLGGs can be distinguished from 2SLGGs largely due to the inclusion of *i*) dual, in-line pump tubes, *ii*) parallel pump tubes, *iii*) spall pillow (or flyer plate) muzzle attachments, and *iv*) preheating of the WG. Although some significant performance improvements are possible, these modifications are not necessarily consistently applied or widely adopted. Often, these modifications are research subjects themselves (see, *e.g.*, [11, 12, 30, 132, 214–217]).

Several approaches to modifying the basic 2SLGG configuration involve incorporating an additional light gas compression stage. For example, the effectiveness of the 2SLGG inspired the creation of one 3SLGG concept, which incorporates an extra *in-line* compression stage to enhance performance (*i.e.*, 2SLGG + LGG). Although this appears a reasonable and natural extension to the 2SLGG, the few instances in which this technique has been attempted have resulted in only modest increases in muzzle velocity (up to roughly 9 km/s) while adding significant design challenges [11, 132, 214]. The energy required to accelerate *two* compression pistons, along with the inevitable frictional losses, offsets any significant increases in projectile muzzle velocity. Consequently, the modest improvements in velocity, combined with higher consumable, construction, and labor costs, have led to its limited adoption. The increased complexity of optimizing performance parameters (powder mass, pump tube pressures, piston masses, *etc.*) for this 3SLGG also makes it less predictable and more operationally complex.

The inclusion of an extra in-line pump tube is distinct from a dual, *parallel* pump tube arrangement. One of the most innovative developments to the light gas compression stage is Fraunhofer EMI's "Twingun," featuring two pressure breech and pump tube assemblies arranged in parallel [30]. The pump tubes share a common central breech. Both pressure breeches are powder driven, and the charges can be detonated with precisely delayed timing. This results in pistons intentionally traveling asynchronously downrange in the

pump tubes. The time difference between the piston arrival times can be controlled to "smoothen" the WG pressure curve and, thus, the projectile acceleration profile. Smoother acceleration profiles generally broaden the type and mass range of projectiles that can be launched by a given 2SLGG, since many projectiles can fail in the launch tube if subjected to sufficient peak accelerations.

Other 2SLGG modifications that do not incorporate an additional compression stage have also been referred to as 3SLGGs. One notable example that has resulted in significant muzzle velocity gains leverages a 2SLGG-launched projectile to initiate an additional launch strategy. The process generally involves using a projectile assembly with varying density to strike a stationary (often metallic) flyer plate [12, 13, 216, 217]. As a result of the impact, transient, structured, high-pressure waves (*e.g.*, 100 GPa) are produced, enabling the relatively gentle acceleration of the plate to extreme speeds without material failure. The design of the variable-density impactor is essential for ensuring the flyer plate's smooth acceleration without excessive heating that could cause melting or vaporization of the flyer plate. Moreover, the pressure wave must be adjusted to prevent the flyer plate from experiencing spall fractures. These requirements are crucial for effectively launching flyer plates to velocities beyond the capabilities of unmodified 2SLGGs. For instance, employing these techniques has allowed the launching of titanium (Ti-6Al-4V) and aluminum (6061-T6) alloy plates with thicknesses between 0.5 mm and 1.0 mm (and masses from 0.1 g to 1 g) to speeds exceeding 15 km/s [13].

An alternative 3SLGG incorporates an extra preheating and filling stage in the pump tube, which enables broader control over the initial energy of the WG (*cf.* [215]). This increase in the initial gas temperature not only allows for potentially higher muzzle velocities but also helps suppress peak pressures in the reservoir, even while increasing the amount of powder charge for higher projectile velocities. In this way, the preheating process can contribute to achieving high velocities while also enabling relatively low projectile accelerations. The latter aspect is particularly useful for testing intricate and delicate projectiles and models. Although this method offers potential advantages, there is a scarcity of available data, and practical obstacles include effectively heating the WG and managing its temperature in an experimentally repeatable manner. Even with the relatively low adoption of these techniques, the featured 3SLGGs demonstrate how innovative modifications to the 2SLGG can enhance muzzle velocity and projectile launch survivability. An overview of these techniques can be found in Table 2.

4. A Brief Comparison of 2SLGG Performance Capabilities

Variations in 2SLGG configurations and operations have given rise to a broad spectrum of performance capabilities. For instance, 2SLGGs that can propel projectiles/models at velocities between 2 and 4 km/s

are typically suitable for most hypersonic applications, whereas projectile velocities must exceed 6 km/s for most MMOD problems. The achievable velocity range alone, however, is an inadequate 2SLGG selection criterion, as a majority of MMOD problems can be addressed by employing relatively small, easily launched metallic spheres of various diameters while hypersonic problems generally require launching larger and more sophisticated projectiles/models. Of course, the range tankage also plays an integral role in the aeroballistic range selection process (see Section 5.1). For these reasons, the performance ceiling of a 2SLGG is often measured by the highest kinetic energy it can transfer to a projectile during launch. Factors such as the gun's size, shape, drive type, and working gas, as well as the projectile's ability to withstand the launch accelerations, heavily influence this performance threshold. In other words, the highest performing 2SLGGs have the greatest achievable kinetic energies.

Comparing a given 2SLGG's maximum muzzle velocity and launch tube diameter (Table 1) provides some indication of its performance capabilities. An increase in launch tube diameter (and thus gun size) generally corresponds to an increase in the projectile mass that can be launched to a given peak muzzle velocity (*i.e.*, peak projectile kinetic energy scales with gun size). However, determining the maximum kinetic energy for all documented 2SLGGs presented a challenge, as most studies did not explicitly provide this information and many 2SLGGs do not operate at full performance capacity. When possible, appropriate projectile mass and velocity data from published experimental results were utilized to calculate representative kinetic energy values. These estimates, along with explicitly reported kinetic energy limits, are provided in Fig. 14 in descending order for a representative sample of operational 2SLGGs. Achievable peak projectile energies range from a few joules to nearly 100 megajoules (roughly equivalent to 25 kg of TNT). The lowest plotted projectile kinetic energy of ∼20 J corresponds to Mississippi State University's (MSU) ∼4 m long, 1 mm bore 2SLGG range (the smallest bore reported, Fig. 15a, [32]), while the highest energy of ∼96 MJ was achieved by AEDC's ∼280 m long, 203 mm bore 2SLGG range (the largest bore reported, Fig. 15b, [116, 117])[1]. The

[1]Drexel's 2SLGG aeroballistic range is actually shorter and has a lower reported maximum kinetic energy (Fig. 14) than MSU's due to its lower performance requirements. The MSU-I 2SLGG has the smallest bore diameter.

Table 2: A list of representative "three-stage light gas gun" (3SLGG) capabilities. Each capability is characterized by the third stage differentiating it from a standard 2SLGG, including dual in-line and parallel pump tubes, spall pillow or flyer plate muzzle modifications, and working gas preheating.

No.	Facility Name	Country	Third Stage
1	National Research Tomsk University [132]	Russia	Dual pump tube, in-line
2	University of Dayton Research Institute (UDRI) [11]	US	Dual pump tube, in-line
3	Fraunhaufer EMI – "Twingun" [30]	Germany	Dual pump tube, parallel
4	Tokyo Institute of Technology [215]	Japan	Dual drive (powder and compressor), preheating
5	Lawrence Livermore National Laboratory [214]	US	Dual pump tube, in-line
6	Sandia National Laboratory [12]	US	Spall pillow/flyer plate
7	European Synchrotron Radiation Facility (ESRF) [216]	France	Spall pillow/flyer plate
8	China Academy of Space Technology [217]	China	Spall pillow/flyer plate

other operational 2SLGGs span the range of achievable kinetic energies. Hence, many space, hypersonic, and military research problems can be readily addressed at a nearly continuous scale of projectile size/mass and impact energy.

The peak projectile kinetic energy does not offer a comprehensive understanding of a 2SLGG's performance capabilities, as it may only apply to a limited number of projectile materials and/or geometries. In particular, this peak value may not translate to a wide range of projectile masses, as heavier/denser projectiles becoming increasingly difficult to launch for a given 2SLGG. For this reason, the range of velocities that can be achieved for designated launch package masses may provide a better comparison metric in the evaluation of 2SLGG performance. Experimentally generating a comprehensive collection of 2SLGG performance data, however, can be cost-prohibitive and time-consuming. Even when such data is available, many facilities do not openly disclose complete and readily accessible datasets. Instead, the range of achievable velocities and projectile sizes are commonly reported, whereas projectile masses are not. Despite these limitations, some representative performance data was obtained from the open literature for a subset of operational 2SLGGs worldwide. This projectile launch velocity *versus* mass data is summarized in Fig. 16, with each marker type corresponding to a different facility. The graph also features lines of constant kinetic energy to give an idea of relative scale and to highlight the extensive range of combined launch capabilities. The listed 2SLGGs cover a kinetic energy range spanning seven orders of magnitude. Moreover, for a specific gun, the maximum muzzle velocity decreases as the projectile mass increases, while the kinetic energy ceiling remains unchanged. Hence, launch mass and velocity data provides a more complete picture of 2SLGG launch capabilities compared to kinetic energy ceilings, peak muzzle velocities, or achievable muzzle velocity ranges.

The breadth of achievable kinetic energies depicted in Figs. 14 and 16 highlights the remarkable potential of modern 2SLGGs to address a diverse array of problems in ballistics, HVIs, hypersonics, shock physics, *etc.* In addition, these tools facilitate the investigation of *scaling effects* on impact physics and aerothermophysics, which is essential for understanding phenomenology and refining modeling techniques (*cf.* [222–224]). As physical phenomena may significantly differ with scale, the ability to vary scale across multiple orders of magnitude in length and energy is of paramount importance. By leveraging these resources, robust scaling laws can be developed while also readily addressing scale-induced changes in energy absorption, deformation/failure behaviors, thermodynamics, and aerodynamics that are governed by factors such as model size, impact energy, event duration, material heterogeneity, and adiabatic heating. Emerging microscopic ballistic testing methods, such as Laser-Induced Particle Impact Testing (LIPIT) [14, 225], have the potential to extend these scaling boundaries, expediting material discovery and phenomenological understanding at even lower energies (nanojoules to microjoules) and higher strain rates (*e.g.*, $>10^9$ s^{-1}; Fig. 2).

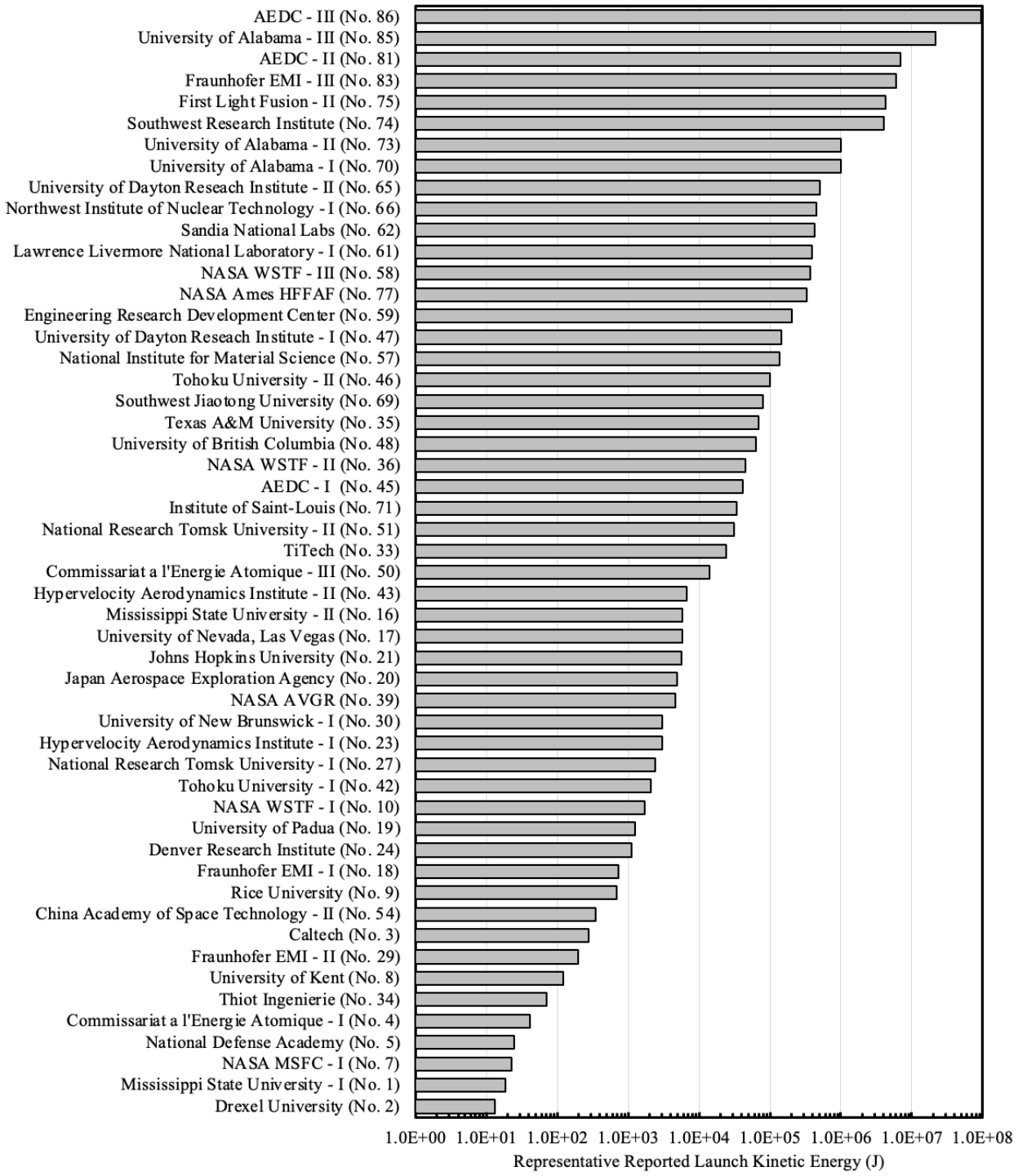

Figure 14: Representative projectile kinetic energy capabilities for 52 out of the 91 2SLGGs included in this study, suggesting that current launch capabilities span roughly seven orders of magnitude. The kinetic energy values reported may not be representative of the *rated* capabilities of the 2SLGGs, as not all reported 2SLGG operate at maximum performance.

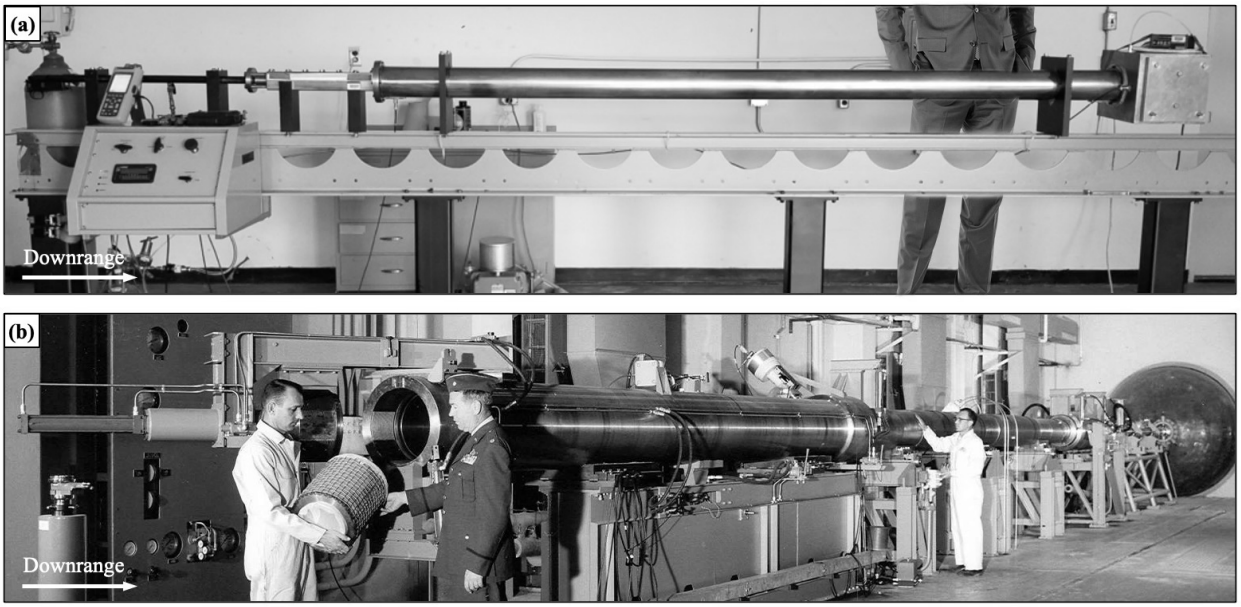

Figure 15: Photos of the smallest and largest operational 2SLGGs: (a) Mississippi State University's ∼4 m long, 1 mm bore 2SLGG range and (b) AEDC's ∼280 m long, 203 mm 2SLGG range. Photos were sourced from Refs. [32] and [218], respectively.

5. Differences in 2SLGG Aeroballistic Ranges

In the preceding sections, key similarities and differences between 2SLGGs worldwide have been presented, with an emphasis on gun working principles, operations, configurations, and performance. However, each 2SLGG is an integral part of a corresponding aeroballistic range. 2SLGGs, single-stage gas guns, single-stage powder guns, rail guns, and three-stage guns can all assemble into their own aeroballistic range. Hence, an aeroballistic range typically consists of a launcher and a characteristic tankage assembly, which can vary significantly across different facilities. The tankage configuration is heavily dependent on the experiments that the range is designed to perform (impact physics, aerothermophysics, planar impacts, and nuclear/pellet injection, *etc.*), specific research application (ultra-high-rate material behavior, planetary science/defense, nuclear physics, spacecraft MMOD protection, hypersonic vehicle performance and survivability, military protective structures, *etc.*), and facility affiliation (government, academic, private, *etc.*). In this section, the key differences in aeroballistic ranges are highlighted, with a focus on tankage assemblies and their corresponding research applications.

5.1. 2SLGG Aeroballistic Range Tankage Assemblies

Aeroballistic range tankage design and construction are at least as diverse and intricate as 2SLGG geometries, sizes, and capabilities. Tankage configurations can differ significantly in form, function, and sophistication, depending on the research requirements. Throughout a given aeroballistic range's lifetime, however, substantial tankage modifications are not uncommon. Despite the wide disparity in aeroballistic

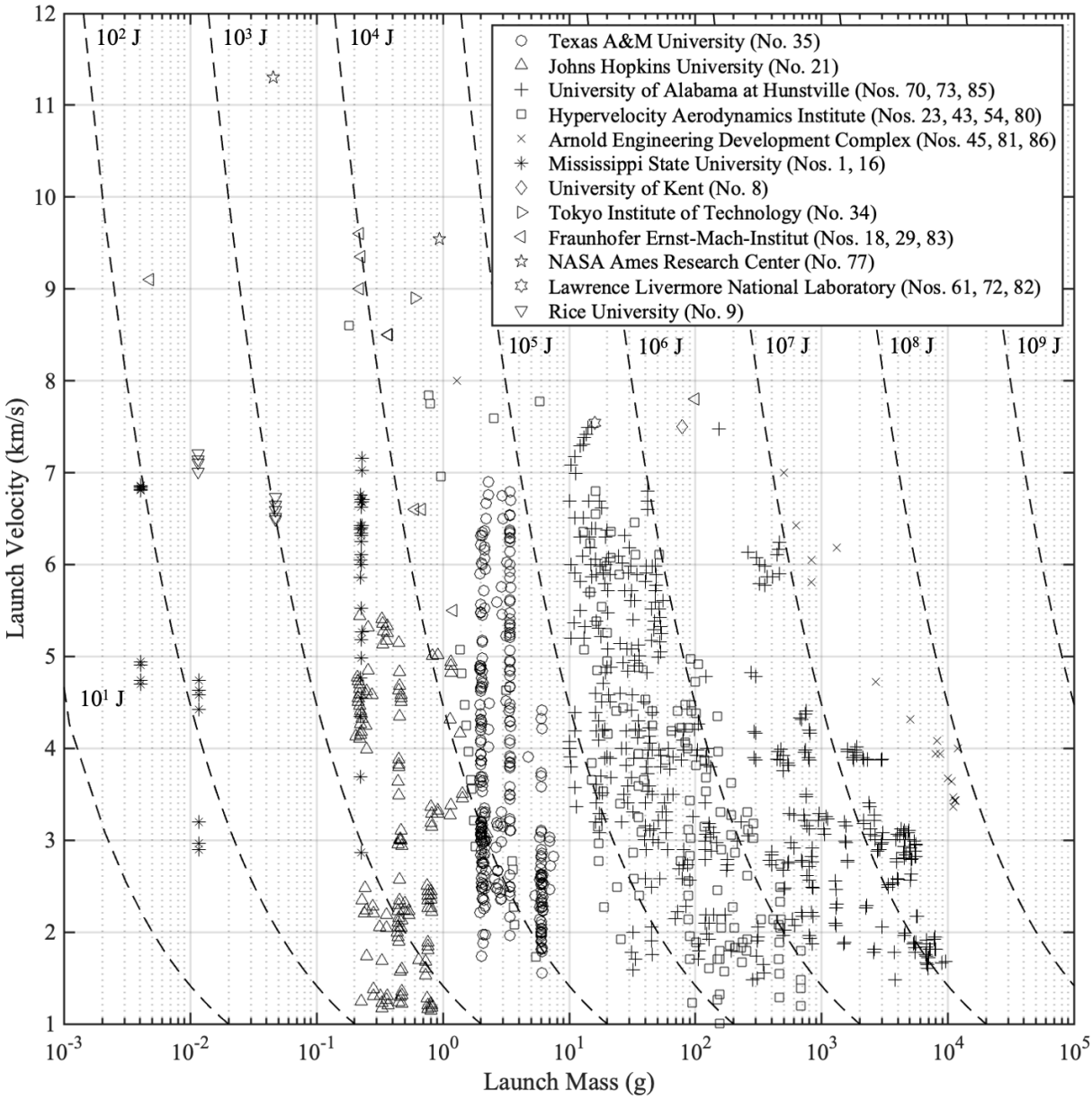

Figure 16: Projectile launch velocities ($N \sim 1100$) from a sampling of 2SLGG facilities, with data sourced from Refs. [15, 58, 104, 126, 163, 219–221]. The results provide valuable insights into 2SLGG performance and potential applications in hypervelocity research, facilitating comparisons between representative research facilities and their equipment.

range complexity and research thrusts, the majority of tankage assemblies can be categorized into three representative configurations: (1) a separated blast tank and target tank, (2) a near-muzzle tank, and/or (3) a combined blast tank and "free flight" range tank. Each configuration has two overarching objectives: to create a well-controlled and well-characterized environment for the desired experiment and to support *in-situ* diagnostic instrumentation.

The first and most predominant tankage configuration consists of two separated tanks [103–105, 109, 119,

123, 126, 127, 134, 141, 154]. The uprange most "blast" tank is positioned in-line with to the downrange target (or terminal) tank. The blast tank serves dual functions: providing a free flight range for the projectile and capturing the hot, high-pressure WG *via* rapid expansion and baffling. The blast tank is typically equipped with access hatches and plumbing ports, which allow for efficient cleaning and gas evacuation. The 2SLGG launch tube muzzle is inserted into the uprange end of the blast tank, where a circumferential seal is created between the barrel's outer diameter and the blast tank. This seal, in conjunction with airtight seals on all hatches, ports, and windows, enables the tankage assembly to be placed under near-vacuum conditions. Such conditions are vital for reducing projectile aerodynamic drag and heating, lowering oxygen concentration, and controlling the internal atmosphere to generate desired test conditions.

Upon exiting the muzzle, the projectile package (often consisting of the projectile and a sabot) commences free flight in the blast tank. Depending on whether the 2SLGG barrel is rifled or smoothbore, the sabot separates from the projectile either through gyroscopic forces induced by barrel rifling or aerodynamic forces induced by the sub-atmospheric pressure of an inert gas (*e.g.*, N_2) in the blast tank. Independent of the separation mechanism, the sabot pieces are typically arrested by an annular metallic plate, known as the sabot stopping or stripping plate, at the downrange end of the blast tank [109, 115, 163, 226]. The projectile then proceeds into the target tank, either directly or through a short ("drift") tube, depending on the tankage layout. Some form of velocimetry system typically captures the projectile velocity just before or just after entering the target tank (see Section 6). For example, laser velocimetry "curtains" can be passed through two sets of optical ports just uprange of the target tank [26, 101, 102, 119, 128, 133, 137, 140, 163, 168, 227–229]. The terminal tank houses the target sample (or equivalently contains an observation volume) for a given experiment and often contains intricate structures for supporting instrumentation and target fixturing. External fixturing equipment, such as optical tables, can be employed to support diagnostic tools and associated equipment [134, 163]. The projectile's flight terminates within the target tank, typically *via* target impact. To facilitate *in-situ* data capture, most target tanks feature a multitude of diagnostic windows and feed-through ports, which support both internal and external diagnostic instrumentation. Different liquids, gasses, and aerosolized particles can also be introduced *via* these feed-through ports to generate different target tank environmental conditions [113, 163, 228, 230–232]. A simple, representative schematic of this tankage configuration is provided in Fig. 17a.

In the separate blast and target tank design, the relatively long free flight path from muzzle to target can lead to significant projectile pitching, yawing, or even tumbling, particularly in smooth bore 2SLGGs, where the projectiles are not spin-stabilized by rifling. This behavior is detrimental to experiments that require high planarity upon impact, rendering the two-tank configuration unfavorable for such purposes. To address this issue, a single chamber, situated directly downrange of the launch tube muzzle, is typically

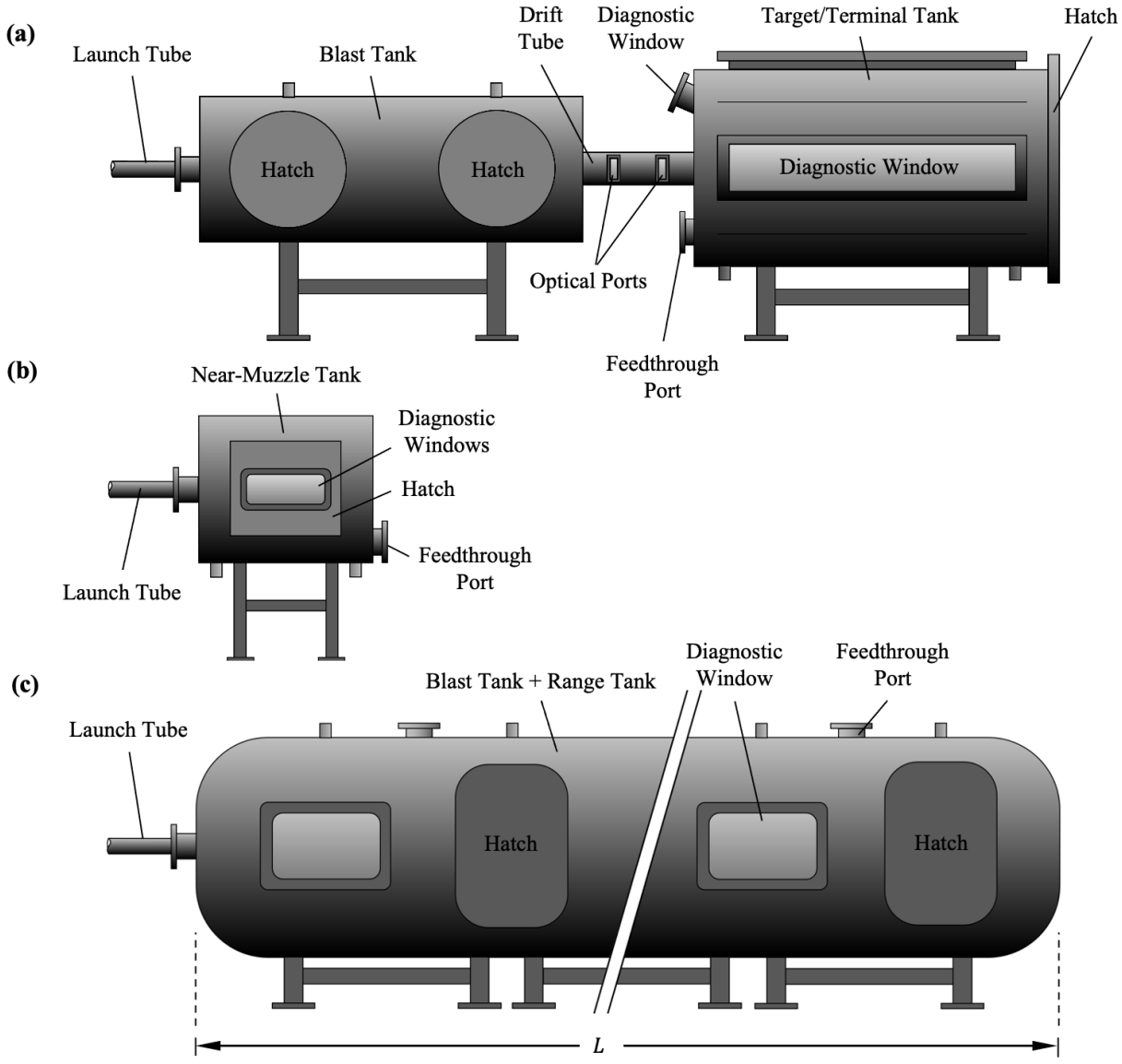

Figure 17: An illustration of common aeroballistic range tankage configurations used with 2SLGGs: (a) the separated blast tank and target tank, (b) the near-muzzle chamber, and (c) the combined blast tank and target tank. The choice of tankage configuration depends on the research area, with (a) separated blast and target tank used most commonly for terminal ballistic investigations, (b) near-muzzle tanks used for shock physics experiments, and (c) combined tanks for hypersonic experiments ($L >>$ gun length).

employed [120, 128, 134]. The launch tube is inserted into this near-muzzle chamber, forming an airtight seal for gas evacuation purposes. However, sabot separation is not possible in this configuration, necessitating the use of i) full-bore, cylindrical sabots with projectiles attached to the downrange end of the sabot or ii) full-bore cylindrical projectiles [58, 233–235]. In other words, the sabot is part of the experiment in some way for near-muzzle chamber experiments. A 2SLGG combined with a near-muzzle chamber can also be used to perform flyer plate experiments [118, 217, 236–239]. Near-muzzle tanks can accommodate various

target geometries, enabling both normal and oblique impacts with high planarity [240, 241]. Similar to the separated tank configuration, near-muzzle chambers are equipped with diagnostic windows, hatches, and feed-through ports. Some facilities have even integrated near-muzzle chambers into their aeroballistic ranges, directly uprange of the blast tank, to support a broader range of experiments [134]. A basic diagram illustrating a typical near-muzzle chamber can be found in Fig. 17b.

For some research applications, it may be crucial to accurately characterize and analyze the shock structure and flow field surrounding projectiles or models during flight. Conventional separated blast and target tank assemblies present significant challenges for such observations, primarily due to their relatively short lengths, which result in short flight durations caused by projectile velocities on the order of km/s. To overcome this limitation, some research facilities utilize an integrated blast tank and range tank assembly that is substantially longer than the associated 2SLGG [15, 110, 117, 242]. This tankage design is typically found in facilities with 2SLGGs on the larger end of the kinetic energy and length scales (*cf.* Fig. 14 and Table 1). These assemblies feature enclosed, large-diameter tubes through which the projectile or model travels. The range tanks' internal conditions can be precisely controlled, enabling hypersonic research under various test conditions, by modifying parameters such as gas pressure, humidity, and composition [15, 228, 231]. Strategically placed diagnostic windows, stations, and hatches along the range tank facilitate *in-situ* characterization of test articles. Guide rails extending the length of the range tank can be employed that help maintain projectile stability and level flight during ballistic hypersonic testing, while feed-through ports allow for the creation of diverse environmental conditions throughout the range tank [15, 116, 117, 231]. Additionally, the tankage assembly can incorporate a target tank, further supporting large-scale impact studies and enhancing research capabilities [15, 110, 117, 242]. Figure 17c shows an illustrative example of a combined blast and range tank, where the tank length (L) is generally much larger than the 2SLGG length. This tankage configuration is a defining feature of AEDC's Range-G, the largest aeroballistic range in routine operation globally [116, 117]. Constructed in 1962, Range-G has been instrumental in the development of defense technology, pioneering many hypersonic and hypervelocity research thrusts. The range is capable of launching projectiles up to 7 km/s, utilizing barrels that can be interchanged to accommodate various projectile diameters, up to 203.2 mm. The 3 m diameter and 305 m long test chamber can be conditioned to pressures from 0.2 torr (26.7 pascals) to 1.7 atmospheres (172 kilopascals). This chamber can also mimic specific weather conditions like rain or snow, providing vital capabilities for the development and assessment of hypersonic vehicle survivability. Along the tankage, the facility is equipped with an extensive assortment of diagnostic instruments, including shadowgraph cameras, high-speed video cameras, and digital X-ray sensors, that allow for detailed *in-situ* analysis and observation.

Operational techniques and technologies pioneered by AEDC's Range-G and similar facilities are being

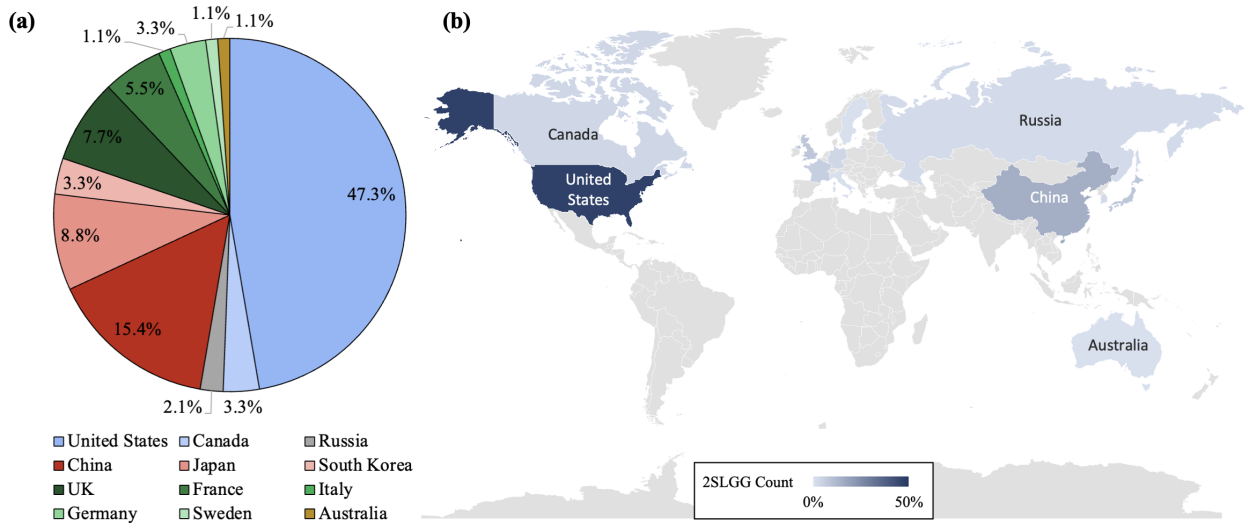

Figure 18: The geographic distribution of 2SLGGs worldwide, featuring (a) a percentage breakdown of 2SLGGs by country and (b) a global heat map highlighting the countries that possess 2SLGGs.

adapted and enhanced in new 2SLGG aeroballistic ranges, such as the Ballistic, Aero-Optics, and Materials (BAM) Test Range at Texas A&M University (TAMU) [191, 192, 242]. Once complete, the BAM Range will include a 67 m long, 10 cm bore 2SLGG; a 12 m long, 3 m diameter HVI target chamber; and a 1 km long, 2.4 m diameter ballistic hypersonics tube with stategically placed state-of-the-art diagnostic stations along its length. The BAM Range will be one of the largest facilities in the world and will be well-suited for evaluating laser propagation, hypersonic aerothermodynamics, and material and structural HVI responses. The BAM Range will complement the existing Range-G and other model-scale facilities dedicated to HVI and hypersonic research.

5.2. 2SLGG Experiment Types and Research Applications

2SLGG aeroballistic ranges have been instrumental in driving groundbreaking advancements across various fields, including experimental impact physics, aerothermophysics, nuclear physics, shock physics, and beyond. Key challenges in these domains are addressed by experiments performed at 2SLGG aeroballistic ranges worldwide, with known facilities in at least a dozen countries including the United States (47.3%), China (15.4%), Japan (8.8%), United Kingdom (7.7%), France (5.5%), Germany (3.3%), Canada (3.3%), South Korea (3.3%), Russia (2.1%), Italy (1.1%), Sweden (1.1%), and Australia (1.1%) (Fig. 18). This global participation highlights the fact that experiment types and research applications are not restricted to a particular country of origin and are truly international endeavors supported by a diverse, multidisciplinary scientific community.

A strong correlation exists between specific aeroballistic range tankage configurations and the experiments conducted at the corresponding facilities. Experiments involving hypervelocity penetration and perforation

mechanics are the most common. Conventional impact experiments typically involve launching a hypervelocity projectile at a specific target, focusing on either the projectile, the target, or their combined response. The majority of aeroballistic ranges that conduct these experiments feature separated blast and target tankage configurations, as detailed previously in Section 5.1 and Fig. 17. Depending on the relative velocity, as well as the materials and geometries of the projectile and target, impacts can involve predominantly penetration (cratering) and/or perforation for a wide range of target obliquities. These events are characterized by a variety of phenomena, including severe deformation, erosion, fragmentation, heating, melting, vaporization, and sublimation of the projectile or target [243–246]. Most studies have adopted a single projectile impact approach, varying the projectile material, geometry, and/or velocity against one or more normal or oblique targets of varying geometry [247]. A wide array of target materials have been studied with this approach, including metals [162, 248–251], polymers [112, 252–254], ceramics [255, 256], composites [199, 257, 258], granular and geo-materials [104, 120, 149, 224, 259–264], reactive materials [265–268], and radioactive materials. Generally, monolithic or composite target geometries have been plates, cylinders, or blocks of defined thickness [247, 269–272]. Target structures, including Whipple shield concepts, are also commonly tested [273, 274]. Projectile materials and sizes also vary, with high density projectiles being more challenging to launch. Projectile materials include metals, polymers, ceramics, composites, and reactive materials [163, 247, 266, 271, 272, 275, 276], while projectile geometries span spheres, ogives, long rods, cylinders, and cones [247, 266, 270, 277–279]. Simultaneously launched distributed particle impacts have also been conducted to study impact interactions and aggregate damage formation mechanics [210, 226, 280–287]. Most research involving hypervelocity penetration/perforation also incorporates analytical modeling or numerical simulations to supplement experimental data [5, 83, 248, 257, 258].

Applications of HVI experiments encompass the development of novel protective materials and structures for military and space purposes, planetary science, defense, hypersonic vehicle survivability, counter-hypersonics, *etc.* Impact testing for protective structure development typically involves launching projectiles that represent realistic threats at candidate materials or structures. In the context of spacecraft protection, targets often include Whipple shields or stuffed Whipple shields [273, 274, 288–293]. Protective structure development for military applications usually entails testing on metals, high-performance concretes, or novel materials and material structures [247, 249, 294–298]. For planetary science or defense, experiments generally involve impacts on granular materials to characterize crater formation and momentum enhancement, as well as perform Hugoniot measurements [104, 120, 149, 224, 259–264]. Representative atmospheric particles, such as dust and ice, have been launched at potential hypersonic vehicle materials and geometries to assess surface damage formation and resulting disturbances to the hypersonic flow field [113, 163, 228, 230, 231, 299].

Immediately following an impact, compressive stress waves propagate through both the projectile and

target, leading to increased internal energy, pressure, and density [7, 300]. When the impact velocity is sufficiently high, the amplitude of these stress waves can exceed the yield stress of the materials involved, causing an elastic precursor wave to be succeeded by a slower-moving plastic wave. Additionally, if the impact-induced wave speed surpasses the local speed of sound in the projectile and target, strong shocks may form. These conditions can result in significant projectile/target temperature rises, plastic deformation, flow and melting, and material fracture and fragmentation. In cases where the impact velocity is even higher, projectile and target vaporization or sublimation may occur [243]. Although this brief overview provides a highly simplified explanation of the impact process, it serves to highlight the complexity of the phenomenon, as shear waves and tensile waves can also form depending on geometries and loading conditions. HVIs often involve complex and coupled projectile/target interactions, making the stress and thermodynamic states challenging to quantify (see Section 2). In response, planar impact experiments have been developed to dramatically simplify the physics of the problem [7, 300]. Facilities that perform planar impact experiments generally use a near-muzzle chamber configuration [120, 128, 129, 134, 216, 237] (see Section 5.1 and Fig. 17b). These experiments typically involve a planar projectile (*i.e.*, flat disc) of known material being launched at a target material of interest, with specialized diagnostic tools measuring arrival times and free surface velocities as stress waves traverse the target material. By combining these measurements with one-dimensional (1D) Rankine-Hugoniot relations, the material shock response can be characterized, informing equations of state and facilitating applications in shock physics, ultra-high-rate material behavior, and Hugoniot data generation. Los Alamos National Laboratory (LANL) has conducted extensive planar impact testing to characterize the shock response of various materials, including metals, polymers, ceramics, *etc.* [76]. The resulting equations of state not only provide a deeper fundamental understanding of material behavior but also support modeling and simulation efforts for penetration and perforation problems [5] (see Section 2).

In 2SLGG experimentation, the focus can shift from traditional impact testing to studying the *projectile's* behavior as it traverses a prescribed atmospheric environment (including aerosolized particles) at hypersonic speeds (>Mach 5, see Section 2). Although such research has been ongoing for decades [228], the increasing global interest in the development of hypersonic weapons and vehicles has prompted the United States and other nations to prioritize the advancement and implementation of hypersonic technologies [28]. Moreover, reentry vehicles also experience hypersonic flight conditions, further underscoring the importance of these experiments [301].

A critical aspect of hypersonic/aerothermophysics experimentation involves characterizing the flow field surrounding the hypersonic model as well as the thermal and mechanical loads to which the vehicle is subjected [302]. Depending on the Mach number, flow phenomena can include strong shocks and expansion

fans, turbulence, and extreme gas pressures and temperatures, with gases potentially ionizing in the vicinity of the hypersonic vehicle [303]. Consequently, much of the research in this field is devoted to vehicle geometry optimization, thermal protection system development and survivability testing, and flow field characterization for computational or theoretical model development and validation [6, 301, 302, 304–310]. Complex flight ranges that incorporate various diagnostic tools and techniques are necessary for such characterization, and it is not uncommon for the projectile itself to be instrumented [6, 116, 117]. Although 2SLGGs are not the only launching devices used (see Section 1), they offer several advantages, such as the ability to achieve hypersonic speeds over a relatively small distance with subscale models and relative ease of implementation in closed, indoor aeroballistic ranges (see Section 1). For hypersonic/aerothermophysics experiments, most range tankage configurations consist of combined blast tanks and range tanks (see Section 5.1 and Fig. 17c) [15, 116, 117, 190–192]. Closed range tankage is generally more desirable, as it allows for control of the internal tank gas pressure, temperature, humidity, and composition, simulating a variety of atmospheric conditions and altitudes. This atmospheric control enables experiments under realistic flight conditions and parametric studies for theoretical and computational fluid dynamics (CFD) model development and implementation. As hypersonic technology continues to be prioritized, the importance of hypersonic/aerothermophysics testing will likely continue to increase.

One particularly unique application of a 2SLGG is in nuclear fusion research. One of the difficulties of maintaining a fusion reaction is consistently providing fuel to sustain the reaction [311–313]. Given the extreme temperatures and pressures required for fusion, material entering the reactor can quickly degrade from usable fusion fuel to waste mass. Some researchers have proposed using 2SLGGs to launch fuel into their reactor cores to prevent the fuel from being degraded before reaching the fusion reaction site. These facilities typically have relatively small bore launch tubes ($\sim$5 mm) and modest velocity ceilings ($\sim$5 km/s) compared to other comparable 2SLGGs, but they have some of the highest experimental cyclic rates in the field ($\sim$1–10 launches per second) [146, 148]. While these 2SLGGs are relatively few in number, they represent a creative application of 2SLGG technology and illustrate its diverse utility.

The experiment types and research applications highlighted herein emphasize the versatility of 2SLGG aeroballistic ranges in addressing a wide variety of complex research problems. Many facilities are designed to facilitate multiple experiment types, whereas some are predominantly reserved for specific testing (*i.e.*, government-affiliated labs that characterize reactive and/or radioactive material). Histograms of aeroballistic range affiliation and experimentation type are provided in Figs. 19a and 19b, respectively, for reference. Affiliations include academic (46%), government (48%), and private (6%), while experiment types performed at the aeroballistic ranges span penetration/perforation mechanics (75%), planar impact (40%), hypersonic/aerothermophysics (20%), flyer plate impact (14%), and nuclear/pellet injection (4%). Essential

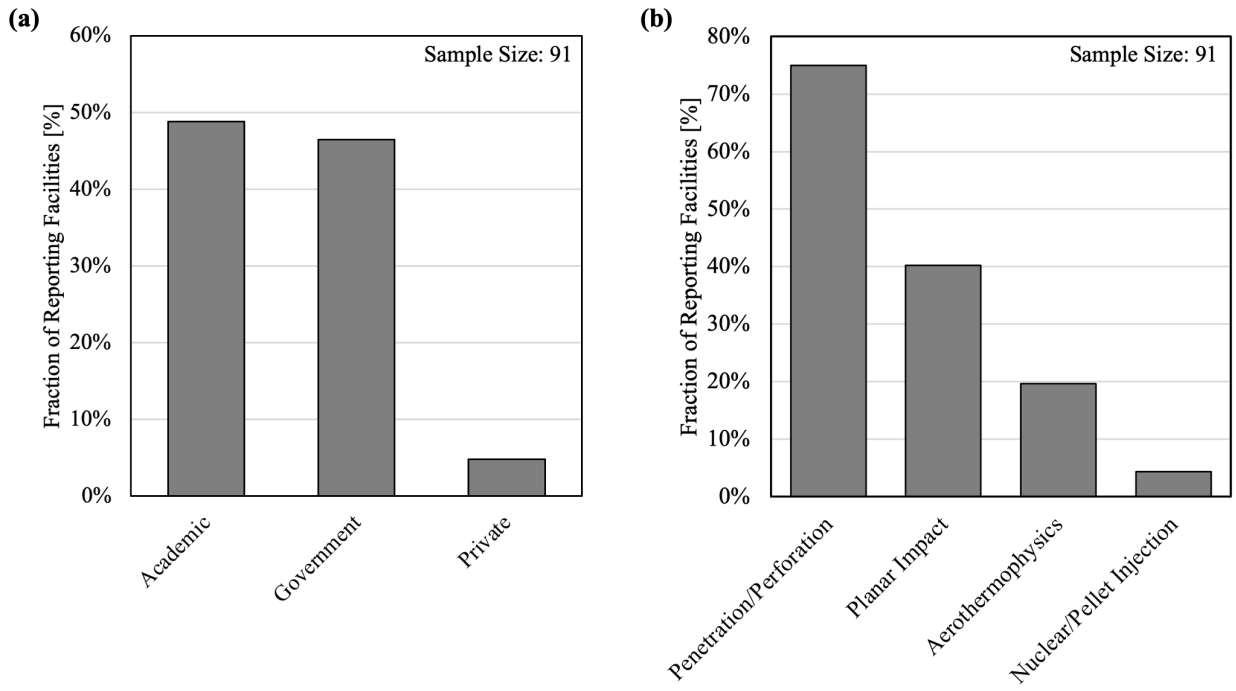

Figure 19: An overview of the research applications of 2SLGGs, detailing (a) the fraction of 2SLGGs used in academic, government, and private laboratories, and (b) the fraction of 2SLGGs employed in various types of experiments, including perforation/penetration mechanics, planar impacts, hypersonic/aerothermophysics, flyer plate impacts, and nuclear/pellet injection.

information on these experiment types, as well as representative applications, can be found in Table 3.

6. Diagnostic Tools and Techniques

The progress in 2SLGG aeroballistic range research has largely depended on the concurrent development of diagnostic techniques and tools. Consequently, the field of *in-situ* diagnostics for ballistic events has a history spanning over 150 years [314]. Given that 2SLGG-launched projectiles can achieve speeds up to 10 km/s, a collection of ultra-high sampling rate diagnostics is typically required for real-time observations

Table 3: A list of key types of experiments performed using a 2SLGG, along with their associated research applications and representative facilities.

Experiment Type	Research Applications
Penetration/Perforation Mechanics (PM)	military protective materials/structures, MMOD spacecraft protection, planetary science and defense, hypersonic vehicle survivability
Planar Impacts (PI)	ultra-high strain rate behavior of materials, shock physics
Hypersonic/Aerothermophysics (HA)	hypersonic vehicle survivability and performance, hypersonic flow field characterization, reentry vehicle survivability and performance
Nuclear/Pellet Injection (N)	nuclear fusion

during experiments [314]. These diagnostic instruments, some specifically designed for 2SLGG laboratories and others adapted from pre-existing technologies, allow researchers to investigate HVI events and hypersonic projectile flight across much of the electromagnetic spectrum (from infrared to X-ray), as well as monitor various shock interactions. Diagnostic options have grown as impact velocities have increased and new technologies have emerged. Apart from *in-situ* diagnostic tools, many laboratories also utilize instruments for "postmortem" forensic analyses of projectiles and targets, although the majority of these tools are not exclusive to aeroballistic range testing and are not discussed in this context.

Diagnostics in 2SLGG aeroballistic range research can generally be grouped according to the method applied or the specific equipment utilized. Notable diagnostic *techniques* encompass still imaging [314], schlieren imaging [113, 299, 315, 316], particle tracking [113, 317–320], shadowgraphy [26, 32, 104–106, 112, 116, 127, 134, 141, 159, 163, 321–324], strobe photography [325, 326], high-speed spectroscopy [327–329], and digital image correlation (DIC) [159, 160, 330]. These methods play a crucial role in capturing and examining projectile/target behavior during HVI and hypersonic flight. To facilitate these techniques, a variety of diagnostic *instruments* are employed. Common tools include high-speed cameras [26, 32, 104–106, 116, 121, 127, 134, 141, 159, 163, 314, 331–335], flash X-ray systems [15, 105, 107, 115, 119, 133, 134, 140, 142, 152, 163, 166, 171, 175, 176, 336, 337], laser Doppler velocimeters [103], velocity interferometer system for any reflector (VISAR) [49, 100, 120, 166, 338, 339], streak cameras [102, 103, 114, 118, 177, 314], high-speed film [314], and photonic Doppler velocimetry (PDV) systems [47, 108, 128, 129, 134, 169, 193, 340, 341]. Moreover, additional diagnostic tools support the analysis, such as X-ray velocimeters [104, 116, 117, 342], laser Doppler vibrometers [264, 343], accelerometers [103, 105, 119], strain gauges [105, 106, 119, 152, 166, 176, 177, 182], load cells [103, 104, 119, 182], and microwave reflectometers [15, 133]. The timeline in Fig. 20 highlights several key milestones in *in-situ* diagnostic development. However, not all prevalent diagnostic platforms could be integrated into the timeline, as some techniques have no clear origin in the literature (*e.g.*, using laser curtains for projectile intervalometry). Together, the mentioned tools and techniques (as well as others) provide a wide range of data types necessary for investigating HVI and hypersonic phenomena. Typically, the selection of diagnostic techniques and tools utilized at a specific facility is closely related to the type of experiment conducted (see Section 5.2). The following passages highlight some of the primary diagnostic methods and instruments employed in 2SLGG aeroballistic range experiments.

In aeroballistic range experiments, the diagnostic triggering mechanism is a critical component due to the high projectile velocities (>2 km/s) and the short event durations of many diagnostic tools (microseconds). Velocimetry systems, which typically consist of two or more velocity "gates," are most commonly employed to provide these diagnostic triggers. As a projectile sequentially passes through each gate, the time difference between the gate arrivals is combined with the known distance between gates to compute a projectile velocity.

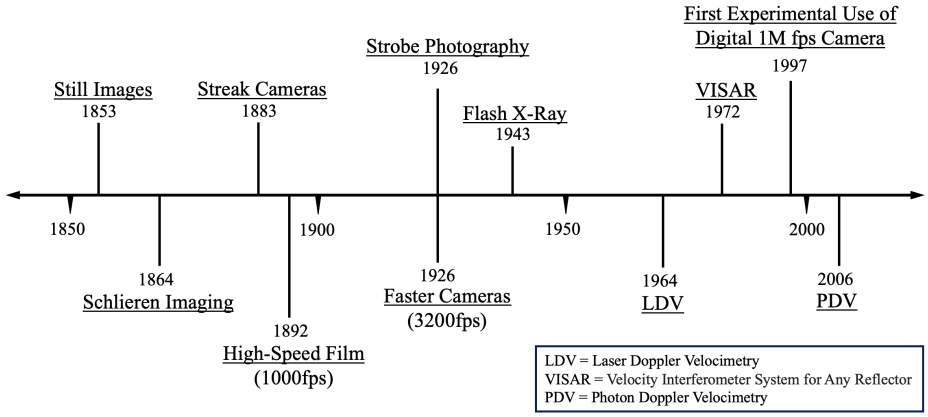

Figure 20: A timeline detailing the development of key diagnostics used in conjunction with 2SLGG aeroballistic ranges. The dates reported in this figure were sourced from Refs. [47, 49, 314, 315, 325, 331, 336, 343].

Concurrently, a preset or dynamic (velocity-dependent) delay trigger signal (*e.g.*, 5 V TTL) is sent to the diagnostic instruments. Although velocimetry systems operate in a similar fashion, various instruments can be employed to capture the projectile velocity, including lasers, induction coils, shorting pins, and continuous X-ray sources.

Many ranges, for instance, often use laser intervalometry or laser velocimetry systems (LVSs) [26, 101, 102, 119, 128, 133, 134, 137, 140, 163, 168, 227–229]. The shift to LVSs was partially driven by the introduction of cheaper and more reliable LED lasers. An LVS involves projecting two or more laser "curtains" perpendicular to the projectile's free flight path, with emitters on one side and photodiodes on the other. Projectile velocity is then calculated by dividing the gate distance by the time between laser curtain voltage drops, as detected by a high sampling rate oscilloscope.

X-ray beams and detectors can also be used instead of laser curtains and photodetectors, resulting in a velocimetry system that can better circumvent false triggers caused by airborne particulates, debris, and muzzle blasts [104, 116, 117, 342]. Induction coils can similarly serve as gates, as a voltage generated when the projectile travels through the coil can be detected by an oscilloscope [234]. Shorting pins, on the other hand, are employed in applications involving direct contact between two bodies [344]. A thin electrically charged wire creates a voltage drop when contacted by a moving body and subsequently bent to make contact with a local "ground." Despite being frequently damaged or destroyed during experiments, shorting pins are still widely utilized in several laboratories due to their usefulness in taking timestamp measurements in confined or heavily shielded spaces where optical techniques are not feasible [114, 120, 168, 344]. These sacrificial methods, in addition to "make" or "break" screens [345], can also be extended to capture the velocity of other relevant objects, such as impact ejecta, debris, or the 2SLGG compression piston, demonstrating their

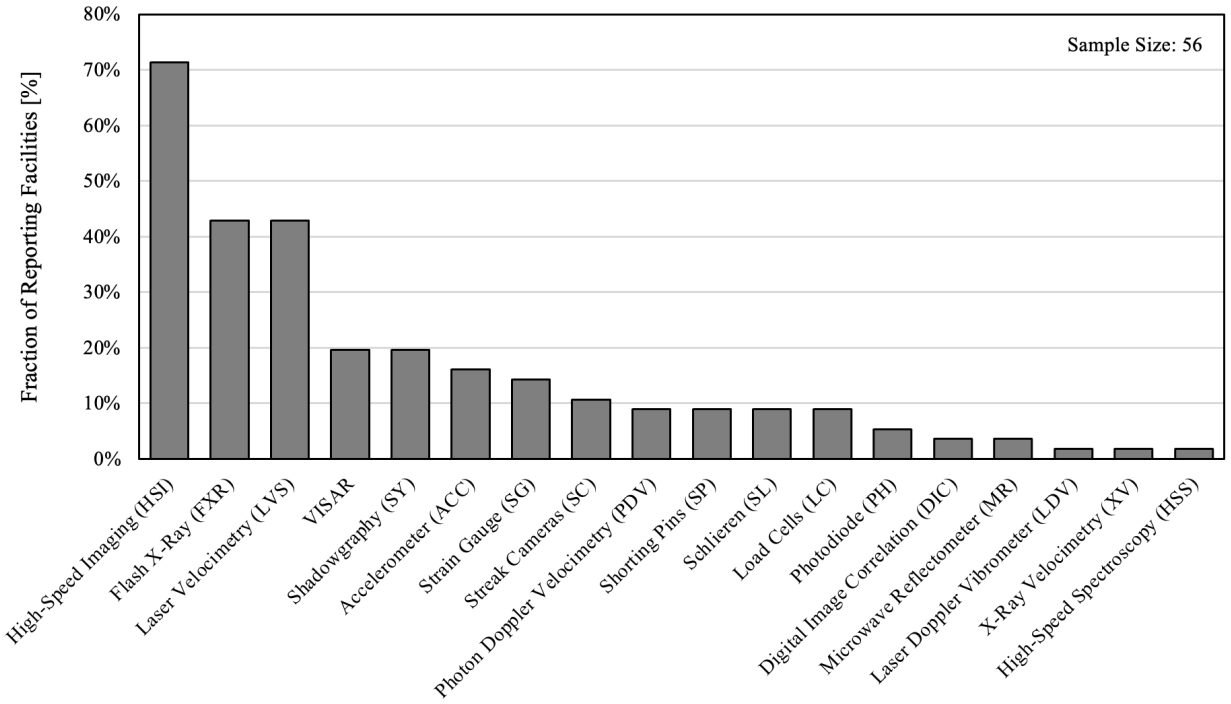

Figure 21: The percentage of key supporting diagnostics and instruments used at 56 of the 91 reporting facilities. Abbreviations correspond to those used in Appendix A, Table 6.

versatility in various experimental contexts.

High-speed imaging (HSI) has become the most prevalent diagnostic tool in 2SLGG facilities; nearly 70% of reporting facilities have implemented HSI (Fig. 21). Historically, researchers utilized various ingenious mechanical techniques to capture impact events or hypersonic flights at megahertz resolution with film cameras [314]. However, over the past three decades, advances in digital computing, memory storage speed, digital optical arrays, and lighting have led to the implementation of digital cameras for video recording [26, 32, 104–106, 116, 121, 127, 134, 141, 159, 163, 198, 314, 331]. Digital images offer two main advantages: (1) ease of duplication and sharing and (2) the ability to harness computerized post-processing techniques to extract more data points and types than possible with film images. Many modern facilities employ commercial cameras like the Hyper Vision (Shimadzu Corp.) [332], Kirana (Specialized Imaging Ltd.) [333], Phantom (Vision Research) [334], and Photron FASTCAM (Photron) [335], with frame rates exceeding $\sim$1 GHz and exposures down to $\sim$50 ns or less. The total number of frames can exceed 100, and the frame rate can be adjusted depending on the experiment duration. In general, an increase in the frame rate is inversely proportional to image resolution and record duration (number of frames). This relationship imposes some limitations, but capabilities are improving as technology advances. Depending on the experiment type, one or more high-speed cameras can be used, and they can support various diagnostic techniques such as shadowgraphy, schlieren imaging, digital particle tracking, and DIC.

Shadowgraphy is one of the most common imaging techniques used in 2SLGG aeroballistic range research [26, 32, 104–106, 112, 116, 127, 134, 141, 159, 163, 321–324]. It involves positioning a high-speed camera on one side of the target tank opposite a high-intensity light source (*e.g.*, a high-intensity LED [346] or flash bulbs [347]). Both the camera and light sources are arranged perpendicular to the launch tube (and projectile flight) axis, allowing maximum light entry through the camera lens. This setup enables image capture at minimal exposure times and maximum frame rates, producing high-contrast images. Schlieren imaging is another established technique for examining density variations in gas flows across subsonic, supersonic, and hypersonic environments [315]. As a result, it can be used to effectively visualize flow characteristics like bow shocks, turbulence, and interactions between shocks and particles. The technique works by selectively obstructing refracted light from areas with high-density gradients, which are then represented through changes in light intensity [315]. Although various schlieren setups exist, a straightforward lens-based system has demonstrated its effectiveness in analyzing structures within hypersonic flows [46, 113, 299, 316].

Videography alone yields only qualitative data and necessitates additional post-analysis tools. To produce more quantitatively significant data, custom image processing algorithms have been developed that utilize high-speed videography images of projectiles, targets, debris fragments, and other elements to obtain time-resolved data on fragment sizes, two-dimensional (2D) positions, velocities, and rotations [113, 317, 318, 320]. This information can be employed to estimate the kinetic energy and momentum of both the incoming projectile and ejecta/debris, as well as the absorption and transfer of impact energy. Another way to extract quantitative information from high-speed images is *via* DIC [159, 160, 330]. Appropriately arranged single (2D DIC) or stereoscopic [three-dimensional (3D) DIC] cameras can be employed to capture the temporal evolution of a random speckle pattern on a target surface. Post-processing algorithms can extract 2D or 3D surface displacements from the images that can be used to approximate the rapidly evolving strain field [348]. In these ways, visible light cameras combined with one or more of the various diagnostic techniques can provide rich qualitative and quantitative data, the quality of which will only improve as technology advances and new techniques emerge.

High-speed visible light cameras offer valuable insights into ultra-high-rate events. During HVI events, however, the ejecta and debris from both the impact and exit sides of the target can obstruct the observation of projectile and target erosion, plastic deformation, fracture, and/or fragmentation processes. Additionally, as the penetration or perforation event progresses, the target itself can obscure the view of the projectile. Flash X-ray (FXR) systems, employed in 45% of surveyed facilities (Fig. 21), address many of these challenges by generating short-duration, high-intensity pulses, to capture a series of high-rate radiographs [15, 105, 107, 115, 119, 133, 134, 140, 142, 152, 163, 166, 171, 175, 176, 337]. Powered by super-capacitors charged up to hundreds of kilovolts, FXR systems can penetrate dense ejecta/debris fields, as well as intact targets, to

more clearly capture projectile/target interactions during impact. FXR systems can be either single-anode or multi-anode [349]. Single anode systems typically consist of one or more "tubes" or cylindrical "heads" fixed at various angles on planes perpendicular to the launch tube axis (projectile flight axis). For each head, a radiograph film is positioned on the opposite side of the target from the X-ray source and alone the head axis. Upon triggering, each head generates a multi-nanosecond pulse of high-energy X-rays at a predetermined voltage, commonly in the range 10–1000 kV, with higher voltages providing greater X-ray penetration capability. However, these single-anode systems have limitations because they can only capture a single instant in time. Multiple heads are required to capture temporally and spatially varying radiographs, but cost and space limitations make multi-head FXR systems unobtainable for many facilities. Multi-anode systems partially overcome these limitations by using a single tube with multiple anodes to generate temporally spaced X-ray pulses [349]. A colinear scintillator screen detects these pulses and produces a rapidly decaying image captured by a high-speed camera [350]. This approach allows operators to capture approximately ten radiographs in a shadowgraph fashion, with the FXR source serving as the illumination. Although FXR systems have numerous potential applications, they are predominantly used in penetration and perforation mechanics experiments (see Section 5.2).

In planar impact experiments, the primary focus lies in studying the transmission and reflection of impact-induced high-amplitude stress or shock waves through a sample (see Section 5.2). High-speed cameras are generally unsuitable for observing shock wave behavior in non-transparent media. Hence, many facilities employ free-surface velocity measurement techniques to determine shock arrival times and free-surface velocity histories. One widely used method in planar impact and shock physics experiments is PDV [108, 128, 129, 134, 169, 193, 340, 341], which was developed at LLNL by Strand *et al.* in 2006 and has largely supplanted the earlier VISAR systems [47]. PDV works by reflecting incident laser light from an optical fiber off a free surface and back into the optical fiber. The movement of the target surface causes the reflected light to undergo a Doppler shift, generating a detectable beat frequency that can be analyzed by an oscilloscope to compute the instantaneous free surface velocity. Faster oscilloscopes enable the measurement of higher free surface velocities. By employing PDV measurements, researchers can characterize a material's shocked state using Rankine-Hugoniot relations to facilitate equation of state development and implementation. PDV arrays offer advantages over VISAR, as they are simpler to assemble using more affordable and more widely available components, allowing laboratories to construct systems with a greater number of data channels than VISAR technology permits [351]. As the technology has matured, complete commercial PDV systems have even become available [352, 353].

The advancement of diagnostic techniques and tools has become a primary focus in 2SLGG aeroballistic range research, as high-fidelity data capture for all experiment types relies heavily on the quality and speed

of data acquisition. In certain instances, the application of existing methods or instruments to a new research problem can render novel, innovative data. For example, digital in-line holography (DIH) is gaining traction as a promising diagnostic technique for 2SLGG aeroballistic ranges [230, 354–356]. Utilizing high-speed cameras, DIH facilitates the acquisition of 3D position, velocity, and acceleration data of hypervelocity and hypersonic particles from 2D images. This method involves capturing the interference pattern generated by the interaction between a reference light and the light scattered by the object of interest [357, 358]. Subsequently, the recorded hologram can be digitally reconstructed, enabling the measurement of the object's size, shape, and position in 3D space for each high-speed image (time step). This innovative approach has significant implications for tracking HVI-induced ejecta and debris, as well as estimating target energy dissipation.

Additionally, ultra-high-speed spectroscopy has emerged as another promising diagnostic tool, offering valuable insights into the chemical composition and physical properties of materials under extreme conditions. For example, this technique has been employed to investigate the bright flash emitted during an HVI, uncovering critical information about the underlying physical processes, such as material ionization and plasma generation [327–329]. By analyzing the emitted light from materials subjected to high temperatures or pressures, researchers can gain a deeper understanding of the material's atomic and molecular structure nanoseconds after impact, thereby elucidating energy absorption and failure mechanisms more comprehensively. Despite significant progress, the current advanced diagnostic methods and technologies provide limited insight into the physical phenomena that take place during crucial hypervelocity, hypersonic, and other ultra-high-speed events. Hence, there is a substantial need to tailor existing technologies to tackle issues associated with aeroballistic range research. Table 4 presents a selection of essential diagnostic methods and tools, as well as their applications.

7. Performance Prediction Methods for Two-Stage Light Gas Guns

Predicting 2SLGG muzzle velocity for a given experiment presents a significant challenge due to the relatively large number of operational parameters (powder mass and type, working gas pressure and type, petal valve burst pressure, projectile mass, *etc.*). This issue is compounded by intrinsic frictional losses and launch tube bore erosion, as well as variations in powder burn rate, piston release pressure, petal valve burst pressure, and other factors. Yet, robust performance predictive tools/methods are necessary to reduce experimental costs and turnaround times. Hence, a number of analysis techniques have been researched since the early development of 2SLGGs [2, 20]. The level of sophistication and accuracy of a given model varies based on its intended application(s). For example, many 2SLGG users need only algorithms for muzzle

velocity prediction. More comprehensive predictive tools used by 2SLGG designers, however, must also be able to resolve breech pressures, pump tube piston and projectile dynamics, compressible flows, petal valve mechanics, precise event timing, bore erosion, *etc.*, in addition to projectile muzzle velocity. As a result, various predictive methodologies have been explored, including empirical models, closed-form solutions, and numerical models. This section highlights some notable 2SLGG performance prediction techniques.

7.1. Empirical Approaches

One simple yet effective way to predict 2SLGG muzzle velocity is through interpolation or careful extrapolation of previous experimental data. Typically, such performance "curve fitting" models seek to reliably predict muzzle velocity *for a given 2SLGG*. Statistical analyses and normalization metrics can, however, enable some comparison between 2SLGGs of different sizes and simplify interpolation operations. Even so, large (and costly) data sets are required to span a given 2SLGG's performance envelope and to quantify its associated random errors for similar or even identical inputs. Many 2SLGG users will fix key operational parameters (*e.g.*, WG and petal valve burst pressures) to reduce random error and simplify prediction procedures. Despite these limitations, simple empirical prediction approaches are usually the most accurate (for a given gun) and, therefore, have historically been the most widely used methods.

More recently, simple curve fitting methods have been augmented with more sophisticated neural networks. Fraunhofer EMI [104, 342] pioneered this effort, developing a neural network to predict 2SLGG muzzle velocity and optimize operational parameters. Efforts to incorporate machine learning have also been reported elsewhere [359]. Many computational resources and advanced regression techniques have recently emerged, including artificial neural networks [360], support vector regression [361], and Gaussian

Table 4: A representative list of diagnostics and instruments commonly utilized in 2SLGG aeroballistic range facilities. The table includes examples of diagnostic and instrument applications, as well as the names of representative facilities that employ each respective diagnostic or instrument.

No.	Experimental Diagnostic/Instrument	Representative Applications
1	High-Speed Imaging (HSI)	Projectile/target characterization (HVI); flow characterization (hypersonic)
2	Flash X-Ray (FXR)	Projectile/target characterization during HVI
3	Laser Velocimetry System (LVS)	Hypervelocity/hypersonic projectile velocimetry
4	VISAR	HVI target free surface velocity measurements
5	Shadowgraphy (SY)	High-contrast hypervelocity/hypersonic projectile/target imaging
6	Accelerometer (ACC)	Target vibration and load measurements during HVI
7	Strain Gauge (SG)	2SLGG performance diagnostics,
8	Streak Cameras (SC)	Phenomena boundary tracking and particle path recording
9	Photon Doppler Velocimetry (PDV)	HVI target free surface velocity measurements; projectile velocity history
10	Shorting Pins (SP)	2SLGG compression piston velocimetry; general velocimetry
11	Schlieren (SL)	Hypersonic flow field visualization
12	Load Cells (LC)	Projectile-target momentum transfer measurements
13	Photodiode (PH)	Muzzle flash detection (diagnostic triggering); projectile velocimetry
14	Digital Image Correlation (DIC)	*In-situ* target deformation measurements during HVI
15	Microwave Reflectometer (MR)	Piston and projectile velocity measurement while inside the barrel
16	Laser Doppler Vibrometer (LDV)	HVI target free surface velocity measurements
17	X-Ray Velocimetry (XV)	Hypervelocity/hypersonic projectile velocimetry through dense debris
18	High-Speed Spectroscopy (HSS)	HVI flash characterization

process regression [362], each with their own complexities, strengths, degree of accuracy, and precision. Neural networks are particularly promising for regression tasks since they function as universal approximators [363]. While not currently in widespread use, neural network and machine learning prediction approaches for 2SLGG performance will undoubtedly become more prevalent as these technologies continue to mature and large empirical data sets become increasingly available.

7.2. Closed Form Solutions

Despite the large number of operational parameters and uncertainties in 2SLGG usage, a number of simple, closed-form solutions/equations have been derived from first principles to estimate the highest possible 2SLGG muzzle velocity (U_P) [2, 10]. Recall, one noteworthy equation, credited to Langweiler [96], calculates U_P based on WG temperature (T), molecular weight (M), and ratio of specific heats (γ), *i.e.,*

$$U_P \approx \sqrt{\frac{2\frac{RT}{M}}{\gamma - 1}}, \tag{1}$$

where Eq. (1) is repeated here for ease of comparison. This expression provides a reasonable estimate of the maximum achievable muzzle velocity, but it does not consider the specifics of the gun or the projectile. In contrast, Swift [6] described a relationship for U_P that takes into account key projectile features:

$$U_p \approx \sqrt{\frac{2Gd_p^3}{m_p}}, \tag{4}$$

where m_p is the total launch mass, d_p is the launch tube diameter, and G is an empirical fitting parameter with units of pressure ($G = 40.0$ GPa for most guns). These models are clearly limited in that they cannot be used to optimize a set of launch parameters. Further, they are typically only applicable over a narrow portion a gun's performance (kinetic energy) envelope. Nevertheless, such closed-form expressions provide valuable insights into the fundamental physics of 2SLGGs. For instance, Eq. (1) illustrates that gun performance is proportional to WG temperature and inversely proportional to WG molecular weight, relationships that can be explained by variations in gas sound speed and the energy required for gas acceleration. Similarly, Eq. (4) reveals that maximum projectile velocity decreases with increasing projectile mass for a given launch tube diameter and that launch tube diameter can be increased to enhance the kinetic energy ceiling.

7.3. Physics-Based Numerical Models

Empirical and analytical prediction methods cannot resolve key processes that ultimately dictate 2SLGG muzzle velocity, such as powder combustion, piston release and translation, frictional heating, WG compression, petal valve rupture, projectile acceleration, and more. 2SLGG operations must be understood and

simulated to effectively design and optimize individual components. Numerical codes rooted in computational fluid dynamics (CFD) principles can be used to probe the physics of 2SLGG launches. In general, the WG dynamics, for example, are captured using established CFD algorithms that approximate the solution to differential equations derived from fundamental fluid flow conservation equations (continuity, momentum, and energy) [364]. Key 2SLGG sub-domains (*e.g.*, pump and launch tube volumes) are generally discretized into cells with set moving boundaries and initial conditions. The Piston Compression Light Gas Gun Performance (PCLGGP) [20] and the Light Gas Gun (LGGUN) [25] codes have been particularly influential and well-adopted. Despite nearly five decades of development and refinement [20, 25, 51, 92, 203], these approaches can have difficulty predicting 2SLGG performance given the wide range of potential operational parameters and configurations.

The PCLGGP code (aka "Charters Code" [20]) evolved from the first CFD-based 2SLGG prediction code developed at the Naval Ordnance Laboratory. This code employs a 1D, Lagrangian, time-implicit, transient, finite volume approach with moving boundary conditions. Compressible flows are modeled using the von Neumann-Richtmyer Artificial Viscosity method, Gaussian-upwind finite difference methods for numerical integration, and equations of state for light gas gun fluids and components. Key assumptions incorporated into PCLGGP include a 1D domain, adiabatic and frictionless flow (non-isentropic flow due to shock waves), and idealized powder gases composed of a perfect mixture of common combustion products. The code does not account for heat transfer, viscous diffusion (except for shock wave damping), turbulence, and heat conduction effects. The tube walls are considered adiabatic and frictionless, and the gun components serve as a fixed, inertial reference frame. The code approximates projectile muzzle velocity along with breech pressures, gas temperatures, piston velocity, projectile acceleration, *etc.* Because of the 2SLGG operational cycle idealizations (neglecting friction, heat loss, *etc.*), PCLGGP tends to over-predict muzzle velocity by ∼10–20%. Despite these limitations, the predictions generally agree with empirical data from numerous experiments and offer helpful guidance for 2SLGG operators and designers in a straightforward manner.

Over 30 years, Bogdanoff *et al.* [25, 51, 92, 203] developed the more sophisticated LGGUN that accounts for the effect of launch tube erosion (*e.g*, the entrainment of droplets of barrel wall material into the WG) in limiting the maximum achievable muzzle velocity for 2SLGGs [92]. In essence, LGGUN is a "quasi-1D," Lagrangian, time implicit, transient, finite volume approach with moving boundary conditions [25] that employs the Godunov method for highly compressible flows and the MacCormic predictor-corrector scheme for time advancement. The code accounts for piston-pump tube wall friction, gas viscosity effects, and has robust, empirically fitted equations of state. The "quasi" one-dimensionality accounts for radial heat transfer through the launch tube wall due to axially accelerating gases/solids during each time-step. In addition, LGGUN can be used model shock tunnels and other 1D, hypersonic flows. The code, however, relies on several

empirical fits and requires sensitive fitting parameters, which makes input data file formation challenging and requires expertise when interpreting predicted results [25]. LGGUN's complexity and theoretical rigor make it less user-friendly than PCLGGP but can provide insight into specific aspects of 2SLGG operational performance.

Both PCLGGP and LGGUN complement empirical and analytical approaches to enable better 2SLGG prediction, development, and optimization. These codes have further motivated other 2LSGG numerical prediction efforts [50, 94, 359, 365–369]. Table 5 presents a partial list of other relevant empirical, analytical, and numerical 2SLGG prediction efforts and provides key details for each.

8. Conclusions

Over the past seven decades, two-stage light gas gun (2SLGG) aeroballistic ranges have been instrumental in advancing the study of material behavior under hypervelocity impacts (HVIs) and hypersonic conditions. This review article provides a broad overview of more than 90 2SLGG aeroballistic ranges that have been operational since 1990, describing their working principles and assessing global experimental capabilities. 2SLGG launch tube diameters range from 1 mm to 203 mm, and aeroballistic ranges span from around a meter in length to hundreds of meters. Maximum muzzle velocities have surpassed 10 km/s for standard 2SLGGs, with even higher velocities for modified 2SLGGs, and kinetic energy thresholds range from a few joules to nearly 100 megajoules. 2SLGG aeroballistic ranges are located worldwide in countries such as the United States (47.1%), China (15.3%), Japan (8.2%), United Kingdom (8.2%), France (5.9%), Germany (3.5%), Canada (3.5%), South Korea (2.4%), Russia (2.4%), Italy (1.2%), Sweden (1.2%), and Australia (1.2%), with affiliations spanning academic (46%), government (48%), and private (6%) sectors. The study delves into the origins and research applications of 2SLGGs, emphasizing their relevance across

Table 5: An overview of analytical, empirical, and numerical prediction techniques for 2SLGG performance, including predictor/model name, classification, and key model details. Prediction techniques without definitive names are identified by reporting authors.

No.	Predictor/Model Name	Class	Key Details
1	Lexow *et al.* (2015) [104, 342]	Empirical	Neural network
2	Shojaei *et al.* (2022) [359]	Empirical	Machine learning; Random forest regression
3	Langweiler (1938) [10]	Analytical	Maximum theoretical muzzle velocity prediction
4	Swift (2005) [6]	Analytical	Maximum muzzle velocity prediction for 2SLGGs
5	Zhuang and Lu (2016) [365]	Numerical	1D ODEs; 2 linked models
6	Patin and Courter (1986) [94]	Numerical	1D; Time-dependent; 4 linked models; Nonlinear ODEs
7	Rajesh *et al.* (2007) [366]	Numerical	No viscosity/heat transfer; 5th order Runge-Kutta
8	Majzoobi *et al.* (2018) [367]	Numerical	Expansion on work by Rajesh *et al.* [366]
9	Dong and Cao (2022) [204]	Numerical	Employed Ansys Fluent, 6DOF, and dynamic mesh
10	LGGUN (Bogdanoff, 1995) [25]	Numerical	Gudunov code; Quasi-1D; includes bore erosion & friction
11	PCLGGP (Charters *et al.*, 1973) [20]	Numerical	Linear ODEs; Ignores heat transfer and friction
12	QUICKGUN (Milora *et al.*, 1990) [368]	Numerical	Uses "method of characteristics"
13	Piacesi *et al.* (1963) [369]	Numerical	Uses Richtyer-von Neuman "q" method
14	Rynearson and Rand (1972) [50]	Numerical	Uses isentropic compression method; nonlinear ODEs

various disciplines, including shock physics, planetary science, defense, nuclear physics, hypersonic vehicle survivability and performance, and spacecraft protection. A synopsis of HVI phenomena accentuates the need for 2SLGGs and clarifies the commonalities and disparities among diverse 2SLGG aeroballistic ranges and supportive methodologies.

2SLGG working principles, configurations, and operations are also examined and compared. The maximum muzzle velocity is inversely proportional to working gas molecular weight and directly proportional to gas temperature, prompting many facilities to adopt hydrogen as the working gas. 2SLGGs can be powder-driven, compressed gas-driven, and gaseous detonation-driven, with powder-driven systems being the most common (80%) and highest-performing. The review presents current 2SLGG performance capabilities and uses facility survey findings to report current aeroballistic range tankage configurations, experiment types, research applications, and diagnostic instruments and techniques. Generally, range tankage can be categorized by one or more of the following configurations: (a) a separated blast tank and target tank, (b) a near-muzzle chamber, or (c) a combined blast tank and free flight range tank. The most prevalent diagnostic tools employed in these facilities include high-speed imaging (70%), flash X-ray (45%), laser velocimetry (45%), and PDV and/or VISAR (30%). In addition, a brief overview of 2SLGG performance prediction methods is presented. While many facilities depend on historical experimental data to predict muzzle velocity, analytical and numerical predictive tools can supplement empirical empirical models/data. Overall, this study underscores the multifaceted and interdisciplinary strategies and capabilities available to characterize HVIs and hypersonic phenomena over a range of environmental conditions and spatial scales.

Acknowledgments

This research is based upon work partially supported by the National Science Foundation Graduate Research Fellowship under Grant No. 1746932. David Strange at Physics Applications, Inc. provided significant guidance on the history and operations of 2SLGGs. In addition, the authors acknowledge Brynn Martin for her support during the initial review stages of this effort. The views and conclusions contained in this document are those of the authors and should not be interpreted as representing the official policies, either expressed or implied, of the Army Research Office or the U.S. Government. The U.S. Government is authorized to reproduce and distribute reprints for Government purposes notwithstanding any copyright notation herein.

Appendix A

This appendix presents a summary of key aeroballistic range features reported in the literature: organization type, diagnostics, research class, and range tankage configuration (open *vs.* closed). These features, distinct from the *2SLGG performance/operational* data presented in Table 1, describe a given range's capabilities rather than the corresponding 2SLGG, itself. This data was instrumental in creating figures and making broad conclusions in this review paper. It provides a broader perspective on the research capabilities and application areas for the 2SLGG aeroballistic ranges reported in Table 1.

Table 6: Aeroballistic range features available in the literature. Here, key reported diagnostic instruments and methods include high-speed imaging (HSI), flash X-ray (FXR), laser velocimetry (LVS), velocity inteferometer system for any reflector (VISAR), shadowgraphy (SY), accelerometers (ACC), strain gauges (SG), streak cameras (SC), photon doppler velocimetry (PDV), shorting pins (SP), schlieren (SL), load cells (LC), photodiode (PH), digital image correlation (DIC), microwave reflectometers (MR), laser doppler vibrometers (LDV), X-ray velocimetry (XV), and high-speed spectroscopy (HSS) (see Fig. 21 and Table 4 in Section 6). Similarly, research classes include penetration/perforation mechanics (PM), planar impacts (PI), hypersonic/aerotherophysics (HA), and nuclear/pellet injection (N) (see Fig. 19 and Table 3 in Section 5.2).

No.	Facility	Organization Type	Diagnostics	Research Class	Range Tankage Configuration
1	Mississippi State University - I	Academic	PH	PM	Closed
2	Drexel University	Academic	HSI	PI, PM	Closed
3	Caltech	Academic	HSI, VISAR, PH	PM	Closed
4	Commissariat a l'Energie Atomique - I	Government	HSI, LVS	PM	Closed
5	National Defense Academy	Academic	LVS	PM	Closed
6	Commissariat a l'Energie Atomique - II	Government	···	N	···
7	NASA MSFC - I	Government	HSI, LVS	PI, PM	Closed
8	University of Kent	Academic	LVS	PM	Closed
9	Rice University	Academic	···	PM	···
10	NASA WSTF - I	Government	ACC, FXR, HSI, LVS, SG SY	PI, PM	Closed
11	Oak Ridge National Lab	Government	···	N	Closed
12	The Open University	Academic	···	PM	Closed
13	NASA JSC	Government	FXR, HSI, LVS	PM	Closed
14	PERC, Chita	Academic	HSI	PI	Closed
15	NASA MSFC - II	Government	···	HA, PM	Closed

Table 6: Aeroballistic range features available in the literature. Here, key reported diagnostic instruments and methods include high-speed imaging (HSI), flash X-ray (FXR), laser velocimetry (LVS), velocity inteferometer system for any reflector (VISAR), shadowgraphy (SY), accelerometers (ACC), strain gauges (SG), streak cameras (SC), photon doppler velocimetry (PDV), shorting pins (SP), schlieren (SL), load cells (LC), photodiode (PH), digital image correlation (DIC), microwave reflectometers (MR), laser doppler vibrometers (LDV), X-ray velocimetry (XV), and high-speed spectroscopy (HSS) (see Fig. 21 and Table 4 in Section 6). Similarly, research classes include penetration/perforation mechanics (PM), planar impacts (PI), hypersonic/aerotherophysics (HA), and nuclear/pellet injection (N) (see Fig. 19 and Table 3 in Section 5.2).

No.	Facility	Organization Type	Diagnostics	Research Class	Range Tankage Configuration
16	Mississippi State University - II	Academic	HSI	PM	Closed
17	University of Nevada, Las Vegas	Academic	PDV, LVS,	PI	Closed
18	Fraunhofer EMI - I	Government	ACC, HSI, LC, LVS, PH, SY, SC	PM	Closed
19	University of Padua	Academic	ACC, LVS, SY	PM	Closed
20	Japan Aerospace Exploration Agency	Government	HSI, PH	PM	Closed
21	Johns Hopkins University	Academic	FXR, HSI, LVS	HA, PI, PM	Closed
22	Cranfield University	Academic	FXR, HSI, SG	PI	Closed
23	Hypervelocity Aerodynamics Institute - I	Government	FXR, HSI, LVS, MI, SL, SY	PM	Closed
24	Denver Research Institute	Academic	···	PI, PM	···
25	Brookhaven National Lab	Government	···	PM	Closed
26	KAIST	Academic	···	PM	Closed
27	National Research Tomsk University - I	Academic	FXR	···	···
28	Corvid	Government	···	PM	···
29	Fraunhofer EMI - II	Government	ACC, HSI, LC, LDV, SC, SY	PM	Closed
30	University of New Brunswick - I	Academic	DIC, HSI	PM	Closed
31	Imperial College London	Academic	···	PI	···
32	Kyushu Institute of Technology	Academic	LVS	PM	···
33	TiTech	Academic	VISAR	PI	Closed
34	Thiot Ingenierie	Private	FXR, HSI, LVS	PI, PM	Closed
35	Texas A&M University	Academic	FXR, HSI, LVS, SL, SY	HA, PM	···
36	NASA WSTF - II	Government	ACC, FXR, HSI, LVS, SG, SY	PI, PM	Closed
37	First Light Fusion - I	Private	HSI, SC, SL, SP, SY	HA, N	Closed
38	Argonne National Lab	Government	PDV	PI, PM	Closed

Table 6: Aeroballistic range features available in the literature. Here, key reported diagnostic instruments and methods include high-speed imaging (HSI), flash X-ray (FXR), laser velocimetry (LVS), velocity inteferometer system for any reflector (VISAR), shadowgraphy (SY), accelerometers (ACC), strain gauges (SG), streak cameras (SC), photon doppler velocimetry (PDV), shorting pins (SP), schlieren (SL), load cells (LC), photodiode (PH), digital image correlation (DIC), microwave reflectometers (MR), laser doppler vibrometers (LDV), X-ray velocimetry (XV), and high-speed spectroscopy (HSS) (see Fig. 21 and Table 4 in Section 6). Similarly, research classes include penetration/perforation mechanics (PM), planar impacts (PI), hypersonic/aerotherophysics (HA), and nuclear/pellet injection (N) (see Fig. 19 and Table 3 in Section 5.2).

No.	Facility	Organization Type	Diagnostics	Research Class	Range Tankage Configuration
39	NASA AVGR	Government	HSI	HA	Closed
40	Naval Surface Warfare Center - I	Government	FXR, HSI, SG, VISAR	PI, PM	···
41	Royal Military College of Science	Academic	FXR, HSI	PM	Closed
42	Tohoku University - I	Academic	HSI	PM	···
43	Hypervelocity Aerodynamics Institute - II	Government	FXR, HSI, LVS, MI, SL, SY	PM	···
44	China Academy of Space Technology - I	Government	···	PI	Closed
45	AEDC - I	Government	···	HA, PM	···
46	Tohoku University - II	Academic	FXR, SC	PM	···
47	UDRI - I	Academic	ACC, FXR, HSI, LC LVS, SG	PI, PM	···
48	University of British Columbia	Academic	SP, LVS	PI	Closed
49	University of New South Wales	Academic	HSI, LVS, PDV	PI, PM	···
50	Commissariat a l'Energie Atomique - III	Government	FXR, HSI, TH, VISAR	PI, PM	Closed
51	National Research Tomsk University - II	Academic	···	PM	···
52	University of California, Davis	Academic	LVS, SP, VISAR	PM	···
53	China Academy of Space Technology - II	Government	···	PI, PM	···
54	Hypervelocity Aerodynamics Institute - III	Government	···	HA	Closed
55	Seoul National University	Academic	HSI, FXR	PM	Closed
56	University of New Brunswick - II	Academic	HSI, DIC	PM	···
57	National Institute for Material Science	Government	VISAR, SG, SC, FXR	PI	···
58	NASA WSTF - III	Government	ACC, FXR, HSI, LVS, SG, SY	PI, PM	···
59	Engineering Research Development Center	Government	HSI	PM	···
60	Wuhan University	Academic	···	PI	Closed
61	Lawrence Livermore National Laboratory - I	Government	FXR, VISAR	PI	Closed

Table 6: Aeroballistic range features available in the literature. Here, key reported diagnostic instruments and methods include high-speed imaging (HSI), flash X-ray (FXR), laser velocimetry (LVS), velocity inteferometer system for any reflector (VISAR), shadowgraphy (SY), accelerometers (ACC), strain gauges (SG), streak cameras (SC), photon doppler velocimetry (PDV), shorting pins (SP), schlieren (SL), load cells (LC), photodiode (PH), digital image correlation (DIC), microwave reflectometers (MR), laser doppler vibrometers (LDV), X-ray velocimetry (XV), and high-speed spectroscopy (HSS) (see Fig. 21 and Table 4 in Section 6). Similarly, research classes include penetration/perforation mechanics (PM), planar impacts (PI), hypersonic/aerotherophysics (HA), and nuclear/pellet injection (N) (see Fig. 19 and Table 3 in Section 5.2).

No.	Facility	Organization Type	Diagnostics	Research Class	Range Tankage Configuration
62	Sandia National Labs	Government	HSI, HSS, PDV, ORVIS, VISAR	HA, PI	···
63	Los Alamos National Lab - II	Government	···	PI	···
64	Chinese Academy of Sciences	Government	···	PM	Closed
65	UDRI - II	Academic	ACC, FXR, HSI, LC, LVS, SG	PI, PM	···
66	Northwest Institute of Nuclear Technology - I	Government	···	PM	Closed
67	Swedish Defence Research Agency	Government	FXR	PI, PM	Closed
68	Eglin Air Force Base	Government	···	PM	Open
69	Southwest Jiaotong University	Academic	···	PI	···
70	University of Alabama - I	Academic	···	HA, PM	Closed
71	Institute of Saint-Louis	Government	FXR, SL, SY	HA, PI, PM	Closed
72	Lawrence Livermore National Laboratory - II	Government	FXR, HSI, SP, LVS, VISAR	PI, PM	···
73	University of Alabama - II	Academic	···	HA, PM	···
74	Southwest Research Institute	Private	···	HA, PM	···
75	First Light Fusion - II	Private	HSI	N	Closed
76	New Mexico Tech - EMRTC	Academic	···	PM	···
77	NASA Ames HFFAF	Government	HSI	HA	···
78	Naval Surface Warfare Center - II	Government	FXR, HSI, SG, VISAR	FPI	···
79	Los Alamos National Lab - I	Government	···	PI, PM	···
80	Hypervelocity Aerodynamics Institute - IV	Government	···	PM	···
81	AEDC - II	Government	···	HA, PM	···
82	Lawrence Livermore National Laboratory - III	Government	FXR, HSI, SP, VISAR	PI, PM	Closed
83	Fraunhofer EMI - III	Governmnet	ACC, HSI, LC, SC, SY, XV	HA, PM	···
84	TAMU Ballistics Aero-Optics and Materials	Academic	···	HA, PM	···

Table 6: Aeroballistic range features available in the literature. Here, key reported diagnostic instruments and methods include high-speed imaging (HSI), flash X-ray (FXR), laser velocimetry (LVS), velocity inteferometer system for any reflector (VISAR), shadowgraphy (SY), accelerometers (ACC), strain gauges (SG), streak cameras (SC), photon doppler velocimetry (PDV), shorting pins (SP), schlieren (SL), load cells (LC), photodiode (PH), digital image correlation (DIC), microwave reflectometers (MR), laser doppler vibrometers (LDV), X-ray velocimetry (XV), and high-speed spectroscopy (HSS) (see Fig. 21 and Table 4 in Section 6). Similarly, research classes include penetration/perforation mechanics (PM), planar impacts (PI), hypersonic/aerotherophysics (HA), and nuclear/pellet injection (N) (see Fig. 19 and Table 3 in Section 5.2).

No.	Facility	Organization Type	Diagnostics	Research Class	Range Tankage Configuration
85	University of Alabama - III	Academic	···	HA, PM	Closed
86	AEDC - III	Government	···	HA, PI, PM	···
87	Agency for Defence Development	Government	HSI, LVS, PDV	PI	Closed
88	Harbin Institute of Technology	Academic	···	PM	···
89	Northwest Institute of Nuclear Technology - II	Government	···	PM	···
90	Beihang University	Academic	···	PM	···
91	Shenyang Ligong University	Academic	HSI	PM	···

References

[1] W. Y. Carman, A history of firearms: from earliest times to 1914, Routledge, 2015.

[2] T. N. Canning, A. Seiff, C. S. James, Ballistic-range technology, Tech. rep., Advisory Group for Aerospace Research and Development Neuilly-Sur-Seine (France) (1970).

[3] E. M. Schmidt, The Aerodynamics Range: A National Historic Mechanical Engineering Landmark, Tech. rep., The American Society of Mechanical Engineers (1983).

[4] S. J. Zaloga, Railway Guns of World War II, Bloomsbury Publishing, 2016.

[5] S. Signetti, A. Heine, Transition regime between high-velocity and hypervelocity impact in metals – a review of the relevant phenomena for material modeling in ballistic impact studies, International Journal of Impact Engineering 167 (2022) 104213. doi:https://doi.org/10.1016/j.ijimpeng.2022.104213.

[6] H. F. Swift, Light-gas gun technology: a historical perspective, in: L. C. Chhabildas, L. Davison, Y. Horie (Eds.), High-Pressure Shock Compression of Solids VIII, Springer-Verlag Berlin Heidelberg, Germany, 2005, Ch. 1, pp. 1–36.

[7] J. D. Walker, Modern impact and penetration mechanics, Cambridge University Press, 2021.

[8] A. Charters, B. P. Denardo, V. J. Rossow, Development of a piston-compressor type light-gas gun for the launching of free-flight models at high velocity, Tech. rep., NASA (1957).

[9] Z. Slawsky, Survey of NOL Hyperballistic Research, U.S. Naval Ordinance Laboratory, White Oak, Silver Spring, Maryland, United States, 1960, pp. 106–123.

[10] J. Corner, Theory of the interior ballistics of guns, Wiley, 1950.

[11] A. Piekutowski, K. Poormon, Development of a three-stage, light-gas gun at the University of Dayton Research Institute, International Journal of Impact Engineering 33 (1-12) (2006) 615–624.

[12] T. Thornhill, L. Chhabildas, W. Reinhart, D. Davidson, Particle launch to 19 km/s for micro-meteoroid simulation using enhanced three-stage light gas gun hypervelocity launcher techniques, International Journal of Impact Engineering 33 (1) (2006) 799–811. doi:https://doi.org/10.1016/j.ijimpeng.2006.09.015.

[13] L. Chhabildas, L. Kmetyk, W. Reinhart, C. Hall, Enhanced hypervelocity launcher - capabilities to 16 km/s, International Journal of Impact Engineering 17 (1) (1995) 183–194, Hypervelocity Impact. doi:https://doi.org/10.1016/0734-743X(95)99845-I.

[14] D. Veysset, J.-H. Lee, M. Hassani, S. E. Kooi, E. L. Thomas, K. A. Nelson, High-velocity micro-projectile impact testing, Applied Physics Reviews 8 (1) (2021) 011319.

[15] S. Liu, Ballistic range, in: Hypervelocity Launchers, Springer, 2016, pp. 23–52.

[16] E. Workman, Development of new gun using helium gas for projectile acceleration, Tech. rep., New Mexico School of Mines (1952).

[17] J. H. Grinstead, M. C. Wilder, D. C. Reda, C. J. Cornelison, B. A. Cruden, D. W. Bogdanoff, Shock tube and ballistic range facilities at NASA Ames Research Center, Tech. rep., NASA (2010).

[18] Aeroballistic Range Association (ARA) History, accessed: 2023-04-29.
URL https://www.aeroballistics.org/history.asp?di=

[19] AEDC's Range-G in operation for 50 Years, accessed: 2023-04-29.
URL https://www.arnold.af.mil/News/Article-Display/Article/804821/aedcs-range-g-in-operation-for-50-years/

[20] A. Charters, D. K. Sangster, Fortran computer program for interior ballistic analysis of light-gas guns, Informal Manual available from Dr. Charters, July (1973).

[21] J. C. Abell, Sept. 9, 1982: 3-2-1 ... liftoff! the first private rocket launch (sep 2009).
URL https://www.wired.com/2009/09/dayintech0909privaterocket/

[22] J. Charles E. Anderson, The Origins of the Hypervelocity Impact Society (2016).
URL https://hvis.org/docs/HVISV12I1.pdf

[23] Thiot Ingenierie: About Us (Dec 2020).
URL https://www.thiot-ingenierie.com/en/about-us/

[24] Physics Applications, Inc. - Company Profile and News, accessed: 2023-04-29.
URL https://www.bloomberg.com/profile/company/0068970D:US#xj4y7vzkg

[25] D. W. Bogdanoff, R. Miller, New higher-order godunov code for modelling performance of two-stage light gas guns, Tech. rep. (1995).

[26] D. Pavarin, A. Francesconi, F. Angrilli, A system to damp the free piston oscillations in a two-stage light-gas gun used for hypervelocity impact experiments, Review of Scientific Instruments 75 (1) (2004) 245–252.

[27] T. Moritoh, N. Kawai, S. Matsuoka, K. G. Nakamura, K. ichi Kondo, M. Katayama, Hypervelocity impact experiments up to 9 km/s by a compact multi-stage light-gas gun, International Journal of Impact Engineering 29 (1) (2003) 459–467. doi:https://doi.org/10.1016/j.ijimpeng.2003.09.042.

[28] A. F. Woolf, Conventional prompt global strike and long-range ballistic missiles: background and issues, Library of Congress Washington DC, 2021.

[29] Private Craft Soars Into Space, History.
URL http://www.cnn.com/2004/TECH/space/06/21/suborbital.test/

[30] R. Putzar, F. Schäfer, EMI's TwinGun Concept for a New Light-gas Gun Type Hypervelocity Accelerator, Procedia Engineering 103 (2015) 421–426. doi:10.1016/j.proeng.2015.04.041.

[31] M. LLC, Thiot Ingenierie reaches a new hypervelocity world record (2016).
URL https://www.thiot-ingenierie.com/en/2016/07/06/thiot-ingenierie-reaches-a-new-hypervelocity-world-record-2/

[32] M. Salvador, Hypervelocity Impact of Spherical Aluminum 2017-T4 Projectiles on Aluminum 6061-T6 Multi-Layered Sheets, Master's thesis, Mississippi State University (2017).

[33] H. Klinkrad, H. Stokes, Hypervelocity impact damage assessment and protection techniques, in: Space Debris, Praxis Publishing Ltd, Chichester, UK, 2006, Ch. 7, pp. 199–214.

[34] W. P. Schonberg, Studies of hypervelocity impact phenomena as applied to the protection of spacecraft operating in the MMOD environment, Procedia Engineering 204 (2017) 4–42. doi:10.1016/j.proeng.2017.09.723.

[35] F. L. Whipple, Meteorites and space travel, The Astronomical Journal 52 (1947) 131. doi:10.1086/106009.

[36] W. P. Schonberg, Hypervelocity impact penetration phenomena in aluminum space structures, Journal of Aerospace Engineering 3 (3) (1990) 173–185. doi:10.1061/(ASCE)0893-1321(1990)3:3(173).

[37] E. L. Christiansen, K. Nagy, D. M. Lear, T. G. Prior, Space station MMOD shielding, Acta Astronautica 65 (7-8) (2009) 921–929. doi:10.1016/j.actaastro.2008.01.046.

[38] W. P. Schonberg, Protecting spacecraft against meteoroid/orbital debris impact damage: an overview, Tech. rep. (2001).

[39] E. L. Christiansen, J. H. Kerr, Projectile shape effects on shielding performance at 7 km/s and 11 km/s 20 (1997) 165–172.

[40] R. Bernhard, E. Christiansen, D. Kessler, Orbital debris as detected on exposed spacecraft, International Journal of Impact Engineering 20 (1) (1997) 111 – 120. doi:https://doi.org/10.1016/S0734-743X(97)87485-4.

[41] E. Christiansen, Micrometeoroid and orbital debris (MMOD) risk overview (2014). doi:https://ntrs.nasa.gov/archive/nasa/casi.ntrs.nasa.gov/20140009950.pdf.

[42] S. Flegel, C. Wiedemann, S. Stabroth, D. Alwes, J. Bendisch, P. Vörsmann, Satellite failure risk due to hypervelocity impacts, in: Proceedings, 19th International Astronautical Congress, 2008.

[43] L. Lamberson, Investigations of high performance fiberglass impact using a combustionless two-stage light-gas gun, Procedia Engineering 103 (2015) 341–348. doi:https://doi.org/10.1016/j.proeng.2015.04.056.

[44] D. Carver, L. Campbell, B. Roebuck, Large-scale, hypervelocity, high-fidelity interceptor lethality development in AEDC's range G, International Journal of Impact Engineering 35 (12) (2008) 1459–1464, Hypervelocity Impact Proceedings of the 2007 Symposium. doi:https://doi.org/10.1016/j.ijimpeng.2008.07.036.

[45] J. Manin, S. A. Skeen, L. M. Pickett, Performance comparison of state-of-the-art high-speed video cameras for scientific applications, Optical Engineering 57 (12) (2018) 1 – 14. doi:10.1117/1.OE.57.12.124105.

[46] G. S. Settles, M. J. Hargather, A review of recent developments in schlieren and shadowgraph techniques, Measurement Science and Technology 28 (4) (2017) 042001.

[47] O. T. Strand, D. R. Goosman, C. Martinez, T. L. Whitworth, W. W. Kuhlow, Compact system for high-speed velocimetry using heterodyne techniques, Review of Scientific Instruments 77 (8) (2006) 083108. doi:10.1063/1.2336749.

[48] H. Swift, High-speed image-forming instrumentation for hypervelocity impact studies, International Journal of Impact Engineering 5 (1) (1987) 623–634, Hypervelocity Impact Proceedings of the 1986 Symposium. doi:https://doi.org/10.1016/0734-743X(87)90077-7.

[49] L. M. Barker, R. E. Hollenbach, Laser interferometer for measuring high velocities of any reflecting surface, Journal of Applied Physics 43 (11) (1972) 4669–4675. doi:10.1063/1.1660986.

[50] R. J. Rynearson, J. Rand, Optimization of a two stage light gas gun, Tech. rep. (1972).

[51] D. Bogdanoff, Optimization study of the Ames 0.5" two-stage light gas gun, International Journal of Impact Engineering 20 (1) (1997) 131–142. doi:https://doi.org/10.1016/S0734-743X(97)87487-8.

[52] A. Francesconi, D. Pavarin, A. Bettella, F. Angrilli, A special design condition to increase the performance of two-stage light-gas guns, International Journal of Impact Engineering 35 (12) (2008) 1510–1515.

[53] D. J. Grosch, J. P. Riegel, Development and optimization of a "micro" two-stage light-gas gun, International Journal of Impact Engineering 14 (1-4) (1993) 315–324.

[54] T. Moritoh, N. Kawai, K. G. Nakamura, K.-i. Kondo, Optimization of a compact two-stage light-gas gun aiming at a velocity of 9 km/s, Review of Scientific Instruments 72 (11) (2001) 4270–4272.

[55] W. Tang, Q. Wang, B. Wei, J. Li, J. Li, J. Shang, K. Zhang, W. Zhao, Performance and modeling of a two-stage light gas gun driven by gaseous detonation, Applied Sciences 10 (12) (2020) 4383.

[56] A. Cable, Upgrade of ballistic range facilities at AEDC, in: 17th Aerospace Ground Testing Conference, 1992, p. 3997.

[57] F. Seiler, O. Igra, Hypervelocity launchers, Springer, 2016.

[58] A. Stilp, Review of modern hypervelocity impact facilities, International Journal of Impact Engineering 5 (1-4) (1987) 613–621.

[59] S. Signetti, A. Heine, Characterization of the transition regime between high-velocity and hypervelocity impact: thermal effects and energy partitioning in metals, International Journal of Impact Engineering 151 (2021) 103774. doi:https://doi.org/10.1016/j.ijimpeng.2020.103774.

[60] G. Jonas, J. A. Zukas, Mechanics of penetration: analysis and experiment, International Journal of Engineering Science 16 (11) (1978) 879–903.

[61] Material characterization and constitutive modelling of ductile high strength steel for a wide range of strain rates, International Journal of Impact Engineering 31 (4) (2005) 401–433. doi:https://doi.org/10.1016/j.ijimpeng.2004.02.005.

[62] G. R. Johnson, A constitutive model and data for materials subjected to large strains, high strain rates, and high temperatures, Proc. 7th Inf. Sympo. Ballistics (1983) 541–547.

[63] G. R. Cowper, P. S. Symonds, Strain-hardening and strain-rate effects in the impact loading of cantilever beams, Tech. rep., Brown University (1957).

[64] F. J. Zerilli, R. W. Armstrong, Dislocation-mechanics-based constitutive relations for material dynamics calculations, Journal of Applied Physics 61 (5) (1987) 1816–1825.

[65] C. Sellars, W. McTegart, On the mechanism of hot deformation, Acta Metallurgica 14 (9) (1966) 1136–1138. doi:10.1016/0001-6160(66)90207-0.

[66] D. L. Preston, D. L. Tonks, D. C. Wallace, Model of plastic deformation for extreme loading conditions, Journal of Applied Physics 93 (1) (2003) 211–220. doi:10.1063/1.1524706.

[67] D. J. Steinberg, S. G. Cochran, M. W. Guinan, A constitutive model for metals applicable at high-strain rate, Journal of Applied Physics 51 (3) (1980) 1498–1504. doi:10.1063/1.327799.

[68] G. R. Johnson, W. H. Cook, Fracture characteristics of three metals subjected to various strains, strain rates, temperatures and pressures, Engineering Fracture Mechanics 21 (1) (1985) 31–48.

[69] Damage accumulation and fracture initiation in uncracked ductile solids subject to triaxial loading, International Journal of Solids and Structures 44 (16) (2007) 5163–5181. doi:10.1016/j.ijsolstr.2006.12.026.

[70] D. Grady, M. Olsen, A statistics and energy based theory of dynamic fragmentation, International Journal of Impact Engineering 29 (1-10) (2003) 293–306.

[71] B. Hopkinson, A method of measuring the pressure produced in the detonation of high explosives or by the impact of bullets, Proceedings of the Royal Society of London. Series A, Containing Papers of a Mathematical and Physical Character 89 (612) (1914) 411–413. doi:10.1098/rspa.1914.0008.

[72] G. I. Taylor, The use of flat-ended projectiles for determining dynamic yield stress i. theoretical considerations, Proceedings of the Royal Society of London. Series A. Mathematical and Physical Sciences 194 (1038) (1948) 289–299. doi:10.1098/rspa.1948.0081.

[73] G. I. Taylor, H. Quinney, The latent energy remaining in a metal after cold working, Proceedings of the Royal Society of London. Series A, Containing Papers of a Mathematical and Physical Character 143 (849) (1934) 307–326.

[74] E. Grüneisen, Theorie des festen zustandes einatomiger elemente, Annalen der Physik 344 (12) (1912) 257–306.

[75] J. H. Tillotson, Metallic equations of state for hypervelocity impact, Tech. rep., General Dynamics San Diego CA General Atomic DIV (1962).

[76] S. P. Lyon, SESAME: the Los Alamos National Laboratory equation of state database, Tech. Rep. LA-UR-92-3407, Los Alamos National Laboratory (1992).

[77] C. E. Anderson, T. G. Trucano, S. A. Mullin, Debris cloud dynamics, International Journal of Impact Engineering 9 (1) (1990) 89–113. doi:https://doi.org/10.1016/0734-743X(90)90024-P.

[78] R. Bjork, A. Olshaker, The role of melting and vaporization in hypervelocity impact, Tech. rep., Rand Corp Santa Monica Ca (1965).

[79] G. E. Duvall, R. A. Graham, Phase transitions under shock-wave loading, Rev. Mod. Phys. 49 (1977) 523–579. doi:10.1103/RevModPhys.49.523.

[80] R. Kinslow, Properties of spherical shock waves produced by hypervelocity impact, Tech. Rep. AD0421578, Arnold Engineering Development Center (1963).

[81] H. Hopkins, H. Kolsky, Mechanics of hypervelocity impact of solids, ARDE, 1960.

[82] J. Wilbeck, Classification of impact regimes, Tech. Rep. 06-9304, Southwest Research Institute (1985).

[83] S. Signetti, A. Heine, Characterization of the transition regime between high-velocity and hypervelocity impact: Thermal effects and energy partitioning in metals, International Journal of Impact Engineering 151 (2021) 103774.

[84] M. Liu, Q. Wang, Q. Zhang, R. Long, Z. Su, Characterizing hypervelocity (∼2.5 km/s)-impact-engendered damage in shielding structures using in-situ acoustic emission: Simulation and experiment, International Journal of Impact Engineering 111 (2018) 273–284. doi:10.1016/j.ijimpeng.2017.10.004.

[85] A. Jaramillo-Botero, M. L. Cable, A. E. Hofmann, M. Malaska, R. Hodyss, J. Lunine, Understanding hypervelocity sampling of biosignatures in space missions, Astrobiology 21 (4) (2021) 421–442, pMID: 33749334. doi:10.1089/ast.2020.2301.

[86] L. Murr, S. A. Quinones, E. Ferreyra T, A. Ayala, O. L. Valerio, F. Hörz, R. Bernhard, The low-velocity-to-hypervelocity penetration transition for impact craters in metal targets, Materials Science and Engineering: A 256 (1) (1998) 166–182. doi:10.1016/S0921-5093(98)00796-5.

[87] H. Fair, Hypervelocity then and now, International Journal of Impact Engineering 5 (1) (1987) 1–11, Hypervelocity Impact Proceedings of the 1986 Symposium. doi:10.1016/0734-743X(87)90027-3.

[88] S. A. Razzaqi, M. K. Smart, Hypervelocity experiments on oxygen enrichment in a hydrogen-fueled scramjet, AIAA Journal 49 (7) (2011) 1488–1497.

[89] S. Paik, S. Kim, Y. Yoo, M. Lee, Protection performance of dual flying oblique plates against a yawed long-rod penetrator, International Journal of Impact Engineering 34 (8) (2007) 1413–1422. doi:10.1016/j.ijimpeng.2006.06.006.

[90] Y.-H. Yoo, H. Shin, Protection capability of dual flying plates against obliquely impacting long-rod penetrators, International Journal of Impact Engineering 30 (1) (2004) 55–68. doi:10.1016/S0734-743X(03)00064-2.

[91] A. E. Seigel, The theory of high speed guns, Tech. rep., Advisory Group for Aerospace Research and Development Neuilly-sur-seine (France) (1965).

[92] D. W. Bogdanoff, Use of a tantalum liner to reduce bore erosion and increase muzzle velocity in two-stage light gas guns, in: Meeting of Aeroballistics Range Association, no. ARC-E-DAA-TN25754, 2015.

[93] W. Crozier, W. Hume, High-velocity, light-gas gun, Journal of Applied Physics 28 (8) (1957) 892–894.

[94] R. Patin, R. Courter, A one-dimensional simulation model for a two stage light gas gun with deformable piston, in: 24th Aerospace Sciences Meeting, 1986, p. 46.

[95] L. C. Chhabildas, L. Davison, Y. Horie, High-pressure shock compression of solids VIII: The science and technology of high-velocity impact, Springer Science & Business Media, 2004.

[96] H. Langweiler, Beitrag zur hydrodynamischen detonationstheorie, Zeitschrift fur Technische Physik 19 (1938) 271–283.

[97] H. Bernier, Scaling and designing large-bore two-stage high velocity guns, Springer-Verlag Berlin Heidelberg, Germany, 2005, Ch. 2, pp. 37–84.

[98] W. D. Crozier, W. Hume, High-velocity, light-gas gun, Journal of Applied Physics 28 (8) (1957) 892–894. doi:10.1063/1.1722882.

[99] M. Bowering, Strain rate effects on energy dissipation during hypervelocity penetration of polymeric materials, Master's thesis, Mississippi State University (2018).

[100] J. M. Mihaly, Investigation of Hypervelocity Impact Phenomena Using Real-Time Concurrent Diagnostics, Ph.D. thesis, California Institute of Technology (Jan 2013).

[101] F. Saito, T. Usui, H. Tamura, Y. Tanaka, M. Shimizu, K.-i. Kondo, Improvement of a "mini" two-stage light-gas gun for hypervelocity impact experiments: Technical devices to accelerate and detect a "minute" projectile efficiently, Review of Scientific Instruments 76 (5) (2005) 055107.

[102] R. Putzar, F. Schaefer, Experimental space debris simulation at EMI's calibre 4 mm two-stage light gas gun, in: Proceedings of the 5th European Conference on Space Debris, Darmstadt, Germany, ESA SP-672, 2009.

[103] S. Ryan, Hypervelocity impact induced disturbances on composite sandwich panel spacecraft structures, School of Aerospace, Mechanical and Manufacturing Engineering Science, RMIT University, Melbourne, Australia (2007).

[104] B. Lexow, M. Wickert, K. Thoma, F. Schäfer, M. Poelchau, T. Kenkmann, The extra-large light-gas gun of the Fraunhofer EMI: Applications for impact cratering research, Meteoritics & Planetary Science 48 (1) (2013) 3–7.

[105] W. L. Ross, D. Henderson, The guns of NASA, Tech. rep.

[106] NASA White Sands, NASA White Sands Test Facility Remote Hypervelocity Test Laboratory, Tech. rep. (2017).

[107] T. See, R. Montes, The Johnson Space Center Experimental Impact Lab: Contributions toward understanding the evolution of the solar system, in: Proceedings of the 43rd Lunar and Planetary Science Conference, 2012.

[108] S. K. Roy, M. Peña, R. S. Hixson, M. Trabia, B. O'Toole, S. Becker, E. Daykin, R. Jennings, M. Matthes, M. Walling, Use of a multiplexed photonic doppler velocimetry (MPDV) system to study plastic deformation of metallic steel plates in high velocity impact, in: Fracture, Fatigue, Failure and Damage Evolution, Volume 8, Springer, 2016, pp. 253–260.

[109] N. Kawai, K. Tsurui, S. Hasegawa, E. Sato, Single microparticle launching method using two-stage light-gas gun for simulating hypervelocity impacts of micrometeoroids and space debris, Review of Scientific Instruments 81 (11) (2010) 115105.

[110] C. Cornelson, E. Fretter, Fact sheet: Range complex, Tech. rep., NASA Ames Research Center (2004).

[111] T. Moritoh, N. Kawai, K. G. Nakamura, K.-i. Kondo, Projectile acceleration aiming at velocities above 9 km/s by a compact gas gun, in: AIP Conference Proceedings, Vol. 620, American Institute of Physics, 2002, pp. 1204–1207.

[112] J. Rogers, P. T. Mead, K. Harrison, K. R. Kota, J. D. Leaverton, G. Lukasik, W. D. Kulatilaka, J. W. Wilkerson, T. E. Lacy, Hypervelocity impact response of polyethylene plates, in: Proceedings of the AIAA Scitech 2021 Forum, 2021, p. 0887. doi:10.2514/6.2021-0887.

[113] G. Lukasik, J. Rogers, K. R. Kota, J. W. Wilkerson, T. E. Lacy, W. D. Kulatilaka, Application of digital particle tracking and schlieren imaging to study debris cloud and shockwave formation during hypervelocity impacts, in: Proceedings of the AIAA Scitech 2021 Forum, 2021, p. 0725. doi:10.2514/6.2021-0725.

[114] T. Ringrose, H. Doyle, P. Foster, M. Betney, J. Skidmore, T. Edwards, B. Tully, J. Parkin, N. Hawker, A hypervelocity impact facility optimised for the dynamic study of high pressure shock compression, Procedia Engineering 204 (2017) 344–351.

[115] N. Fellows, P. Barton, Royal Military College of Science light gas gun facility, Review of Scientific Instruments 68 (10) (1997) 3823–3827.

[116] Arnold Engineering Development Complex (AEDC), Test Facility Guide, Tech. rep. (2018).

[117] A. E. D. Complex, Test Capabilties Guide, Tech. rep. (2021).

[118] Y. Syono, T. Goto, Shock wave facilities for high-pressure experiments at tohoku university, in: AIP Conference Proceedings, Vol. 78, American Institute of Physics, 1982, pp. 701–705.

[119] K. Poormon, MMOD hypervelocity impact test & piggyback sensing, in: In-Space Inspection Workshop 2017, University of Dayton Research Institute, 2017.

[120] S. Stewart, D. Spaulding, The Shock Compression Laboratory at the University of California, Davis, in: Proceedings of the Lunar and Planetary Science Conference, no. 1964, 2017, p. 2154.

[121] G. Vankirk, J. Sherburn, W. Heard, E. Chappell, Initial study of ultraordnance impact experiments on concrete, in: Proceedings of the 2021 SEM Annual Conference on Experimental Applied Mechanics, Virtual, 2021.

[122] V. Henson, Science and technology review June 2004, Tech. Rep. UCRL-TR-52000-04-6, Lawrence Livermore National Laboratory (2004).

[123] W. D. Reinhart, Sandia National Laboratories Star Facility yesterday, today, tomorrow, Tech. rep., Sandia National Lab.(SNL-NM), Albuquerque, NM (United States) (2017).

[124] D. B. Longcope, Analysis of the second stage of the STAR 28 mm two-stage light gas gun, International Journal of Impact Engineering 17 (4-6) (1995) 527–537.

[125] A. Piekutowski, A new technique for achieving impact velocities greater than 10 km/s, in: Space Technology Conference and Exposition, 2001, p. 4591.

[126] W. Hubbs, B. Roebuck, M. Zwiener, B. Wells, Southern Impact Testing Alliance (SITA), in: National Space and Missile Materials Symposium, 2009.

[127] D. J. Grosch, J. D. Walker, Large Two-Stage Light-Gas Gun Facility, Tech. rep. (2017).

[128] D. Baum, Testing and diagnostic capabilities at LLNL, Tech. rep., Lawrence Livermore National Laboratory, Livermore, CA (1998).

[129] A. Martinez, S. Sheffied, M. Whitehead, H. Olivas, J. Dick, New LANL gas driven two-stage gun, in: AIP Conference Proceedings, Vol. 309, American Institute of Physics, 1994, pp. 1643–1646.

[130] New Mexico Tech - Energetic Materials Research Testing Center, Energetic Materials Research and Testing Center (EMRTC) promotional brochure, Tech. rep. (2020).

[131] W. Zonghao, H. Jie, S. Anhua, S. Qiang, L. Sen, Hypersonic boundary layer transition visualization in CARDC hypervelocity ballistic range.

[132] Y. F. Khristenko, S. A. Zelepugin, A. V. Gerasimov, New light-gas guns for the high-velocity throwing of mechanical particles, ARPN Journal of Engineering and Applied Sciences 12 (22) (2017) 6606–6610.

[133] S. Liu, Y. Li, J.-F. Zhou, A.-m. Xie, J.-y. Luo, J. Huang, Debris cloud characteristics of mono-and multi-plates under hypervelocity impact, Target 25 (2010) 25mm.

[134] G. Simpson, M. Shaeffer, K. Ramesh, HyFIRE: Hypervelocity facility for impact research at Johns Hopkins University, Bulletin of the American Physical Society 64 (2019).

[135] A. R. Martinez, S. A. Sheffied, M. C. Whitehead, H. D. Olivas, J. J. Dick, New LANL gas driven two-stage gun, AIP Conference Proceedings 309 (1) (1994) 1643–1646. doi:10.1063/1.46403.

[136] L. E. Lamberson, P. A. Boettcher, Compressed gas combined single- and two-stage light-gas gun, Review of Scientific Instruments 89 (2) (2018) 023903. doi:10.1063/1.5000912.

[137] R. Hibbert, M. Cole, M. C. Price, M. Burchell, The hypervelocity impact facility at the University of Kent: Recent upgrades and specialized capabilities., Procedia Engineering 204 (2017) 208–214.

[138] C. G. Lamontagne, G. N. Manuelpillai, J. H. Kerr, E. A. Taylor, R. C. Tennyson, M. J. Burchell, Projectile density, impact angle and energy effects on hypervelocity impact damage to carbon fibre/peek composites, International Journal of Impact Engineering 26 (1-10) (2001) 381–398.

[139] N. Espinoza Magana, Evaluation of superelastic nitinol as a shielding material for hypervelocity impact, Ph.D. thesis, RICE University (1999).

[140] H. Abdulhamid, P. Héreil, P. Deconinck, J. Mespoulet, C. Puillet, Study of hypervelocity impacts on space shields above 7 km/s, in: Proceedings of the 7th European Conference on Space Debris, 2017.

[141] F. Plassard, J. Mespoulet, P. Hereil, Hypervelocity impact of aluminium sphere against aluminium plate: Experiment and LS-DYNA correlation, in: Proceedings of the 8th European LS-DYNA Users Conference, 2011, pp. 1–11.

[142] K. Pianthong, A. Matthujak, K. Takayama, T. Saito, B. E. Milton, Visualization of supersonic liquid fuel jets, Journal of Flow Visualization and Image Processing 13 (3) (2006).

[143] V. Tolkachev, O. Ivanova, N. Pakhnutova, Experimental studying and predicting the consequences of high-velocity impact of rod projectiles with layered and spaced targets, in: Journal of Physics: Conference Series, Vol. 1709, IOP Publishing, 2020, p. 012025.

[144] D. Hébert, G. Seisson, J.-L. Rullier, I. Bertron, L. Hallo, J.-M. Chevalier, C. Thessieux, F. Guillet, M. Boustié, L. Berthe, Hypervelocity impacts into porous graphite: experiments and simulations, Philosophical Transactions of the Royal Society A: Mathematical, Physical and Engineering Sciences 375 (2085) (2017) 20160171.

[145] Y. Michel, A. Moussi, C. Durin, C. Espinosa, J.-M. Chevalier, J.-C. Mandeville, Damaging and ejection processes during hvi on brittle targets: experimental data and comparison with numerical simulation using an sph method, in: 4th European Conference on Space Debris, Vol. 587, 2005, p. 419.

[146] J. Perin, A. Geraud, 3400 m/s deuterium pellet injector for tore supra, Tech. rep. (1994).

[147] S. Combs, C. Foust, D. Fehling, J. McGill, S. Meitner, L. Baylor, J. Caughman, S. Milora, A. Frattolillo, S. Migliori, F. Bombarda, S. Podda, M. Capobianchi, G. Ronci, B. Coppi, G. Roveta, Status of ORNL/ENEA-Frascati Collaboration on IGNITOR High-Speed Pellet Injector, Tech. rep., Oak Ridge National Lab, Oak Ridge, TN (2011).

[148] A. Frattolillo, S. Migliori, F. Scaramuzzi, S. Combs, L. Baylor, C. Foust, M. Gouge, S. Milora, High-speed repeating hydrogen pellet injector for long-pulse magnetic confinement fusion experiments, Review of Scientific Instruments 67 (5) (1996) 1834–1841.

[149] J. McDonnell, The Open University planetary impact facility: A compact two-stage light gas gun for all impact angles, International Journal of Impact Engineering 33 (1-12) (2006) 410–418.

[150] K. Kurosawa, R. Moriwaki, G. Komatsu, T. Okamoto, H. Sakuma, H. Yabuta, T. Matsui, Shock vaporization/devolatilization of evaporitic minerals, halite and gypsum, in an open system investigated by a two-stage light gas gun, Geophysical Research Letters 46 (13) (2019) 7258–7267.

[151] K. Kurosawa, Y. Nagaoka, H. Senshu, K. Wada, S. Hasegawa, S. Sugita, T. Matsui, Dynamics of hypervelocity jetting during oblique impacts of spherical projectiles investigated via ultrafast imaging, Journal of Geophysical Research: Planets 120 (7) (2015) 1237–1251.

[152] Institute of Shock Physics: Annual Review 2014, Tech. rep., Imperial College of London (2014).

[153] B. Corbett, Numerical simulations of target hole diameters for hypervelocity impacts into elevated and room temperature bumpers, International Journal of Impact Engineering 33 (1-12) (2006) 431–440.

[154] C. R. Morse, F. S. Stepka, Effect of projectile size and material on impact fracture of walls of liquid-filled tanks, Tech. rep., NASA (1966).

[155] G. Ciccarelli, M. Subudhi, R. Hall, Raptor gas gun testing experiment, Tech. rep., Brookhaven National Laboratory (BNL), Upton, NY (1998).

[156] C. G. Kim, I. J. Kim, G. Lim, B. I. Yoon, The ballistic impact characteristics of woven fabrics impregnated with a colloidal suspension and flattened rolls, Advances in Science and Technology 71 (2011) 74–79.

[157] J.-H. Cha, Y. Kim, S. K. S. Kumar, C. Choi, C.-G. Kim, Ultra-high-molecular-weight polyethylene as a hypervelocity impact shielding material for space structures, Acta Astronautica 168 (2020) 182–190.

[158] C. Technologies, By capability: Corvid provides end-to-end solutions including concept development, design and optimization, prototype build, test and manufacture, accessed: 2023-04-29 (2021).
URL `https://www.corvidtec.com/capabilities`

[159] J. Spray, P. Gores, Experimental hypervelocity impact of anorthosite at 1.8 to 6.7 km/s: Ejecta parameters, crater shapes and shock effects, LPI Contributions 2136 (2019) 5078.

[160] P. A. Gores, J. G. Spray, Hypervelocity impact of anorthosite: Excavation, spallation and crater reconstruction, International Journal of Impact Engineering 160 (2022) 104078.

[161] Y. Akahoshi, Y. Qu, T. Koura, S. Fukushige, M. Tadaoka, J. Kitagawa, Measurement of delay time from propellant ignition to projectile launch in two-stage light gas gun using electrothermal-chemical gun technology, in: 4th European Conference on Space Debris, Vol. 587, 2005, p. 391.

[162] M. Higashide, M. Tanaka, Y. Akahoshi, S. Harada, F. Tohyama, Hypervelocity impact tests against metallic meshes, International Journal of Impact Engineering 33 (1-12) (2006) 335–342.

[163] J. A. Rogers, N. Bass, P. T. Mead, A. Mote, G. D. Lukasik, M. Intardonato, K. Harrison, J. D. Leaverton, K. R. Kota, J. W. Wilkerson, et al., The Texas A&M University Hypervelocity Impact Laboratory: A modern aeroballistic range facility, Review of Scientific Instruments 93 (8) (2022) 085106. doi:10.1063/5.0088994.

[164] T. Graber, Dynamic Compression Sector Update, Tech. rep., Argonne National Laboratory (2012).

[165] J. S. Karcz, D. Bowling, C. Cornelison, A. Parrish, A. Perez, G. Raiche, J.-P. Wiens, The Ames Vertical Gun Range, in: Proceedings of the Lunar and Planetary Science Conference, 2016.

[166] A. J. Zakraysek, G. T. Sutherland, H. D. Sandusky, D. Strange, A new gun facility dedicated to performing shock physics and terminal ballistics experiments, in: AIP Conference Proceedings, Vol. 505, American Institute of Physics, 2000, pp. 1091–1094.

[167] Z. Gong, F. Dai, J. Yang, M. Hou, J. Zheng, J. Tong, H. Pang, The recent research progresses in space debris hypervelocity impact test in cast, in: APS Shock Compression of Condensed Matter Meeting Abstracts, 2009, pp. CKE–50.

[168] D. J. Deforge, Performance of the ubc two-stage light-gas gun, Ph.D. thesis, University of British Columbia (1993).

[169] J. P. Escobedo-Diaz, C. Neel, M. Gonzales, Dynamic behaviour of multi-phase materials, Tech. rep., University of New South Wales Kensington Australia (2019).

[170] University of New South Wales - Two-Stage Light Gas Gun, https://unsw.adfa.edu.au/our-research/facilities/gas-gun, accessed: 2022-02-18.

[171] W. Harrison, C. Loupias, P. Outrebon, D. Turland, Experimental data and hydrocode calculations for hypervelocity impacts of stainless steel into aluminium in the 2–8 km/s range, International Journal of Impact Engineering 17 (1-3) (1995) 363–374.

[172] M.-A. Courty, J.-M. Martinez, Terrestrial carbonaceous debris tracing atmospheric hypervelocity-shock aeroplasma processes, Procedia Engineering 103 (2015) 81–88.

[173] Y. Jiyun, Z. Jidong, G. Zizheng, P. Hewei, Damage analysis for hypervelocity impact experiments on spaceship windows glass, in: EPJ Web of Conferences, Vol. 6, EDP Sciences, 2010, p. 39001.

[174] Z. Pin-Liang, G. Zi-Zheng, J. Guang-Fu, W. Qing-Song, S. Zhen-Fei, C. Yan, W. Xiang, Shock compression of the new 47Zr45Ti5Al3V alloys up to 200 GPa, Chinese Physics Letters 30 (6) (2013) 066401.

[175] Extreme Performance Testing Center, Tech. rep., Seoul National University (ND).

[176] T. Sekine, S. Tashiro, T. Kobayashi, T. Matsumura, The nirim two-stage light-gas gun: Performance test results, in: AIP Conference Proceedings, Vol. 370, American Institute of Physics, 1996, pp. 1201–1204.

[177] M. Martin, T. Sekine, T. Kobayashi, L. Kecskes, N. Thadhani, High-pressure equation of the state of a zirconium-based bulk metallic glass, Metallurgical and Materials Transactions A 38 (2007) 2689–2696.

[178] X. Hu, G. Yang, B. Zhao, P. Li, J. Yang, C. Leng, H. Liu, H. Huang, Y. Fei, Shock compression behavior of a mixture of cubic and hexagonal boron nitride, Journal of Applied Physics 123 (17) (2018) 175903.

[179] C. Konrad, R. Braddy, M. Martinez, Joint Actinide Shock Physics Experimental Research (JASPER) facility overview, Tech. rep., Bechtel Nevada Corporation (US) (2001).

[180] R. K. Paul, J. L. Jordan, Shock and detonation physics group, Tech. rep., Los Alamos National Lab.(LANL), Los Alamos, NM (United States) (2017).

[181] B. Jensen, B. Sturtevant, J. Lang, T. Salyer, C. Chiquete, Shock and detonation physics group (m-9), Tech. rep., Los Alamos National Laboratory (LANL), Los Alamos, NM (2020).

[182] A. Piekutowski, A new technique for achieving impact velocities greater than 10 km/s, in: Space Technology Conference and Exposition, 2001, p. 4591.

[183] Z. Yu-rong, Z. Xiang-rong, S. Xian-zhong, L. Guan-lan, T. Shu-shun, J. Ji-yong, On the development of a Φ100/30mm-caliber gas-driven two-stage light gas gun, Journal of Experimental Mechanics 25 (3) (2010).

[184] P. Lundberg, Interface defeat and penetration: two modes of interaction between metallic projectiles and ceramic targets, Ph.D. thesis, Acta Universitatis Upsaliensis (2004).

[185] G. Butler, D. King, G. Abate, M. Stephens, Ballistic range tests of store separation at supersonic to hypersonic speeds, in: 29th Aerospace Sciences Meeting, 1991, p. 199.

[186] E. L. Baker, N. Al-Shehab, K. Tomasello, K. Kennision, D. Hunter, Fragment impact gun testing technology and issues, in: 2015 Insensitive Munitions & Energetic Materials Technology Symposium, Rome, Italy, 2015.

[187] Y. Zhang, T. Sekine, H. He, Y. Yu, F. Liu, M. Zhang, Shock compression of Fe-Ni-Si system to 280 GPa: Implications for the composition of the Earth's outer core, Geophysical Research Letters 41 (13) (2014) 4554–4559.

[188] E. Lach, C. Anderson, V. Schirm, G. Koerber, Hypervelocity impact into a high strength and ductile steel alloy, International Journal of Impact Engineering 35 (12) (2008) 1625–1630.

[189] E. Escauriza, R. Barker, M. Read, G. Burdiak, H. Doyle, N. Hawker, Ablation of a solid obstacle with a radiative shock driven by gas gun plate impact, Bulletin of the American Physical Society (2022).

[190] C. Park, An overview of ames experimental aerothermodynamics, in: Shock Waves: Proceedings of the 18th International Symposium on Shock Waves, Held at Sendai, Japan 21–26 July 1991, Springer, 1992, pp. 591–596.

[191] George H.W. Bush Combat Development Complex (BCDC), Ballistic, Aero-Optics, and Materials Test Range, accessed: 2023-04-30.
URL https://bcdc.tamus.edu/facilities/bam/

[192] Texas A&M University System (TAMUS), Texas A&M System Regents ok $60.3 million for army innovation, accessed: 2023-04-30 (Nov 2021).
URL https://www.tamus.edu/texas-am-system-regents-ok-60-3-million-for-army-innovation/

[193] Y. Hong, K. Moon, Experimental research on ice particle impact on aluminum alloys, Wear 382-383 (2017) 102–106. doi:10.1016/j.wear.2017.04.024.

[194] P. Baojun, Z. Wei, L. Dekun, Z. Zehua, Experimental investigation into water-filled pressurized vessels damaged by high-velocity projectile impact, European Space Agency-Publications-Esa Sp 473 (2001) 603–606.

[195] D. Zhang, R. Tang, J. Lin, X. Zhang, Y. Zhu, Development of a new type gas-driven two-stage light gas gun, Acta Armamentarii 1 (2004).

[196] Z. Gong, M. Hou, K. Xu, J. Zheng, J. Niu, Y. Cao, Experimental Study on Hypervelocity Impact Characteristics of New Types of Gong-Hou Shield, in: 6th European Conference on Space Debris, Vol. 723, 2013, p. 109.

[197] E. Tang, M. Xu, Q. Zhang, S. Liu, M. Wang, S. Xiang, J. Xia, L. He, Y. Han, L. Zhang, et al., Research on the ionization degree of the plasma generated by 2A12 aluminum target during hypervelocity impact, IEEE Transactions on Plasma Science 44 (8) (2016) 1333–1340. doi:10.1109/TPS.2016.2580909.

[198] M. H. Bowering, Strain rate effects on energy dissipation during hypervelocity penetration of polymeric materials, Mississippi State University, 2018.

[199] S. Khatiwada, C. A. Armada, E. V. Barrera, Hypervelocity impact experiments on epoxy/ultra-high molecular weight polyethylene fiber composites reinforced with single-walled carbon nanotubes, in: Procedia Engineering, Vol. 58, Elsevier Ltd, 2013, pp. 4–10. doi:10.1016/j.proeng.2013.05.003.

[200] J. S. Curtis, An accelerated reservoir light-gas gun, NASA, 1962.

[201] G. Bird, The effect of wall shape on the degree of reinforcement of a shock wave moving into a converging channel, Journal of Fluid Mechanics 5 (1) (1959) 60–66.

[202] O. Laporte, On the interaction of a shock with a constriction, Tech. rep., Los Alamos Scientific Laboratory (LANL) (1954).

[203] D. W. Bogdanoff, Design of a two-stage light gas gun for muzzle velocities of 10-11 km/s, in: Aeroballistic Range Association Meeting, no. ARC-E-DAA-TN35142, 2016.

[204] J. Dong, B. Cao, Numerical simulation analysis of the flow field in the bore of a two-stage light gas gun, Journal of Physics: Conference Series 2365 (1) (2022) 012024. doi:10.1088/1742-6596/2365/1/012024.

[205] C. J. Cornelison, E. T. Watts, Results of two-stage light-gas gun development efforts and hypervelocity impact tests of advanced thermal protection materials, Tech. Rep. TM-1998-112234, NASA Ames Research Center (1998).
URL https://ntrs.nasa.gov/api/citations/19980236871/downloads/19980236871.pdf

[206] X. Chang, K. Shimomura, S. Taki, Development and performance examination of a two-stage detonation light gas gun, Transactions of the Japan Society of Mechanical Engineers, Part B 62 (Jul 1996).

[207] D. Zhang, R. Tang, J. Lin, X. Zhang, Y. Zhu, Development of a new type gas-driven two-stage light gas gun, Acta Armamentarii 1 (2004).

[208] H. Bernier, Flat scored high pressure diaphragms as quick opening valves, in: Proceedings of the 42nd ARA Meeting, Adelaide, Australia, 1991.

[209] H. Swift, D. Strange, Sabot discard technology, Physics Applications Inc., Internal Report (1987).

[210] A. J. Stilp, Sabot designs for launching penetrators and projectiles, in: High-pressure shock compression of solids VIII, Springer, 2005, pp. 201–225.

[211] D. Siegelman, J. Wang, E. SCHMIDT, Sabot design optimization, in: 7th Atmospheric Flight Mechanics Conference, 1981, p. 1903.

[212] H. Swift, D. Strange, Analyses of sabot operation, in: Proceedings of the 49th ARA Meeting, Salisbury, Australia.

[213] R. E. Berggren, R. M. Reynolds, The light-gas-gun model launcher, Ballistic range technology (1970) 9–54.

[214] L. A. Glenn, Optimization studies of a three-stage light gas gun, in: AIP Conference Proceedings, Vol. 429, American Institute of Physics, 1998, pp. 963–966.

[215] K. Kondo, O. Fat'yanov, Y. Hironaka, T. Moritoh, S. Ozaki, Performance of the three-stage light-gas gun with a preheating stage, in: AIP Conference Proceedings, Vol. 505, American Institute of Physics, 2000, pp. 1167–1170.

[216] E. Escauriza, J. Duarte, D. Chapman, M. Rutherford, L. Farbaniec, J. Jonsson, L. Smith, M. Olbinado, J. Skidmore, P. Foster, et al., Collapse dynamics of spherical cavities in a solid under shock loading, Scientific Reports 10 (1) (2020) 8455.

[217] X. Wang, C. Dai, Q. Wang, L. Hao, J. Bai, Y. Yu, Q. Wu, H. Tan, J. Hu, G. Luo, et al., Development of a three-stage gas gun launcher for ultrahigh-pressure hugoniot measurements, Review of Scientific Instruments 90 (1) (2019) 013903.

[218] AEDC's Range-G in operation for 50 years, accessed: 2023-04-30.
URL https://www.arnold.af.mil/News/Article-Display/Article/804821/aedcs-range-g-in-operation-for-50-years/

[219] J. Warren, M. Cole, S. Offenberger, K. R. Kota, T. E. Lacy, H. Toghiani, M. Burchell, S. Kundu, C. U. Pittman, Hypervelocity impacts on honeycomb core sandwich panels filled with shear thickening fluid, International Journal of Impact Engineering 150 103803.

[220] J. Warren, K. R. Kota, S. M. Westberg, T. Lacy, S. Kundu, H. Toghiani, C. U. Pittman Jr, et al., Hypervelocity impacts of shear thickening fluid imbibed metallic foam core sandwich panels, in: 30th technical conference of American Society of Composites, East Lansing, USA, 2015, pp. 28–30.

[221] J. Moreno, M. Shaeffer, P. Malhotra, G. Simpson, Y. Kim, K. Ramesh, In situ characterization and visualization of high-speed impacts at the HyFIRE facility, in: Proceedings of the 71st Aeroballistic Range Association Meeting, 2022.

[222] S. Chocron, J. D. Walker, D. J. Grosch, A. J. Carpenter, D. D. Durda, K. R. Housen, Hypervelocity impact on pumice: scale effects on experiments and simulations, Procedia Engineering 204 (2017) 154–161.

[223] P. S. Westine, S. A. Mullin, Scale modeling of hypervelocity impact, International Journal of Impact Engineering 5 (1-4) (1987) 693–701.

[224] K. A. Holsapple, The scaling of impact processes in planetary sciences, Annual Review of Earth and Planetary Sciences 21 (1) (1993) 333–373.

[225] J.-H. Lee, D. Veysset, J. P. Singer, M. Retsch, G. Saini, T. Pezeril, K. A. Nelson, E. L. Thomas, High strain rate deformation of layered nanocomposites, Nature Communications 3 (1) (2012) 1164.

[226] M. J. Burchell, M. J. Cole, J. McDonnell, J. C. Zarnecki, Hypervelocity impact studies using the 2 mv van de graaff accelerator and two-stage light gas gun of the University of Kent at Canterbury, Measurement Science and Technology 10 (1) (1999) 41.

[227] G. Seisson, D. Hébert, I. Bertron, J.-M. Chevalier, L. Hallo, E. Lescoute, L. Videau, P. Combis, F. Guillet, M. Boustie, et al., Dynamic cratering of graphite: experimental results and simulations, International Journal of Impact Engineering 63 (2014) 18–28.

[228] A. Finchum, M. Nehls, W. Young, P. Gray, B. Suggs, N. M. Lowrey, Capabilities of the Impact Testing Facility at Marshall Space Flight Center, in: Proceedings of the 62nd Annual Meeting of the Aeroballistic Range Association, no. M11-1008, 2011.

[229] K. Sakuraba, Y. Tsuruda, T. Hanada, J.-C. Liou, Y. Akahoshi, Investigation and comparison between new satellite impact test results and nasa standard breakup model, International Journal of Impact Engineering 35 (12) (2008) 1567–1572.

[230] G. Lukasik, C. Schweizer, J. Rogers, T. E. Lacy, W. D. Kulatilaka, Ultra-high-speed digital in-line holography for three-dimensional tracking of hypervelocity projectiles, in: Proceedings of the AIAA Scitech 2023 Forum, 2023, p. 0805.

[231] M. H. Bowman, The History and Advancement of the Weather Encounter Capabilities in the AEDC Hyperballistic Range G, in: Proceedings of the AIAA Scitech 2021 Forum, 2021, p. 1874.

[232] A. Dworzanczyk, N. J. Parziale, N. Mueschke, D. Grosch, P. C. Bueno, High-speed imaging of droplet impact on a hypervelocity projectile, in: Proceedings of the AIAA Scitech 2023 Forum, 2023, p. 0464.

[233] A. Jones, W. Isbell, C. Maiden, Measurement of the very-high-pressure properties of materials using a light-gas gun, Journal of Applied Physics 37 (9) (1966) 3493–3499.

[234] M. Yokoo, N. Kawai, Y. Hironaka, K. G. Nakamura, K.-i. Kondo, Diagnostic system to measure spatial and temporal profiles of shock front using compact two-stage light-gas gun and line reflection method, Review of Scientific Instruments 78 (4) (2007) 043904.

[235] A. K. Hopkins, H. F. Swift, Planar shock wave experiments using very small bore guns, Review of Scientific Instruments 42 (6) (1971) 863–867.

[236] W. D. Reinhart, L. C. Chhabildas, D. E. Carroll, T. K. Bergstresser, T. F. Thornhill, N. A. Winfree, Equation of state measurements of materials using a three-stage gun to impact velocities of 11 km/s, International Journal of Impact Engineering 26 (1-10) (2001) 625–637.

[237] Y. Syono, T. Goto, A two-stage light gas gun for shock wave research, Scientific Reports of the Research Institute, Tohoku University 29 (1980) 17–31. doi:10.50974/00043219.

[238] T. Mashimo, A. Sawaoka, A measurement system for interior projectile motion and particle-velocity histories for impact shock study with a two-stage light gas gun, Japanese Journal of Applied Physics 20 (5) (1981) 963.

[239] W. Sun, X. Li, K. Hokamoto, Fabrication of graded density impactor via underwater shock wave and quasi-isentropic compression testing at two-stage gas gun facility, Applied Physics A 117 (2014) 1941–1946.

[240] Q. Wei, K. Ramesh, T. C. Hufnagel, J. Wilkerson, J. A. El-Awady, J. Kimberley, B. Ravaji, S. P. Joshi, Insights from the mede program: An overview of microstructure–property linkages in the dynamic behaviors of magnesium alloys, Mechanics of Materials 163 (2021) 104084.

[241] P. D. Asimow, Failure of soda-lime glass at extreme conditions: New experimental frontiers, Tech. rep., California Institute of Technology (2019).

[242] Texas A&M Regents OK World-Class Engineering Feat (Nov 2020).
URL https://www.tamus.edu/texas-am-regents-ok-world-class-engineering-feat/

[243] W. Herrmann, J. S. Wilbeck, Review of hypervelocity penetration theories, International Journal of Impact Engineering 5 (1-4) (1987) 307–322. doi:10.1016/0734-743X(87)90048-0.

[244] W. P. Schonberg, A. J. Bean, K. Darzi, Hypervelocity impact physics, Tech. rep., NASA (1991).

[245] A. Fletcher, S. Close, D. Mathias, Simulating plasma production from hypervelocity impacts, Physics of Plasmas 22 (9) (2015) 093504.

[246] N. Lee, S. Close, D. Lauben, I. Linscott, A. Goel, T. Johnson, J. Yee, A. Fletcher, R. Srama, S. Bugiel, et al., Measurements of freely-expanding plasma from hypervelocity impacts, International Journal of Impact Engineering 44 (2012) 40–49.

[247] B. G. Cour-Palais, Hypervelocity impact in metals, glass and composites, International Journal of Impact Engineering 5 (1-4) (1987) 221–237.

[248] F. K. Schäfer, M. Herrwerth, S. J. Hiermaier, E. E. Schneider, Shape effects in hypervelocity impact on semi-infinite metallic targets, International Journal of Impact Engineering 26 (1-10) (2001) 699–711.

[249] S. K. Roy, M. Trabia, B. O'Toole, R. Hixson, S. Becker, M. Pena, R. Jennings, D. Somasoundaram, M. Matthes, E. Daykin, et al., Study of hypervelocity projectile impact on thick metal plates, Shock and Vibration 2016 (2016).

[250] T. Takano, Y. Murotani, K. Maki, T. Toda, A. Fujiwara, S. Hasegawa, A. Yamori, H. Yano, Microwave emission due to hypervelocity impacts and its correlation with mechanical destruction, Journal of Applied Physics 92 (9) (2002) 5550–5554.

[251] W. P. Schonberg, R. A. Taylor, Penetration and ricochet phenomena in oblique hypervelocity impact, AIAA Journal 27 (5) (1989) 639–646. doi:10.2514/3.10155.

[252] I. Mohagheghian, G. J. McShane, W. J. Stronge, Impact perforation of monolithic polyethylene plates: projectile nose shape dependence, International Journal of Impact Engineering 80 (2015) 162–176. doi:10.1016/j.ijimpeng.2015.02.002.

[253] S. M. Sajadi, C. F. Woellner, P. Ramesh, S. L. Eichmann, Q. Sun, P. J. Boul, C. J. Thaemlitz, M. M. Rahman, R. H. Baughman, D. S. Galvão, et al., 3D printed tubulanes as lightweight hypervelocity impact resistant structures, Small 15 (52) (2019) 1904747. doi:10.1002/smll.201904747.

[254] L. Lamberson, V. Eliasson, A. Rosakis, In situ optical investigations of hypervelocity impact induced dynamic fracture, Experimental Mechanics 52 (2) (2012) 161–170. doi:10.1007/s11340-011-9521-0.

[255] P. Colombo, A. Arcaro, A. Francesconi, D. Pavarin, D. Rondini, S. Debei, Effect of hypervelocity impact on microcellular ceramic foams from a preceramic polymer, Advanced Engineering Materials 5 (11) (2003) 802–805. doi:10.1002/adem.200300397.

[256] Y. Kitazawa, A. Fujiwara, T. Kadono, K. Imagawa, Y. Okada, K. Uematsu, Hypervelocity impact experiments on aerogel dust collector, Journal of Geophysical Research: Planets 104 (E9) (1999) 22035–22052. doi:10.1029/1998JE000554.

[257] J.-M. Sibeaud, L. Thamié, C. Puillet, Hypervelocity impact on honeycomb target structures: Experiments and modeling, International Journal of Impact Engineering 35 (12) (2008) 1799–1807. doi:10.1016/j.ijimpeng.2008.07.037.

[258] M. Wicklein, S. Ryan, D. White, R. Clegg, Hypervelocity impact on CFRP: Testing, material modelling, and numerical simulation, International Journal of Impact Engineering 35 (12) (2008) 1861–1869. doi:10.1016/j.ijimpeng.2008.07.015.

[259] J. D. Walker, S. Chocron, D. D. Durda, D. J. Grosch, N. Movshovitz, D. C. Richardson, E. Asphaug, Momentum enhancement from aluminum striking granite and the scale size effect, International Journal of Impact Engineering 56 (2013) 12–18. doi:10.1016/j.ijimpeng.2012.08.003.

[260] J. D. Walker, S. Chocron, D. J. Grosch, Size scaling of hypervelocity-impact ejecta mass and momentum enhancement: Experiments and a nonlocal-shear-band-motivated strain-rate-dependent failure model, International Journal of Impact Engineering 135 (2020) 103388.

[261] M. Yasui, M. Arakawa, H. Okawa, S. Hasegawa, Cratering experiments on granular targets with a variety of particle sizes: Implications for craters on rubble-pile asteroids, Journal of Geophysical Research: Planets 127 (8) (2022) e2021JE007172.

[262] T. Kenkmann, K. Wünnemann, A. Deutsch, M. H. Poelchau, F. Schäfer, K. Thoma, Impact cratering in sandstone: The memin pilot study on the effect of pore water, Meteoritics & Planetary Science 46 (6) (2011) 890–902.

[263] R. Schmidt, Meteor crater: Energy of formation-implications of centrifuge scaling, in: Proceedings of the Lunar and Planetary Science, Vol. 11, 1980, pp. 2099–2128.

[264] T. Hoerth, F. Schäfer, J. Hupfer, O. Millon, M. Wickert, Momentum transfer in hypervelocity impact experiments on rock targets, Procedia Engineering 103 (2015) 197–204.

[265] S. Ren, Q. Zhang, Q. Wu, Y. Xue, K. Zheng, Y. Lu, H. Liang, Influence of impact-induced reaction characteristics of reactive composites on hypervelocity impact resistance, Materials & Design 192 (2020) 108722.

[266] C. Shang, T. Ren, Q. Zhang, Y. Lu, R. Long, X. Guo, X. Hu, Experimental research on damage characteristics of multi-spaced plates with long rods of steel and W-Zr reactive material at hypervelocity impact, Materials & Design 216 (2022) 110564.

[267] S. Ren, Q. Zhang, Q. Wu, R. Long, H. Liang, L. Gong, A debris cloud model for hypervelocity impact of the spherical projectile on reactive material bumper composed of polytetrafluoroethylene and aluminum, International Journal of Impact Engineering 130 (2019) 124–137.

[268] M. J. Burns, R. L. Gustavsen, B. D. Bartram, One-dimensional plate impact experiments on the cyclotetramethylene tetranitramine (hmx) based explosive edc32, Journal of Applied Physics 112 (6) (2012) 064910.

[269] W. Harrison, C. Loupias, P. Outrebon, D. Turland, Experimental data and hydrocode calculations for hypervelocity impacts of stainless steel into aluminium in the 2–8 km/s range, International Journal of Impact Engineering 17 (1-3) (1995) 363–374.

[270] R. Tennyson, C. Lamontagne, Hypervelocity impact damage to composites, Composites Part A: Applied Science and Manufacturing 31 (8) (2000) 785–794.

[271] J. A. Rogers, A. Mote, P. T. Mead, K. Harrison, G. D. Lukasik, K. R. Kota, W. D. Kulatilaka, J. W. Wilkerson, T. E. Lacy, Hypervelocity impact response of monolithic UHMWPE and HDPE plates, International Journal of Impact Engineering 161 (2022) 104081. doi:10.1016/j.ijimpeng.2021.104081.

[272] S. Katz, E. Grossman, I. Gouzman, M. Murat, E. Wiesel, H. Wagner, Response of composite materials to hypervelocity impact, International Journal of Impact Engineering 35 (12) (2008) 1606–1611.

[273] K. Wen, X.-w. Chen, Y.-g. Lu, Research and development on hypervelocity impact protection using whipple shield: An overview, Defence Technology 17 (6) (2021) 1864–1886.

[274] A. Pai, R. Divakaran, S. Anand, S. B. Shenoy, Advances in the whipple shield design and development: A brief review, Journal of Dynamic Behavior of Materials (2022) 1–19.

[275] N. Kawai, K. Tsurui, D. Shindo, Y. Motoyashiki, E. Sato, Fracture behavior of silicon nitride ceramics subjected to hypervelocity impact, International Journal of Impact Engineering 38 (7) (2011) 542–545.

[276] K. Harrison, K. R. Kota, J. A. Rogers, P. T. Mead, A. Mote, W. D. Kulatilaka, T. E. Lacy Jr, et al., Hypervelocity impact response of stitched CFRP laminates, in: Proceedings of the American Society for Composites—Thirty-Sixth Technical Conference on Composite Materials, 2021.

[277] G. Fei, Z. Guokai, J. Yuguo, C. Jianyu, Response characteristics of hypervelocity ogive-nose projectile penetrating into mortar target, Acta Armamentarii 41 (10) (2020) 1979.

[278] A. J. Piekutowski, Debris clouds generated by hypervelocity impact of cylindrical projectiles with thin aluminum plates, International Journal of Impact Engineering 5 (1-4) (1987) 509–518.

[279] K. Taniyama, H. Tamura, Y. Itagaki, A. Takashima, Hypervelocity impact cratering on 5052-aluminum-alloy targets by flat-head cylindrical impactors of multipartite structure, International Journal of Impact Engineering 163 (2022) 104161.

[280] M. E. Graham, J. D. Carlyle, T. L. Menna, Facility for high-speed particle impact testing, Review of Scientific Instruments 46 (9) (1975) 1221–1225. doi:10.1063/1.1134449.

[281] A. E. Williams, A New Hypervelocity Shotgun, International Journal of Impact Engineering 5 (1987) 703–708. doi:10.1016/0734-743X(87)90085-6.

[282] P. Tsou, D. Brownlee, M. Laurance, L. Hrubesh, A. Albee, Intact Capture of Hypervelocity Micrometeoroid Analogs, in: Proceedings of the 19th Lunar and Planetary Sciences Conference, Lunar and Planetary Institute, Houston, TX, 1988, pp. 1205–1206.

[283] P. V. Kryukov, Review of Investigations Under Way on the Large-Scale Tsniimash Ballistic Facility, International Journal of Impact Engineering 23 (1) (1999) 501–508. doi:10.1016/S0734-743X(99)00099-8.

[284] S. A. Finnegan, M. D. Alexander, Parametric Studies of Multiple Fragment Interactions with Plate Array Targets, Tech. rep., Naval Weapons Center, China Lake, CA (1990).

[285] J. S. Penson, M. Burchell, Hypervelocity impact studies on space tethers, in: 54th International Astronautical Congress of the International Astronautical Federation (IAF), the International Academy of Astronautics and the International Institute of Space Law, Vol. 1, 2003, pp. 1865–1874. doi:10.2514/6.iac-03-i.5.04.

[286] W. Schonberg, S. Evans, M. D. Bjorkman, Hypervelocity impact testing of Multiwall targets using multiple simultaneously launched projectiles, Journal of Spacecraft and Rockets 50 (2) (2013) 358–364. doi:10.2514/1.A32118.

[287] W. Schonberg, S. Evans, M. D. Bjorkman, A Comment On The Use Of Simultaneously Launched Projectiles In The Development Of Ballistic Limit Curves For Multi-Wall Targets, in: Proceedings of the 6th European Conference on Space Debris, ESA, Darmstadt, Germany, 2013, pp. 22–25.

[288] X. Zhang, T. Liu, X. Li, G. Jia, Hypervelocity impact performance of aluminum egg-box panel enhanced whipple shield, Acta Astronautica 119 (2016) 48–59.

[289] D. C. Hofmann, L. Hamill, E. Christiansen, S. Nutt, Hypervelocity impact testing of a metallic glass-stuffed whipple shield, Advanced Engineering Materials 17 (9) (2015) 1313–1322.

[290] J. H. Cha, Y. H. Kim, S. K. Sathish Kumar, C. Choi, C. G. Kim, Ultra-high-molecular-weight polyethylene as a hypervelocity impact shielding material for space structures, Acta Astronautica 168 (2020) 182–190. doi:10.1016/j.actaastro.2019.12.008.

[291] X. Huang, Z. Ling, Z. Liu, H. Zhang, L. Dai, Amorphous alloy reinforced whipple shield structure, International Journal of Impact Engineering 42 (2012) 1–10.

[292] E. L. Christiansen, Design and performance equations for advanced meteoroid and debris shields, International Journal of Impact Engineering 14 (1-4) (1993) 145–156.

[293] S. Ryan, E. L. Christiansen, Hypervelocity impact testing of advanced materials and structures for micrometeoroid and orbital debris shielding, Acta Astronautica 83 (2013) 216–231.

[294] D. Shockey, D. Curran, P. De Carli, Damage in steel plates from hypervelocity impact. I. Physical changes and effects of projectile material, Journal of Applied Physics 46 (9) (1975) 3766–3775. doi:10.1063/1.322162.

[295] K. Qu, C. Wu, J. Liu, Y. Yao, Y. Deng, C. Yi, Ballistic performance of multi-layered aluminium and uhmwpe fibre laminate targets subjected to hypervelocity impact by tungsten alloy ball, Composite Structures 253 (2020) 112785.

[296] Y. Mei, J. Liu, Y. Cui, F. Li, X. Tang, M. Sun, R. Chi, Y. Zhang, A. Zhang, K. Chen, Mechanically excellent nacre-inspired protective steel-concrete composite against hypervelocity impacts, Scientific Reports 11 (1) (2021) 1–12.

[297] T. Atou, Y. Sano, M. Katayama, S. Hayashi, Damage evaluation of reinforced concrete columns by hypervelocity impact, Procedia Engineering 58 (2013) 348–354.

[298] A. Dawson, S. Bless, S. Levinson, B. Pedersen, S. Satapathy, Hypervelocity penetration of concrete, International Journal of Impact Engineering 35 (12) (2008) 1484–1489.

[299] G. Lukasik, J. Rogers, K. R. Kota, R. D. Bowersox, T. E. Lacy, W. D. Kulatilaka, Ultra-highspeed optical diagnostics of water droplet impact, breakup and shock boundary layer interactions of hypervelocity projectiles. doi:10.2514/6.2022-1656.

[300] M. A. Meyers, Dynamic behavior of materials, John Wiley & Sons, 1994.

[301] D. Glass, R. Dirling, H. Croop, T. Fry, G. Frank, Materials development for hypersonic flight vehicles, in: 14th AIAA/AHI Space Planes and Hypersonic Systems and Technologies Conference, 2006, p. 8122.

[302] V. T. Le, N. San Ha, N. S. Goo, Advanced sandwich structures for thermal protection systems in hypersonic vehicles: A review, Composites Part B: Engineering 226 (2021) 109301.

[303] D. Van Wie, D. Drewry, D. King, C. Hudson, The hypersonic environment: required operating conditions and design challenges, Journal of Materials Science 39 (2004) 5915–5924.

[304] Y.-z. Yang, J.-l. Yang, D.-n. Fang, Research progress on thermal protection materials and structures of hypersonic vehicles, Applied Mathematics and Mechanics 29 (2008) 51–60.

[305] Z. Yinhai, P. Wei, X. Ruina, P. Jiang, Review on active thermal protection and its heat transfer for airbreathing hypersonic vehicles, Chinese Journal of Aeronautics 31 (10) (2018) 1929–1953.

[306] E. Schülein, Experimentelle hyperschallversuchsanlagen und messtechniken, in: Besonderheiten des Hyperschallflugs, 2019.

[307] A. Strawa, G. Chapman, T. Canning, J. Arnold, Ballistic range and aerothermodynamic testing, Journal of Aircraft 28 (7) (1991) 443–449.

[308] P. C. Bueno, N. Mueschke, E. LaLonde, C. S. Combs, Spectroscopic imaging of the flow around hypersonic vehicles, in: Proceedings of the AIAA Scitech 2022 Forum, 2022, p. 2224.

[309] C. J. Roy, F. G. Blottner, Review and assessment of turbulence models for hypersonic flows, Progress in Aerospace Sciences 42 (7-8) (2006) 469–530.

[310] J. T. Parker, A. Serrani, S. Yurkovich, M. A. Bolender, D. B. Doman, Control-oriented modeling of an air-breathing hypersonic vehicle, Journal of Guidance, Control, and Dynamics 30 (3) (2007) 856–869.

[311] L. J. Spitzer, D. J. Grove, W. E. Johnson, L. Tonks, W. F. Westendorp, Problems of the stellarator as a useful power source, Tech. Rep. NYO-6047; PM-S-14, Princeton University, NJ (Aug 1954).
URL `https://www.osti.gov/biblio/4294054`

[312] D. Ashby, M. Hughes, Dynamic burn control of a tokamak reactor by fuel injection, Nuclear Fusion 20 (4) (1980) 451.

[313] D. J. Rose, Feasibility of power by nuclear fusion., Tech. rep., Oak Ridge National Lab., Tenn. (1968).

[314] P. W. Fuller, Some highlights in the history of high-speed photography and photonics as applied to ballistics, in: High-Pressure Shock Compression of Solids VIII, Springer, 2005, pp. 251–298.

[315] G. Settles, Schlieren and Shadowgraph Techniques: Visualizing phenomena in transparent media, Springer-Verlag Berlin, 2001.

[316] J. D. Yeager, P. R. Bowden, D. R. Guildenbecher, J. D. Olles, Characterization of hypervelocity metal fragments for explosive initiation, Journal of Applied Physics 122 (3) (2017) 035901.

[317] E. Watson, M. Gulde, L. Kortmann, M. Higashide, F. Schaefer, S. Hiermaier, Optical fragment tracking in hypervelocity impact experiments, Acta Astronautica 155 (2019) 111–117.

[318] E. Watson, N. Kunert, R. Putzar, H.-G. Maas, S. Hiermaier, Four-view split-image fragment tracking in hypervelocity impact experiments, International Journal of Impact Engineering 135 (2020) 103405.

[319] E. Watson, M. Gulde, S. Hiermaier, Fragment tracking in hypervelocity impact experiments, Procedia Engineering 204 (2017) 170–177.

[320] X. Tian, X. Wang, Y. Song, G. Wei, R. Zeng, A tracking algorithm for debris cloud fragments produced by different hypervelocity impacts through image processing, IEEE Transactions on Aerospace and Electronic Systems (2023).

[321] N. Kawai, M. Nagano, S. Hasegawa, E. Sato, In-situ observation of damage evolution in polycarbonate subjected to hypervelocity impact, International Journal of Impact Engineering 142 (2020) 103584.

[322] N. Kawai, Y. Kuroda, M. Nagano, S. Hasegawa, E. Sato, Stress-wave propagation and damage formation associated with hypervelocity penetration into polycarbonate, Procedia Engineering 204 (2017) 255–261. doi:10.1016/j.proeng.2017.09.733.

[323] Q. Zhang, Y. Chen, F. Huang, R. Long, Experimental study on expansion characteristics of debris clouds produced by oblique hypervelocity impact of LY12 aluminum projectiles with thin LY12 aluminum plates, International Journal of Impact Engineering 35 (12) (2008) 1884–1891.

[324] K. Ohtani, D. Numata, T. Kikuchi, M. Sun, K. Takayama, K. Togami, A study of hypervelocity impact on cryogenic materials, International Journal of Impact Engineering 33 (1-12) (2006) 555–565.

[325] T. E. of Encyclopaedia Britannica, Harold edgerton: American electrical engineer and photographer (2022).

[326] V. C. Draxler, High-speed diagnostics for ballistics and explosive studies, High-Pressure Shock Compression of Solids VIII: The Science and Technology of High-Velocity Impact (2005) 227–249.

[327] J. D. Tandy, J. M. Mihaly, M. Adams, A. Rosakis, Examining the temporal evolution of hypervelocity impact phenomena via high-speed imaging and ultraviolet-visible emission spectroscopy, Journal of Applied Physics 116 (3) (2014) 034901.

[328] R. J. Lawrence, W. D. Reinhart, L. C. Chhabildas, T. F. Thornhill, Spectral measurements of hypervelocity impact flash, International Journal of Impact Engineering 33 (1-12) (2006) 353–363.

[329] M. Intardonato, S. Davis, J. A. R. Matthew Hay, G. Lukasik, T. E. L. Jr., , W. D. Kulatilaka, Time-Resolved Spectroscopic Characterization of Hypervelocity Impacts on Metal Targets, in: Proceedings of the 70th JANNAF Propulsion Meeting, 2023.

[330] Hadland Imaging: Ultra High-Speed Digital Image Correlation Solutions (2022).
URL https://hadlandimaging.com/wp-content/uploads/2022/05/Hadland-Imaging-2022-DIC-brochure-v2.pdf

[331] N. E. Howard, D. W. Gardner, D. R. Snyder, Million-frame-per-second ccd camera with 16 frames of storage, in: Ultrahigh- and High-Speed Photography and Image-based Motion Measurement, Vol. 3173, SPIE, 1997, pp. 40–47.

[332] Shimadzu Hyper Vision HPV-X2 (2017).
URL https://www.shimadzu.com/an/sites/shimadzu.com.an/files/pim/pim_document_file/brochures/10336/402_c220e015c.pdf

[333] Kirana Specialized Imaging Kirana7M.
URL https://www.specialised-imaging.com/application/files/8416/2124/6779/SI_KIRANA_01_Q01_A4.pdf

[334] Phantom UHS-SERIES Vision Research v2512/v2012 (2021).
URL https://www.phantomhighspeed.com/-/media/project/ameteksxa/visionresearch/documents/datasheets/web/wdsuhsfam.pdf?download=1

[335] SA-Z FASTCAM Series by Photron (2021).
URL https://photron.com/wp-content/uploads/2021/08/SA-Z-2021.pdf

[336] L. Hoddeson, P. W. Henriksen, G. Baym, R. A. Meade, C. L. Westfall, Critical assembly: a technical history of Los Alamos during the Oppenheimer years, 1943-1945, Cambridge University Press, 1993.

[337] J. Crews, E. Christiansen, The nasa jsc hypervelocity impact test facility (hit-f), in: Space Programs and Technologies Conference, 1992, p. 1640.

[338] T. Moritoh, S. Matsuoka, T. Ogura, K. G. Nakamura, K.-i. Kondo, M. Katayama, M. Yoshida, Dynamic failure of steel under hypervelocity impact of polycarbonate up to 9 km/s, Journal of Applied Physics 93 (10) (2003) 5983–5988.

[339] C. Mabire, P. L. Hereil, Shock induced polymorphic transition and melting of tin, in: AIP Conference Proceedings, Vol. 505, American Institute of Physics, 2000, pp. 93–96.

[340] P. E. Kalita, P. E. Specht, S. Root, N. Sinclair, A. Schuman, M. White, A. Cornelius, J. Smith, S. Sinogeikin, Dynamic XRD Shock and Static Compression of CaF2., Tech. rep., Sandia National Laboratory (SNL), Albuquerque, NM (2017).

[341] M. D. Furnish, S. Root, P. Samuels, Equation-of-state and shock homogeneity of imx-101 and imx-104., Tech. rep., Sandia National Lab.(SNL-NM), Albuquerque, NM (United States) (2014).

[342] B. Lexow, A. Bueckle, M. Wickert, S. Hiermaier, The xllgg–a hypervelovity launcher for impact cratering research., Bridging the Gap III: Impact Cratering In Nature, Experiments, and Modeling 1861 (2015) 1046.

[343] S. Rothberg, M. Allen, P. Castellini, D. Di Maio, J. Dirckx, D. Ewins, B. Halkon, P. Muyshondt, N. Paone, T. Ryan, H. Steger, E. Tomasini, S. Vanlanduit, J. Vignola, An international review of laser doppler vibrometry: Making light work of vibration measurement, Optics and Lasers in Engineering 99 (2017) 11–22. doi:10.1016/j.optlaseng.2016.10.023.

[344] A. Mitchell, W. Nellis, Diagnostic system of the Lawrence Livermore National Laboratory two-stage light-gas gun, Review of Scientific Instruments 52 (3) (1981) 347–359.

[345] AMOtronics Digital Fragment Testing for Ballistic Test Facilities (2021).
URL https://www.amotronics.de/download/AMOtronics-FragmentTesting.pdf

[346] REL SURE-Bright Profusion X Gen2 LED Lighting System (2019).
URL https://hadlandimaging.com/wp-content/uploads/2021/11/Hadland-REL-Visible-Spectrum-LED-2021-Brochure-v2.pdf

[347] Specialized Imaging AD-500: Single or multiple head high intensity flash system (2021).
URL https://www.specialised-imaging.com/application/files/3616/6387/9942/SI_AD500-MSFH_01_Q01_A4.pdf

[348] Correlated Solutions: VIC-3D Ultra High-Speed (UHS) digital image correlation system (2021).
URL https://www.correlatedsolutions.com/specialized-systems-ref/ultra-high-speed

[349] Scandiflash: Modular Instruments and Solutions for Materials Research in Dynamic Processes (2022).
URL https://scandiflash.com/wp-content/uploads/2022/10/scf-systems-a4-20230203-v03-low-res.pdf

[350] Scandiflash: Get Ultra fast sequential imaging with Absolute Minimal parallax (2022).
URL https://scandiflash.com/wp-content/uploads/2022/10/SCF-MAT-A4-20220912-v02-low-res.pdf

[351] L. Zhao, M. Jin, J. Li, A generally applicable laser doppler velocimetry, in: Proceedings of the 2015 International Power, Electronics and Materials Engineering Conference, Atlantis Press, 2015/05, pp. 773–777. doi:https://doi.org/10.2991/ipemec-15.2015.143.

[352] Quantifi Photonics: Photonics Test & Measurement Experts, https://www.quantifiphotonics.com/, accessed: 04-29-2023.

[353] Hadland Imaging: Amotronics Saturn transient recorder system, https://hadlandimaging.com/amotronics-saturn-transient-recorder-system/, accessed: 04-29-2023.

[354] Z.-l. Xue, A.-m. Xie, Y.-q. Zhu, Y.-h. Zhong, Y.-c. Wu, Y.-g. Zhou, X.-c. Wu, 3D characterisation of debris clouds under hypervelocity impact with large-field pulsed digital in-line holography, International Journal of Impact Engineering 154 (2021) 103875.

[355] Y. Zhou, Z. Xue, Y. Wu, A. Xie, X. Wu, Three-dimensional characterization of debris clouds under hypervelocity impact with pulsed digital inline holography, Applied Optics 57 (21) (2018) 6145–6152.

[356] M. Mansoor, J. Trolinger, J. George, Towards three-dimensional characterization of hypervelocity impact events using ultrahigh-speed digital holography, International Journal of Impact Engineering 172 (2023) 104421.

[357] D. Gabor, Microscopy by reconstructed wave-fronts, Proceedings of the Royal Society of London. Series A. Mathematical and Physical Sciences 197 (1051) (1949) 454–487.

[358] U. Schnars, C. Falldorf, J. Watson, W. Jüptner, U. Schnars, C. Falldorf, J. Watson, W. Jüptner, Digital holography, Springer, 2015.

[359] P. Shojaei, M. Trabia, B. O'Toole, R. Jennings, Predicting the projectile velocity of a two-stage gas gun using machine learning, in: Proceedings of the Pressure Vessels and Piping Conference, Vol. 86168, American Society of Mechanical Engineers, 2022, p. V003T05A014. doi:10.1115/PVP2022-79815.

[360] D. Chen, F. Hu, G. Nian, T. Yang, Deep residual learning for nonlinear regression, Entropy 22 (2) (2020) 193.

[361] A. J. Smola, B. Schölkopf, A tutorial on support vector regression, Statistics and Computing 14 (3) (2004) 199–222.

[362] C. E. Rasmussen, Evaluation of gaussian processes and other methods for non-linear regression, Ph.D. thesis, University of Toronto Toronto, Canada (1997).

[363] K. Hornik, M. Stinchcombe, H. White, Multilayer feedforward networks are universal approximators, Neural Networks 2 (5) (1989) 359–366.

[364] J. D. Anderson, J. Wendt, Computational fluid dynamics, Vol. 206, Springer, 1995.

[365] Y. Zhuang, X. Lu, Mathematical Modeling and Numerical Simulation of a Two-Stage Light-Gas Launcher, pp. 255–261. doi:10.1142/9789814759687_0031.

[366] G. Rajesh, R. Mishra, H. Kang, H. Kim, Computational analysis of the compressible flow driven by a piston in a ballistic range, Journal of Thermal Science 16 (2007) 360–369.

[367] G. Majzoubi, M. Ghaed Rahmati, M. Kashfi, Performance of a two-stages gas gun: Experimental, analytical and numerical analysis, International Journal of Engineering 32 (5) (2019) 759–768.

[368] S. Milora, S. Combs, M. Gouge, R. Kincaid, Quickgun: An algorithm for estimating the performance of two-stage light gas guns, Tech. rep., Oak Ridge National Lab. (1990).

[369] R. Piacesi, D. Gates, A. Seigel, Computer analysis of two-stage hypervelocity model launchers, Tech. rep., Naval Ordnance Lab White Oak MD (1963).